Provenance and magmatic-tectonic setting of Campanian-aged volcaniclastic sandstones of the Kannaviou Formation in western Cyprus: evidence for a Southern Neotethyan continental margin volcanic arc

Provenance and magmatic-tectonic setting of Campanian-aged volcaniclastic sandstones of the Kannaviou Formation in western Cyprus: evidence for a Southern Neotethyan continental margin volcanic arc

Guohui Chen*, Alastair H. F. Robertson

School of GeoSciences, University of Edinburgh, West Mains Road, Edinburgh, EH9 3JW, UK

* Corresponding author (Guohui.Chen@live.cn)

Abstract

Regionally developed late Cretaceous subduction-related magmatism in the eastern Mediterranean records progressive closure of the Southern Neotethys. In western Cyprus the late Cretaceous (c. 90 Ma) Troodos ophiolite is depositionally overlain by volcaniclastic sandstones (up to 750 m thick) that are dominated by redeposited pyroclastic fallout, interbedded with both non-calcareous and calcareous radiolarian-bearing mudstones. The sands were mainly deposited by channelised mass flow processes and to a lesser extent by turbidity currents in a deep-water forearc basin. The succession was folded and locally thrust-deformed related to latest Cretaceous emplacement of adjacent Mesozoic continental margin and oceanic units (Mamonia Complex). SIMS U-Pb analysis of euhedral to subhedral magmatic zircon crystals yielded a weighted mean $^{206}Pb/^{238}U$ age of 80.1±1.1 Ma (Campanian). Sandstone petrography including compositional framework ($Q_{12}F_{21}L_{67}$) suggests sediment supply from a volcanic arc. Subordinate continentally derived detritus suggests

a continental margin arc setting for the mafic to felsic fallout ash. SIMS analysis of little-altered volcanic glass indicates high Th/Nb and Th/La ratios that suggest the involvement of continental crust and/or subducted terrigenous sediments in magma genesis. Whole-rock chondrite-normalised REE patterns have comparable trends to modern and ancient forearc basin volcaniclastic sands and sandstones (e.g., northwest Pacific region). Trace element chemistry, although scattered towards the continental island arc fields on some geochemical diagrams (e.g., Th-Sc-Zr), mainly suggests an oceanic island arc source for the Kannaviou Formation sandstones, with variable enrichments in V-Cr-Ni-Sc, depletion in Nb-Ta, and relatively low trace element ratios (e.g., La/Co, Th/Co, La/Sc, Th/Sc). An explanation for this apparent discrepancy is that the volcaniclastic sandstones were derived from a relatively primitive arc constructed on previously depleted, rifted (thinned) Neotethyan continental crust. The inferred continental margin arc developed during early-stage northward subduction of Southern Neotethys beneath a Tauride microcontinent to the north. Large volumes of volcanic ash were derived from continental margin arc volcanism, probably in the vicinity of the Kyrenia Range in northern Cyprus.

Keywords: late Cretaceous, volcaniclastic sediments, continental margin arc, provenance analysis, Southern Neotethys, Cyprus

1. Introduction

Volcanic edifices are commonly localised and may be concealed or eroded, whereas their volcaniclastic products are commonly widely disseminated and easily recognisable in the stratigraphic record (e.g., Fisher and Schmincke, 1984; Yamamoto, 2009; Carey and Schneider, 2011). Volcaniclastic sediments (either primary or reworked) preserve petrographic and geochemical evidence that is indicative of magma genesis and tectonic setting of eruption.

Here, we present and discuss the results of a comprehensive study on the late Cretaceous volcaniclastic sandstones of the Kannaviou Formation in western Cyprus. We utilise a combination of field-based sedimentology, structural geology, thin-section petrography, and geochemical studies (whole-rock composition, mineral and glass composition) together with U-Pb dating of zircon, in the light of the regional geological setting. The main driver, building on previous studies, is to provide geochemical data for the volcaniclastic sandstones and to date the timing of the related volcanism, both of which are essential to understand the regional tectonic-magmatic setting. For example, it was unknown whether the volcanism relates to either continental or oceanic arc volcanism, and whether or not the source volcanism and the background depositional ages are synchronous. Specifically our objectives are: (1) to understand the deposition of the volcaniclastic sediments, taking account of the stratigraphy, structure and field sedimentary features; (2) to determine the magmatic setting of the source rocks using a combination of petrographic, mineralogical and geochemical studies; (3) to determine the absolute age of the related arc volcanism using U-Pb zircon dating; (4) to compare the Kannaviou Formation with modern and ancient counterparts; and (5) to propose

a new magmatic-tectonic model for the late Cretaceous magmatism in the context of the Southern Neotethys in the eastern Mediterranean region. Taken together, the results allow a significant advance in understanding in the tectonic-magmatic development of the Southern Neotethys in the eastern Mediterranean, with implications for comparable volcaniclastic sediments and tectonic settings elsewhere.

The most noteworthy feature of the Southern Neotethys in the eastern Mediterranean region is the late Cretaceous Troodos ophiolite (92-90 Ma) (Mukasa and Ludden, 1987). This is generally accepted to have formed during initial stages of northward subduction of the Southern Neotethys (Gass, 1968; Moores and Vine, 1971; Robinson and Malpas, 1990; Robertson, 1990, 2002; Robertson and Xenophontos, 1993; Pearce and Robinson, 2010). The volcaniclastic sedimentary rocks of the Kannaviou Formation depositionally overlie the Troodos ophiolite in the west of the island (Lapierre, 1968, 1975; Robertson, 1977a) and are therefore critical to interpretation of the regional tectonic setting (Fig. 1). Previous studies of the Kannaviou Formation provided field observations, whole-rock analysis, some mineral chemical analysis (Lapierre, 1975; Robertson, 1977a; Gilbert and Robertson, 2013) and paleontological dating (Urquhart and Banner, 1994; Lord et al., 2000). However, this is the first study to include evidence of geochemistry and volcanic source age. The source area of the Kannaviou Formation was previously suggested to be in the Kyrenia Range of northern Cyprus (Robertson, 1977a; Gilbert and Robertson, 2013) (Fig. 1a), a hypothesis that is tested here using new U-Pb dating of detrital zircons.

2. Geological setting

Below, we outline key features of the geology of Cyprus that are specifically relevant to an understanding of the late Cretaceous volcaniclastic sediments.

2.1. Setting of the Kannaviou Formation relative to the Troodos ophiolite

The Troodos Massif in central and southern Cyprus comprises the late Cretaceous Troodos ophiolite and its *in situ* sedimentary cover including the Kannaviou Formation. Based on paleomagnetic evidence, the Troodos ophiolite and its sedimentary cover underwent anticlockwise rotation of up to c. 90°, between the late Campanian and early Eocene (Clube et al., 1985; Clube and Robertson, 1986; Morris, 1996; Inwood et al., 2009). The Kannaviou Formation has to be rotated by 90° clockwise when interpreting its regional tectonic-magmatic formation.

The ophiolite is overlain, first by Fe-Mn-rich metalliferous sediments (umbers) of the Campanian Perapedhi Formation (up to c. 10 m thick) (Robertson and Hudson, 1974; Robertson, 1975). In western Cyprus, the Perapedhi Formation begins with localised umbers, as elsewhere in Cyprus (Robertson, 1977a), and passes upwards first into radiolarian mudstones, and then into volcaniclastic sandstones that represent the base of the Kannaviou Formation (Robertson, 1977a; Urquhart and Banner, 1994; Gilbert and Robertson, 2013).

The Kannaviou Formation mainly crops out around the western periphery of the Troodos Massif, from near Kannaviou village, the type area, northwards to around Istinjo and Kinousa (Lapierre, 1968) (Fig. 1b). The formation comprises alternating bentonitic claystone, radiolarian mudstone and

volcaniclastic sandstone, up to 750 m thick (Robertson, 1977a; Gilbert and Robertson, 2013) (Fig. 2). A Campanian-early Maastrichtian age has been determined mainly using radiolarians (Urquhart and Banner, 1994; Bragina and Bragin, 1995; Lord et al., 2000). In its type area, the Kannaviou Formation passes upwards into submarine debris-flow deposits, known as the Kathikas Formation (Swarbrick and Naylor, 1980) (Fig. 2). Local interbeds of pelagic chalk are dated as late Maastrichtian (Swarbrick and Naylor, 1980; Urquhart and Banner, 1994; Lord et al., 2000). The Kannaviou Formation and/or the Kathikas Formation in different local areas are conformably overlain by deep-sea pelagic carbonates of the Lefkara Formation, ranging in age from Maastrichtian to Oligocene (Robertson, 1976; Lord et al., 2000) (Fig. 2). Lateral facies equivalents of the Kannaviou Formation along the southern margin of the Troodos Massif are restricted to bentonitic clays and radiolarian siltstone, c. 160 m thick (Moni Member) (Robertson, 1977b; Swarbrick and Robertson, 1980). In contrast, the formation is entirely absent along the northern and eastern margins of the Troodos Massif (Robertson and Hudson, 1974), which has a bearing on the regional tectonic setting.

2.2. Mamonia Complex

The Mamonia Complex of western Cyprus is relevant here because it represents a likely source of terrigenous sediment to the late Cretaceous Kannaviou Formation. The Mamonia Complex is dominated by two different tectono-stratigraphic units (Fig. 1b) of late Triassic to early Cretaceous age: (1) Sandstone gravity-flow deposits, pelagic and redeposited limestone, chert, mudstone and radiolarite of the sedimentary Ayios Photios Group (Lapierre, 1975; Robertson and Woodcock, 1979; Swarbrick and Robertson, 1980; Torley

and Robertson, 2018); and (2) basaltic volcanics, together with volumetrically subordinate shallow-water carbonate, hemipelagic calcilutite, chert and mudstone of the Dhiarizos Group (Lapierre, 1975; Robertson and Woodcock, 1979; Swarbrick and Robertson, 1980; Malpas et al., 1992; Lapierre et al., 2007). The two stratigraphic groups are separated by tectonic contacts, and the Mamonia Complex as a whole has been juxtaposed with the Troodos Massif by a combination of thrusting and strike-slip faulting along steep arcuate fault lineaments during the late Cretaceous (Robertson and Woodcock, 1979; Swarbrick, 1980; Robertson, 1990; Morris et al., 1990; Bailey et al., 2000). The Mamonia Complex is restored as a part of the earliest-formed oceanic crust (Dhiarizos Group) and adjacent passive margin (Ayios Photios Group) of the Southern Neotethys that rifted from the northern margin of Gondwana (Robertson and Woodcock, 1979; Torley and Robertson, 2018). The volcanic rocks are also relevant to the composition of the source mantle lithosphere that may have affected the composition of subsequent arc magmatism in the region.

2.3. Transform faulting

Oceanic transform faulting is relevant to the Kannaviou Formation because it is inferred to have created a sea-floor topography that greatly influenced the deposition of the Kannaviou Formation during the late Cretaceous. The Troodos ophiolite in central-south Cyprus is cut by the east-west-trending South Troodos Transform Fault Zone, up to c. 15 km wide (Moores and Vine, 1971; Murton, 1986; MacLeod, 1990; Morris et al., 1990; MacLeod and Murton, 1993) (Fig. 1a). Transform faulting was active during the late Cretaceous genesis of the Troodos ophiolite at a spreading axis (Murton and Gass, 1986; MacLeod and Murton, 1993). Critically, the transform fault extends westwards beneath

the late Cretaceous-Cenozoic sedimentary cover and links with the arcuate fault-bounded lineaments in western Cyprus (Robertson, 1977a; Malpas et al., 1992, 1993; Morris et al., 1998) (Fig. 1b). The lineaments entrain fragments of late Cretaceous ophiolitic rocks and their sedimentary cover including the Kannaviou Formation (Robertson, 1977a; Gilbert and Robertson, 2013), together with slivers of late Cretaceous amphibolite facies and greenschist facies metamorphic rocks (Lapierre, 1975; Swarbrick, 1980, 1993; Malpas et al., 1992). The Troodos Massif including the Kannaviou Formation was tectonically juxtaposed with the Mamonia Complex during the late Cretaceous (pre- to syn-Maastrichtian) (Robertson and Woodcock, 1979; Swarbrick, 1980, 1993; Malpas et al., 1992, 1993; Morris et al., 1998; Bailey et al., 2000).

2.4. Cenozoic-recent development

The post-depositional geological development needs to be taken into account to understand the sedimentary development of the Kannaviou Formation. In particular, western Cyprus was affected by extension along a c. north-south axis during late Miocene to recent, related to formation of the Polis graben (Robertson, 1977c; Payne and Robertson, 1995, 2000; Balmer et al., 2019). The main Kannaviou Formation outcrop lies within the eastern part of the graben. The formation together with the Troodos Massif as a whole was uplifted and exposed mainly during the Pleistocene (Robertson, 1977c; Poole and Robertson, 1998; Morag et al., 2016). The effects of the Cenozoic faulting (e.g., relative movement of fault blocks) and the Pleistocene uplift (e.g., landslipping) were taken account of when interpreting the Kannaviou Formation.

2.5. Kyrenia Range

The Kyrenia Range in northern Cyprus is mentioned in this paper mainly because it is a possible source of the volcaniclastic sands that supplied the Kannaviou Formation. If correct, the tectonic setting of the Kyrenia Range during the late Cretaceous has a direct bearing on the provenance and tectonic-magmatic setting of the volcanism represented by the Kannaviou Formation. The Kyrenia Range is dominated by Triassic-Cretaceous platform carbonates that were metamorphosed under greenschist facies conditions during the late Cretaceous (Baroz, 1979). Late Cretaceous felsic volcanics (Fourkovouno (Selvilitepe) Formation) (Robertson and Woodcock, 1986; Huang et al., 2007; Robertson et al., 2012; Chen, 2018) have been suggested as the source of the Kannaviou Formation volcaniclastic sediments (Robertson, 1977a; Gilbert and Robertson, 2013). The succession continues with Maastrichtian-early Cenozoic basaltic volcanics and both pelagic and redeposited carbonates. The Kyrenia Range is interpreted as part of the northern active continental margin of the Southern Neotethys (Robertson and Woodcock, 1986; Robertson et al., 2012) that was juxtaposed with the Troodos Massif, possibly by the late Eocene and certainly by the late Miocene (Robertson et al., 2012, 2014). The Kyrenia Range escaped the major anticlockwise tectonic rotation of the Troodos Massif (Morris et al., 2015), and effectively forms the southern limit of Tauride continental crust (Fig. 1a).

213 # 3. Methods

214 ## 3.1. Fieldwork and sampling

215 Previous geological maps (Lapierre, 1975; Robertson, 1977a) were compared
216 and field checked. The type area of the Kannaviou Formation was remapped
217 to illustrate the structure and sediment distribution (Fig. 3). More northerly
218 exposures in the Sarama-Peristerona and Kinousa areas, and in the southern
219 part of the Akamas Peninsula, were studied for comparison (see
220 Supplementary material) (Robertson, 1977a). In addition, sedimentary logs of
221 well-exposed local successions were measured to shed light on depositional
222 processes and to aid sampling (Fig. 4). Fault distribution and kinematic studies
223 were carried out to determine regional stress regimes during different time
224 periods (see Supplementary material). During this study we used a combination
225 of new and previously collected samples (n=20 and 18, respectively), and also
226 new and existing laboratory data, as summarised in Table 1.

227 ## 3.2. Petrography

228 Sandstones of medium to coarse grain size were studied using an optical
229 microscope to determine their mineralogy and petrography. Scanning electron
230 microscopy (SEM) was used to study grain fabric and texture. Fourteen
231 medium-grained sandstones with well-preserved textures were selected for
232 point counting (Table 1). At least 400 points was counted for each sample using
233 a Swift Automatic point-counter, which gave a statistically meaningful result with
234 95% confidence limits (Van der Plas and Tobi, 1965). The Gazzi-Dickinson
235 point-counting method was utilised to maximise source rock data while
236 minimising the effects of grain size variation (Graham et al., 1976; Dickinson
237 and Suczek, 1979; Ingersoll et al., 1984). The recorded components (with

238 explanatory notes) are listed in Table 2. The raw data (by percentage), and the
239 calculated framework parameters are given in the Supplementary material.

240 3.3. Whole-rock major, trace, and rare earth element geochemistry

241 Whole-rock major and trace element concentrations of the sandstones (both
242 new and previous samples) were analysed by X-ray fluorescence (XRF) at the
243 School of GeoSciences, University of Edinburgh, using the methods of Fitton
244 et al. (1998) and Fitton and Godard (2004) (see Table 1). Accuracy and
245 precision estimates are comparable to those of these authors.

246 Ten newly collected samples (Table 1) were analysed at the ACME
247 Laboratories, Vancouver for trace and rare-earth elements (REEs) by
248 inductively coupled plasma mass spectrometer, following lithium
249 metaborate/tetraborate fusion and nitric acid digestion. As an indication of
250 precision, the major intra-lab standard (Reference Material STD SO-18/19) was
251 analysed together with the samples, resulting in standard deviations (≤6%) for
252 all trace and rare earth elements. For further information on the procedures,
253 geostandards and precision for the elements analysed see http://acmelab.com.
254 All of the analytical data for the major, trace and rare earth elements are listed
255 in the Supplementary material.

256 3.4. Glass and mineral chemistry

257 Two polished thin sections (nos. 1074 and 2164 of Robertson, 1977a) that
258 contain abundant well-preserved undevitrified volcanic glass and feldspar were
259 selected for analysis of major elements, using a Cameca SX100 electron
260 microprobe (EMPA) at the School of GeoSciences, University of Edinburgh.
261 Previous analyses of glass, feldspar and pyroxene used the same method
262 (Gilbert and Robertson, 2013) (Table 1). Details of the analytical conditions and

methods are given by Hayward (2011) and by Hartley and Thordarson (2013). The accuracy of major element determinations is better than ±1 % of total value. All analytical data for glass, feldspar and pyroxene are given in the Supplementary material.

Trace-element analyses of undevitrified volcanic glass were performed on four new polished thin sections (nos. 14-11, 14-14, 16-20, 16-22) (Table 1) using a Cameca IMS-4f ion probe at the School of GeoSciences, University of Edinburgh. The analytical data, standardization protocols and errors are given in the Supplementary material.

3.5. U-Th-Pb secondary ion microscopy (SIMS) geochronology

Zircon crystals were selected from the 50-125 μm fraction that was extracted from c. 20 kg of medium to coarse-grained sandstone (sample nos. 14-04, 14-11, 14-14) (Table 1). A Wilfley table, Frantz Isodynamic magnetic separator and a high density solution (lithium polytungstate; 2.85 g/ml) were used to aid separation. Zircon grains (n=18) were randomly picked under a binocular microscope and finally mounted in epoxy resin and polished down to expose the grain interior. Internal structures were studied with the SEM using cathodoluminescence (CL) at the School of GeoSciences, University of Edinburgh. U-Pb analysis was then performed on a Cameca ims-1270 SIMS at the School of GeoSciences, University of Edinburgh, using the methods detailed by Kelly et al. (2008) and Ustaömer et al. (2012). Errors on the reported ages are ±1σ. Geochronological plots were produced using the Excel Macro program ISOPLOT (Ludwig, 2012). Analytical results are listed in the Supplementary material.

4. Results

4.1. Field relationships

4.1.1. Structure

Structural analysis was required to understand the stratigraphy of the Kannaviou Formation. The main part of the outcrop southeast of Kannaviou village is deformed into a large-scale syncline with a c. east-west-trending axis, as inferred by the presence of outcrops of ophiolitic basement both to the north and south (Fig. 3a-b). The core of the fold is made of variably folded mudstones and volcaniclastic sandstones, typically up to hundreds of metres in scale. Locally, the sandstone is structurally inverted, as indicated by overturned cross-bedding and normal grading. West of Kannaviou village, the succession is deformed into a large anticline (Fig. 3c). The core of this structure comprises thick-bedded, medium to coarse-grained volcaniclastic sandstone, siltstone and calcareous claystone. The Troodos ophiolitic lavas north of Kannaviou village (near Ezousa River) are affected by top-to-the northeast thrusting (Fig. 3). In the south, the main Kannaviou Formation outcrop is overthrust by arcuate lineaments of highly sheared ophiolitic serpentinite, as well exposed west of Statos (Fig. 3). Also, in the south of the Akamas Peninsula, ophiolitic rocks are thrust westwards over the Kannaviou Formation (Lapierre, 1975; Robertson, 1977a) (Fig. 1b).

The Kannaviou Formation is affected by two main generations of faulting. Overall, compression-related faulting relates to latest Cretaceous (Maastrichtian) emplacement of the Mesozoic continental margin and oceanic rocks of the Mamonia Complex (Robertson, 1977a; Swarbrick and Naylor, 1980). This was followed by mainly extensional faulting related to formation of

313 the Neogene Polis graben (Payne and Robertson, 1995, 2000). Mapping and
314 kinematic analysis (see Supplementary material) show that faulting offsets
315 parts of the succession but does not greatly disrupt the stratigraphy of the
316 Kannaviou Formation.

317 4.1.2. Sedimentary succession

318 The lower part of the Kannaviou Formation (c. 100 m) is dominated by non-
319 calcareous to variably calcareous claystone (Fig. 4a-b), interbedded with thin-
320 bedded volcaniclastic mudstone (Figs. 4c, 5a). Several fine-grained, lenticular
321 volcaniclastic sandstone packages, up to 10 m thick, are locally present (Figs.
322 4a-d, 5b). Bioturbation (<3 cm long) is commonly well developed (Fig. 5c). The
323 mudstone and sandstone locally contain basalt, hyaloclastite breccia and/or
324 palagonite clasts, 3-45 cm in diameter, with a matrix-supported fabric, as seen
325 near the Troodos extrusive rock contact (Figs. 4b, 5d).

326 The middle part of the succession is characterised by thick-bedded,
327 medium to coarse-grained volcaniclastic sandstone (Fig. 4a, e-h). The
328 individual sandstone depositional unit is much thicker (up to 30 m), more
329 massive and virtually structureless compared to those beneath. A prominent c.
330 25 m thick nearly homogeneous tabular sandstone northeast of Kannaviou
331 village (Fig. 4a) exhibits occasional planar lamination, low-angle cross
332 lamination and indistinct normal grading. Convolute lamination (up to 25 cm
333 thick) and evidence of slumping occur locally (Figs. 4h, 5e). Cross-bedding
334 measurements from small outcrops (e.g., near Istinjo) show a general preferred
335 orientation of foreset lamination towards the southeast (Robertson, 1977a).
336 This is consistent with the absence of the Kannaviou Formation farther east,

where pelagic chalks of the Lefkara Formation directly overlie the Perapedhi Formation or the Troodos ophiolitic lavas (Robertson, 1977a).

The upper part of the succession is dominated by claystone and volcaniclastic mudstone (Fig. 4e-g, i-j). Lenticular sandstone units (up to 20 m thick) are interbedded with structureless claystone and weakly-bedded volcaniclastic mudstone, for example around Sarama-Lasa (Figs. 4e-f, 5f). Sandstone, where present, is generally thin to medium-bedded, and forms lenses up to c. 300 m long. Individual sandstones are fine to medium-grained, well-laminated and normal-graded. Elsewhere, low-angle cross-bedding, planar cross-bedding and horizontal stratification are present. Mud rip-up clasts are locally present near the base of individual beds, and some beds are rich in plant material (i.e., branches, twigs and leaf debris). Dark epiclastic grains of basalt are commonly visible in hand specimen (<1 mm in size).

4.2. Petrography and detrital modes

Framework grains are characterised by sub-angular to sub-rounded morphologies and poorly to moderately-sorted fabrics. Quartz (2-18 modal %) and feldspar (6-21 modal %; up to 1200 μm) are common. Abundant volcaniclastic material is present, mostly as transparent volcanic glass with only rare phenocrysts (see Section 4.2.2). In contrast, volcanic grains (mostly angular) range in composition from mafic to intermediate (dark coloured; <4%), to felsic (pale coloured; 2-15%) and commonly contain phenocrysts (see Section 4.2.2) (Fig. 6a). Grains of pyroxene (<3%, up to 500 μm), biotite (<2%) and hornblende (<2%) occur variably. Clasts of radiolarian chert, mica-schist and foraminiferal pelagic limestone also occur locally (Fig. 6b-c). Microfossils are widespread, mostly radiolarians, planktic foraminifera and sponge spicules

(Fig. 6d). The sandstones are generally matrix-supported and carbonate-cemented. The matrix constitutes 6-48 modal %, and mainly comprises clay minerals, together with minor tiny detrital fragments of volcanic glass, feldspar and mica.

4.2.1. Compositional variation

The sandstones show considerable compositional variation from the base of the succession upwards. The lowermost sandstones (sample nos. 14-14, 19.1) are relatively fine-grained (c. 150-300 μm), generally non-calcareous, rich in quartz (including polycrystalline quartz; QFL%Q=17-19) but low in feldspar (QFL%F=13-15). Mica-schist is common and also locally chert. A medium to coarse-grained sandstone sample (no. 18.5) from near the Paleomylon River contains abundant feldspar (QFL%F=24) and lithic fragments (QFL%L=70) that are mostly of volcanic origin (97%). Where the Kannaviou Formation is exposed along the arcuate tectonic lineaments (Fig. 1b) only the base of the succession is exposed restricted to fine-grained, thin-bedded sandstone (Gilbert and Robertson, 2013). A typical sandstone (no. 14.5) from the lineament south of Episkopi is fine to medium-grained, carbonate-bearing litharenite with abundant polycrystalline quartz and metamorphic lithics (e.g., mica-schist).

In the middle part of the succession (sample nos. 14-12, 14-13, 21.2, 22.1), the grain size of the sandstone is typically c. 180-250 μm but reaches 400 μm locally (e.g., south of Kannaviou village; no. 22.1). Quartz (including polycrystalline quartz) decreases (QFL%Q=6-13), whereas feldspar increases (QFL%F=10-32). Volcanic lithics slightly increase and chert becomes common. Dolomite and carbonate cements become more abundant. Sandstones from the upper part of the succession (sample nos. 14-11, 23.1) are generally

coarse-grained (c. 300-500 μm) with more abundant volcanic lithics (LmLvLs%Lv=96-99). Polycrystalline quartz and mica-schist are sparse. Devitrified volcanic glass and recrystallised limestone are rarely present.

Four medium-grained, thick-bedded sandstones from the middle to upper part of the succession in the Sarama-Lasa area are characterised by marked compositional variation, with generally low textural maturity. Two sandstones (nos. 2124, 2158) have abundant lithic fragments (QFL%L=72-80) but few quartz grains (QFL%Q<5). Two other sandstones (nos. 2141, 2156) have a higher abundance of quartz, especially polycrystalline quartz (QFL%Q=15-20) and subhedral feldspar (QFL%F=26) but less lithic fragments (QFL%L=54-59). Volcanic lithics predominate (LmLvLs%Lv=92-96) in these two sandstones, with subordinate metamorphic (no. 2141; LmLvLs%Lm=6) and sedimentary (no. 2156; LmLvLs%Ls=4) fractions.

4.2.2. Glass morphology

The grain size is typically c. 100-700 μm but reaches 1200 μm locally (Fig. 7). Colourless glass is mainly felsic (Robertson, 1977a; Gilbert and Robertson, 2013), constituting over 75% of the grains analysed (see Section 4.3.1). Pinkish or brownish glass is of mafic to intermediate composition (Robertson, 1977a) (see Supplementary material). Taken together, the relative abundances of glass morphologies, glass colour (related to composition), textures and vesicle abundances allow four general glass groups to be recognised (Fig. 7): (1) transparent, highly vesicular pumiceous glass with a common fluid-like or rarely frothy texture; (2) colourless glass as blocky shards, cuspate bubble wall, and rarely tubular or spindle-shaped glass, all of up to moderate vesicularity; (3)

411 pinkish glass composed of generally vesicular cuspate shards and blocky
412 shards; and (4) brownish glass with a microlitic texture.

413 4.2.3. Modal proportions

414 On the QFL diagram of McBride (1963) (Fig. 8a), sandstones from all sample
415 localities are feldspathic litharenite. An undissected arc basin is indicated on
416 the QFL diagram (e.g., Dickinson et al., 1983) (Fig. 8b) as the dominant
417 provenance, especially for the Kannaviou and Paleomylon River area
418 sandstones. Two samples from Sarama-Lasa (nos. 2141, 2156) and one from
419 south of Episkopi (no. 14.5) plot in the transitional arc field. Plotted on the QFL
420 and LmLvLs diagrams of Marsaglia and Ingersoll (1992) (Fig. 8c-d), the
421 Kannaviou and Paleomylon River area samples plot in the continental arc field.
422 The average Kannaviou Formation composition falls in the continental arc field
423 ($Q_{12}F_{21}L_{67}$) (Fig. 8c) or the overlapping field of intra-oceanic and continental
424 arcs ($Lm_2Lv_{94}Ls_4$) (Fig. 8d).

425 4.3. Glass and mineral chemistry

426 4.3.1. Volcanic glass

427 Volcanic glass of different morphology and from different localities shows
428 considerable compositional variation (Fig. 9). The volcanic glass analysed
429 (n=102) is divisible into two main chemical groups according to silica content:
430 i.e., mafic/intermediate (<57 wt. % SiO_2), and felsic (>70 wt. % SiO_2). All of the
431 glass samples have moderate Na_2O+K_2O contents (2.3-8.1 wt. %), typical of
432 the subalkaline/tholeiitic series (Fig. 9). Glass from the Lempa (no. 4.2),
433 Paleomylon (no. 18.5) and Sarama-Lasa (no. 2164) areas is felsic. Glass from
434 the Kannaviou area (nos. 19.1, 21.1, 21.2, 23A.1) is largely felsic (91%), rarely

435 trending towards intermediate/mafic (9%). Glass from the Akamas area (no.
436 1074) is bimodal, mostly mafic (88%) and to a lesser extent felsic (12%).

437 Oxides such as TiO_2, Al_2O_3, CaO and FeO are tightly grouped and exhibit
438 positive correlations with MgO (see Supplementary material). MgO contents
439 cluster around 0-1 wt. % and 4-6 wt. %. FeO exhibits a wide range (0.6-13.7
440 wt. %), as does CaO (0.7-10.9 wt. %). Al_2O_3 content is relatively high (c. 10.1-
441 19.5 wt. %), whereas TiO_2 is typically low (0.1-1.6 wt. %). Na_2O, K_2O and P_2O_5
442 are scattered.

443 The trace-element composition of the glass was also plotted on a normal
444 mid-ocean ridge basalt (N-MORB)-normalised multi-element spider diagram
445 (Fig. 10). Glass from near Kannaviou (nos. 14-11, 14-14) and from south of
446 Lapithiou (nos. 16-20, 16-22) is compositionally similar, characterised by
447 relative enrichment in Ba and Th (10-200×N-MORB), and also in Ta, Nb and
448 La (1-10×N-MORB). Concentrations of Zr and Sm lie nearly parallel to N-MORB.
449 Ti and Y are relatively depleted at 0.05-1×N-MORB concentrations.

450 4.3.2. Feldspar

451 Eighty-one feldspar grains were analysed from samples from five different
452 localities (Table 1) (Fig. 11a). All of the feldspar grains have low orthoclase
453 contents (<4.8%). Feldspar from the Akamas area (no. 1074; n=9) shows a
454 wide range in anorthite content (55-91%; labradorite-bytownite to anorthite),
455 whereas feldspar grains from the Kannaviou area (nos. 19.1, 21.1, 21.2, 23A.1;
456 n=37) are more variable (40-95%; andesine-anorthite). A bimodal distribution
457 of feldspar compositions exists in samples from the Lempa (no. 4.2; n=10),

458 Paleomylon (no. 18.5; n=12) and Sarama-Lasa (no. 2164; n=13) areas, with
459 anorthite contents of mainly 30-50% (andesine) and 70-90% (bytownite).

460 4.3.3. Clinopyroxene

461 Forty-two clinopyroxene grains were analysed from the Kannaviou (nos. 19.1,
462 21.1, 21.2, 23A.1; n=24), Lempa (no. 4.2; n=8) and Paleomylon (no. 18.5; n=10)
463 areas. Clinopyroxene grains show relatively uniform compositional proportions
464 and are mainly augite (Morimoto, 1988) with one exception from the Lempa
465 area (Fig. 11b).

466 4.3.4. Amphibole

467 Eight grains of amphibole from the Kannaviou (nos. 19.1, 21.1, 23A.1), Lempa
468 (no. 4.2) and Paleomylon (no. 18.5) areas have relatively uniform
469 magnesiohornblende compositions (Leake et al., 1997) (Fig. 11c).

470 4.4. Zircon U-Pb dating

471 Zircon grains are generally sparse and commonly poorly preserved. Most are
472 euhedral and 50-100 μm long (Fig. 12). The crystals display variable internal
473 structures including magmatic oscillatory zoning (zircon 1), inherited
474 (xenocrystic) cores (zircon 5) and metamict structures (zircon 8). The zircon
475 grains have high Th/U ratios (0.18-1.47), suggestive of a magmatic origin
476 (Rubatto, 2002). The 18 analysed zircon grains have concordance levels
477 ranging from 99-106%. The calculated $^{206}Pb/^{238}U$ age with the generally lowest
478 possible error was used for age determination.

479 Zircon grains from the Armou area (no. 14-4; n=6) have a dominant age
480 population of 81.9-85.7 Ma (n=5) (Fig. 13a), together with one grain of 578.9
481 Ma (zircon 6). Zircon grains from sandstones near Kannaviou village (nos. 14-

12, 14-14; n=12) have a significant zircon population of 78.1-83.6 Ma (n=11) (Fig. 13b). One grain was dated at 560.8 Ma (zircon 12). The only concordant or near concordant data (99-102%) within the dominant (relatively young) age distribution are represented by magmatic-textured euhedral zircon grains (nos. 4, 7, 9, 10, 13, 14, 16, 17) (Fig. 13c). These analyses yield a mean weighted mean $^{206}Pb/^{238}U$ age of 80.1±1.1 Ma (MSWD=1.7) (Fig. 13d), which is assumed to be the maximum age of the sandstone deposition, and also the probable age of the volcanic source.

Some of the zircon age data were excluded from the weighted age for the following reasons: The older zircon grains (nos. 6, 12) are rounded with a patchy xenocrystic texture that is suggestive of recycled origin (Fig. 12). Five zircon grains (nos. 1, 3, 8, 15, 18) show slightly reverse discordance, possibly due to slight loss of U and/or variable excess radiogenic Pb (e.g., Söderlund et al., 2010). Zircon grains 2 and 11 have relatively high common ^{204}Pb at 2.9 and 3.5 ppb, respectively. Zircon grain 5 that has an inherited core with a slightly older age (85.7 Ma) and zircon 7 with a relatively old age (83.6 Ma) were also excluded.

4.5. Whole-rock geochemistry

4.5.1. Major-element variation

The Kannaviou Formation sandstones show a wide compositional range (SiO_2 contents of 32-63 wt. %) (Fig. 14), characterised by low TiO_2 (<0.7 wt. %), Na_2O (0.9-2.9 wt. %), K_2O (0.4-1.8 wt. %) and Fe_2O_3 (2.8-5.4 wt. %). Al_2O_3 values are relatively high (typically 11-18 wt. %), as are CaO (5.0-26.6 wt. %) (see Supplementary material). Loss on ignition values are high (3-22 wt. %), as

506 expected given the common carbonate cement. As a result, we focus on trace
507 element contents and inter-element ratios.

508 4.5.2. Trace-element variation

509 Selected trace element concentrations for the Kannaviou Formation
510 sandstones are shown in multi-element diagrams (Fig. 15), normalised to upper
511 continental crust (UCC). Patterns of sandstones from Armou, Lempa, Sarama-
512 Lasa and south of Lapithiou are similar. Their trace element concentrations are
513 well below UCC with the exceptions of Y, Tm and Yb. The Armou, Sarama-
514 Lasa and south of Lapithiou area sandstones are mainly highly depleted in Th,
515 U, Nb and La, whereas the Lempa samples (nos. 4.1, 4.2) are relatively
516 enriched in these elements (with a more restricted range). In addition, one
517 sample (no. 21.1) from the Kannaviou area is characterised by positive
518 anomalies of Th, U, La and Ce but pronounced depletions in Ba and Sr,
519 whereas others (e.g., nos. 14-12, 19.1, 23A.1) are similar to Lempa (no. 4.2) or
520 Sarama-Lasa (no. 16-39). In contrast, the Paleomylon River area sandstones
521 are highly depleted in all trace elements, with pronounced positive anomalies
522 of Sr and wide ranges of U, K, Nb and La. However, Sr and probably also Y
523 (no. 16-04) are slightly enriched. A sample from near Ezousa River (no. 16-30)
524 is strongly depleted in U and has moderate negative anomalies of Ba, Sr and
525 Zr.

526 Positive anomalies generally exist compared to UCC, especially for Sr, Ba
527 and probably also for K, controlled by feldspar and/or K-bearing clay mineral
528 content (e.g., illite, mica) (Nesbitt et al., 1980; McLennan et al., 1983; Feng and
529 Kerrich, 1990). In contrast, negative anomalies of Zr, Hf, Th and U can be
530 explained by a reduced detrital heavy mineral fraction (Taylor and McLennan,

1985) and/or relatively mafic provenance (Bauluz et al., 2000). The generally positive anomalies of Y and probably also of P, especially from the Sarama-Lasa area samples (nos. 16-33, 16-34), imply weathering enrichment of Y related to phosphatic clay and/or a detrital heavy minerals (Wronkiewicz and Condie, 1987).

4.5.3. Rare earth element variation

Chondrite-normalised rare earth element (REE) patterns of selected sandstones from the Kannaviou Formation and reference data from UCC (Rudnick and Gao, 2003; Hu and Gao, 2008) and deep-sea sands from various settings (McLennan et al., 1990) are shown in Figure 16. Sandstones from the Kannaviou area (nos. 14-11, 14-12, 14-14) show moderately fractionated REE patterns with $(La/Yb)_N$=1.83-3.93 and $(Gd/Yb)_N$=0.99-1.16, generally negative Eu anomalies (0.73-1.0) and relatively low total REE contents (45.1-67.9 ppm). Sandstones from the Paleomylon River area (nos. 16-04, 16-13, 16-14) are comparatively enriched in LREE, have negative Eu anomalies (0.81-0.83) and flatten out towards HREEs. Sandstone from Sarama-Lasa (no. 16-34) has a fractionated REE pattern with a moderate $(La/Yb)_N$=2.01, a negative Eu anomaly (0.71) and relative HREE enrichment. Sandstones from south of Lapithiou (nos. 16-22, 16-23, 16-29) are similar to the Kannaviou area, but with considerably more pronounced REE fractionation and lower HREE concentrations. In contrast, the reference data (McLennan et al., 1990) show much less variation. In general, the average Kannaviou Formation sandstone parallels average forearc basin sand composition.

555 # 5. Discussion

556 ## 5.1. Local geological influences

557 The thickness and facies variation of the sandstone, especially in the lower part
558 of the Kannaviou Formation, were strongly influenced by the contemporaneous
559 sea-floor topography. The northeasterly limit of the Kannaviou Formation
560 coincides with the tectonically controlled relief that was created by the westward
561 extension of the c. east-west-trending South Troodos Transform Fault
562 (Robertson, 1977a) (Fig. 17). The transform fault zone formed a bathymetric
563 depression with a strongly rising fault-controlled topography to the north and
564 northeast of the type area around Kannaviou. Fault scarp-derived (epiclastic)
565 lava breccia and relatively coarse-grained, thick-bedded sandstone and minor
566 conglomerate accumulated near the northern limit of the transform, as seen in
567 the Paleomylon River valley (Fig. 4b). After its accumulation during the
568 Campanian (c. 80 Ma) the Kannaviou Formation was affected by north to
569 northeast-directed compression in its type area around Kannaviou. The
570 compression relates to docking of the relatively allochthonous Triassic-
571 Cretaceous continental margin and oceanic rocks of the Mamonia Complex
572 (Robertson and Woodcock, 1979; Malpas et al., 1992; Bailey et al., 2000) (Fig.
573 4d). During the Paleogene, the Kannaviou Formation was covered by the
574 pelagic chalks of the Lefkara Formation (Figs. 3, 4e). The formation was later
575 transected by c. northwest-southeast-trending steep extensional faults related
576 to the Polis graben during late Miocene-Pliocene (Payne and Robertson, 1995,
577 2000; Balmer et al., 2019) (see Supplementary material). The present-day
578 exposure is locally influenced by landsliding, triggered by the Pleistocene uplift
579 of Cyprus and related earthquakes (Mercier et al., 1973; Robertson, 1977c;

580 Poole and Robertson, 1998; Morag et al., 2016). It was necessary to take
581 account of all of these features to understand the primary deposition of the
582 volcaniclastic sediments.

583 5.2. Deposition of the volcaniclastic sandstone

584 The non-calcareous claystone and radiolarian mudstone in the lower part of the
585 succession (e.g., Fig. 4a-b) accumulated relatively slowly, near or beneath the
586 carbonate compensation depth (CCD) based mainly on the carbonate and
587 microfossil content of the interbedded fine-grained sediments (Robertson,
588 1977a). The near-basal matrix-supported basaltic clasts and occasional
589 lenticular, amalgamated sandstone packages with composite bedding (Figs. 4b,
590 5b) are indicative of relatively rapid, channelised emplacement by mass flows.
591 The petrographic evidence of basaltic epiclasts near the base of the succession
592 (no. 18.5) (Fig. 4b), partially degraded hyaloclastite (Gilbert and Robertson,
593 2013), and the high abundance of fine-grained matrix (see Supplementary
594 material), indicate derivation from the adjacent, then submerged Troodos
595 ophiolite.

596 Upwards, the increased occurrence of calcareous claystone, mudstone
597 and volcaniclastic sandstone, with local evidence of convolute lamination,
598 record relatively high sedimentation rates and common tectonic instability (see
599 Section 4.1.2) (e.g., Figs. 4h, 5e). Sporadic, indistinct planar and low-angle
600 cross-lamination are indicative of subordinate turbidity current deposition in
601 parts of the succession (Robertson, 1977a) (Fig. 4a). The relatively coarse
602 grain size, the increase in subhedral feldspar grains, and the occurrence of
603 subangular chert and mica-schist grains (see Section 4.2.1), together suggest
604 that source lithologies were being rapidly degraded and reworked.

605 The relatively thick (up to 20 m thick by c. 300 m long), lenticular
606 volcaniclastic sandstones, locally rich in mud rip-up clasts (see Section 4.1.2)
607 are indicative of rapid, pulsed, channelised accumulation (Robertson, 1977a),
608 similar to that reported from comparable sediments elsewhere (e.g., Nishimura
609 et al., 1991). The appearance of locally abundant although fragmentary plant
610 material indicates input from land (see Section 4.1.2). The upward presence of
611 calcareous mudstone interbeds (e.g., Fig. 4e-g, i-j) with calcareous microfossils
612 indicates a change to deposition above the CCD.

613 The vast amount of vesicular pyroclastic material (Fig. 7) is interpreted to
614 have originated from explosive volcanic eruptions (Robertson, 1977a; Gilbert
615 and Robertson, 2013), similar to many volcaniclastic deposits elsewhere
616 (Schindlbeck et al., 2013; Kutterolf et al., 2014). Excellent examples were
617 recently documented from the northwest Pacific region (Busby et al., 2017;
618 Kutterolf et al., 2018; Robertson et al., 2018). The restriction of the pyroclastic
619 material to sand-sized or smaller (see Section 4.2.2) points to initial explosive
620 eruption, followed by dominantly aeolian ash transport. The eruptions are likely
621 to have been subaerial but could also have been in shallow water (< c. 300 m)
622 where hydrostatic pressure was insufficient to prevent explosive release of ash
623 into the atmosphere. Such phreatic eruptions are for example known from the
624 1965 eruption of Taal Volcano, Philippines (Moore et al., 1966), and the 1975-
625 1977 activity of La Soufrière de Guadeloupe (Lesser Antilles) (Boichu et al.,
626 2011). After initial ash fallout, and probable local current reworking, the
627 volcaniclastic sediment represented by the Kannaviou Formation was carried
628 downslope by mass flows in submarine channels, individually up to 25 m deep
629 by up to 300 m wide (Figs. 4b, 5f). Sequences of repeated turbidites are not

developed in contrast to many deep-sea successions in modern and ancient forearc basins (Dickinson, 1995; Pickering and Hiscott, 2016). Also, undisturbed primary ash fallout deposits are effectively absent. The lack of conglomeratic or pyroclastic debris-flows deposits within the Kannaviou Formation hints at long-distance aeolian transport that left such coarse-grained material behind. Alternatively, a topographic barrier (e.g., ocean floor fault zone) (Fig. 17) could have isolated the depositional area from coarser-grained supply. The dominance of thick, channelised mass-flow (Fig. 4), relative to classical turbidites points, points to relatively proximal deposition in an upper to mid-fan setting (Howell and Normark, 1982). It is therefore unlikely that the sands were transported very long distances (hundreds to thousands of km) by axial flow as in some modern trench settings, such as the Peru-Chile trench (Schweller et al., 1981) or the Aleutian trench (Piper et al., 1973). However, initial long-distance sediment transport by wind and currents is not precluded, as discussed further below.

5.3. Factors affecting sandstone composition

5.3.1. Alteration of mineral and glass grains

In thin section, calcium is relatively abundant in the form of foraminifera, calcite spar (cement), clay minerals and feldspar (up to 14.5 modal %). Relatively high values of CaO, together with positive correlations of CaO and loss on ignition (LOI) values, are consistent with the carbonate content (Fig. 18a). Dissolved feldspar grains are relatively common. Some detrital pyroxene grains show superficial alteration to chlorite. In places, secondary porosity including small late-stage cracks is infilled by clay minerals or calcite spar. Only rarely are glass

654 shards partly devitrified, in which case they typically have thin clay or carbonate
655 cement coatings.

656 The relatively unaltered nature of the glass (c. 86% of the grains) is
657 supported by the analytical totals of typically >92 wt. % (see Supplementary
658 material). A few glass grains, mainly from Sarama (no. 2164), gave totals of 89-
659 91 wt. %. The typically high average totals of c. 95 wt. % are similar to those
660 reported from a range of Pleistocene deep-sea sediments, including tephra
661 from the Mediterranean Sea (90-99 wt. %) (Clift and Blusztajn, 1999), Central
662 America (c. 93 wt. %) (Kutterolf et al., 2008a, b), New Zealand (92-99 wt. %)
663 (Lowe et al., 2008) and also Neogene tephra from the northwest Pacific (90-
664 100 wt. %) (Bryant et al., 2003; Kutterolf et al., 2018). A possible explanation of
665 the relatively unaltered nature of the Kannaviou Formation sandstones,
666 especially the volcanic glass, is because of the protective effects of diagenetic
667 carbonate cement (e.g., Ulmer-Scholle et al., 2015).

668 A few glass grains (especially two from the Kannaviou area) have
669 unusually low analytical totals (89-90 wt. %) and high silica contents (61-71
670 wt. %); this could have several explanations: (1) loss of Na and K during
671 analysis (Nielsen and Sigurdsson, 1981; Clift and Fitton, 1998); (2) relatively
672 high eruptive volatile contents, following crystal fractionation (Burnham and
673 Jahns, 1962); and (3) secondary hydration (Clift and Dixon, 1994). The majority
674 of the glass grains have high silica contents similar, for example, to
675 Mediterranean tephra (Clift and Blusztajn, 1999). The relationship between
676 measured volatile-loss (100%-Total) and silica content (Clift and Dixon, 1994)
677 (Fig. 18b) suggests that little secondary hydration of the Kannaviou Formation
678 glass has generally taken place.

679 5.3.2. Grain-size, weathering, sorting and recycling

680 Several factors can affect sandstone chemical composition, including grain-size
681 variation, weathering, sorting and recycling (e.g., Wronkiewicz and Condie,
682 1987; Cullers, 1995). Some elemental concentrations and ratios can be
683 selectively affected by grain-size variation. However, MnO, CaO, K_2O and Sr
684 concentrations, and also La/Co, Th/Co, La/Ni and Th/Cr ratios are normally not
685 much affected (Cullers, 1995). Finer-grained fractions typically comprise
686 relatively homogeneous detritus and therefore generally have relatively
687 consistent elemental concentrations and ratios (Cullers, 1995, 2000). These
688 fractions are typically characterised by relatively high Al_2O_3, Fe_2O_3, MgO, TiO_2,
689 Th, Sc, Nb, Y and REE, low SiO_2, Na_2O and Ba, and relatively low Eu/Eu*,
690 La/Sc and Th/Sc (Taylor and McLennan, 1985; Cullers, 1995). In the Kannaviou
691 Formation sandstones Na_2O (correlation coefficient r=0.83), TiO_2 (r=0.67), Sc
692 (r=0.68), Be (r=0.61), Ga (r=0.92), Hf (r=0.70), V (r=0.47), Zr (r=0.48), Eu
693 (r=0.90) and HREE (r=0.4-0.6) all correlate with Al_2O_3 (see Supplementary
694 material), which suggests a clay mineral influence (e.g., clayey matrix, illite,
695 kaolinite) on chemical composition (e.g., Roser and Korsch, 1986; Feng and
696 Kerrich, 1990). To overcome these effects, trace element ratios, namely La/Co,
697 Th/Co, Th/Cr, Eu/Eu*, La/Sc, Th/Sc, Zr/Sc and La/Th were used to characterise
698 provenance and tectonic setting (Taylor and McLennan, 1985; Bhatia and
699 Crook, 1986; Condie and Wronkiewicz, 1990; Cullers, 1995, 2000). However,
700 caution is required because some plots (e.g., La-Th-Sc, Th-Sc-Zr) can be
701 influenced by local sorting, and by mafic/heavy mineral variation (Bhatia and
702 Crook, 1986; Floyd et al., 1991).

703 Th/U ratios can indicate source area weathering and sedimentary recycling
704 (e.g., Taylor and McLennan, 1985; McLennan et al., 1993). The majority of the
705 Kannaviou Formation sandstones have Th/U ratios of 1.83-4.0, generally
706 similar to active margin-derived turbidites (McLennan et al., 1990). The low
707 values suggest derivation from little weathered magmatic arc-related source
708 rocks (McLennan et al., 1993). In contrast, relatively elevated Th/U ratios (5-28)
709 in some samples (nos. 16-16, 16-20, 16-25, 16-39, 21.1) point to enhanced
710 subaerial weathering.

711 The absence of significant zircon enrichment (37-99 ppm) precludes
712 marked sediment recycling or sorting effects (McLennan et al., 1993). The
713 depositional age from microfossils (Campanian-early Maastrichtian; 84-72 Ma)
714 (Urquhart and Banner, 1994; Bragina and Bragin, 1995) is broadly coeval with
715 the related volcanism as indicated by zircon geochronology (c. 80 Ma). This
716 evidence rules out chemical differentiation resulting from long-term
717 sedimentary recycling.

718 5.4. Source rock characteristics

719 5.4.1. Petrographic constraints

720 The QFL diagram (Fig. 8b) illustrates entire grain populations and emphasises
721 grain stability, weathering, transport mechanisms and source rocks. All of the
722 samples plot near the lithic apex with the main contribution being from volcanic
723 glass, consistent with a magmatic arc source (e.g., Dickinson et al., 1983).
724 Sandstones from south of Episkopi (no. 14.5) and near Sarama-Lasa (nos.
725 2141, 2156) cluster towards the recycled field, with relatively high quartz
726 abundances (especially polycrystalline quartz at 2-3 modal %). These clastic
727 materials were probably supplied from petrographically similar quartzose

sandstones in the adjacent Mamonia Complex, especially those of late Triassic age (Robertson, 1977a). The mean composition of the Kannaviou Formation plots in the area of overlapping fields (Fig. 8d) in the LmLvLs diagram is explained by the high volcanic glass content (15-47 modal %). Despite this, the relatively high average quartz content (QFL%Q=12) in the Kannaviou Formation sandstones supports input from a continental margin arc (Marsaglia and Ingersoll, 1992; Marsaglia et al., 2016).

5.4.2. Constraints from glass composition

The volcanic glass has relatively low abundances of Na_2O (1.9-4.4 wt. %), K_2O (0.2-4.6 wt. %), TiO_2 (0.1-1.6 wt. %) and P_2O_5 (<0.2 wt. %), typical of incipient subduction-related volcanism (Woodhead et al., 1993; Straub, 2003). Enrichment in Ba and Th, together with depletion in Ti and Nb, support an arc origin (e.g., Pearce, 1983). The glass compositions plot close to the tholeiitic trend on the ternary Na_2O+K_2O-FeO-MgO (AFM) diagram (Fig. 19a). The trend towards the alkaline apex likely represents arc magmatic maturity (Kuno, 1966; Geringer et al., 1986), and is consistent with differentiation of a single parental basaltic magma (Gilbert and Robertson, 2013).

Volcanic glass composition is critical to evaluate continental versus oceanic sediment provenance (Bryant et al., 2003; Kutterolf et al., 2014). Elevated U/Th, Ba/La and Sm/La ratios indicate pelagic sediment and/or fluid influence on magmatic composition (Patino et al., 2000; Straub and Layne, 2003; Plank, 2005; Carr et al., 2007). Elevated ratios of Th/La, Rb/Hf and Th/Nb suggest continental crust and/or subducted terrigenous sediment influence (Hannah et al., 2002; Bryant et al., 2003; Stern et al., 2003). The relatively elevated Th/Nb and Th/La ratios in the Kannaviou Formation glass (Fig. 19b-c)

753 therefore support the involvement of continental crust and/or subducted
754 terrigenous sediment in magma genesis.

755 5.4.3. Constraints from mineral analysis

756 The dominance of augite, with one rare diopside (Fig. 11b), suggests a mafic
757 igneous source (Deer et al., 2013). The clinopyroxene compositions, as shown
758 in the ternary TiO_2-MnO-Na_2O discriminant plot (after Nisbet and Pearce, 1977)
759 (Fig. 19d), indicate a volcanic arc affinity for all of the grains analysed. In
760 addition, the two Ediacaran zircon grains (560 and 578 Ma) originated from
761 older continental crust. The Triassic-Cretaceous sedimentary succession of the
762 adjacent Mamonia Complex is a likely source for the grains of these ages based
763 on detrital zircon geochronology (Chen, 2018).

764 5.4.4. Constraints from whole-rock geochemistry

765 The relatively uniform ratios of La/Co, Th/Co and Th/Cr, together with La/Sc
766 and Th/Sc in the Kananviou Formation sandstones, are consistent with
767 derivation from predominantly mafic source rocks, with a subordinate variable
768 input from felsic rocks (Cullers, 1995, 2000) (Table 3). Sandstones with unusual
769 La/Sc or Th/Sc represent locally increased detrital felsic input (e.g., feldspar,
770 muscovite) or reduced mafic contribution (Taylor and McLennan, 1985; Condie
771 and Wronkiewicz, 1990; Cullers, 2000). Th/Sc vs. Zr/Sc and La/Th vs. Hf
772 diagrams indicate similar compositional variations (Fig. 20a-b).

773 Moderately fractionated REE patterns, low ΣREE abundances (45-79 ppm)
774 and low $(La/Yb)_N$ (1.8-6.2), together indicate dominant derivation from mafic to
775 intermediate-composition rocks. Slight HREE enrichment in one sample (no.
776 16-34) from directly beneath the Kathikas Formation in the Sarama-Lasa area
777 (Fig. 4f) probably resulted from heavy mineral enrichment (e.g., zircon) and/or

778 input of relatively degraded fine-grained material (Taylor and McLennan, 1985),
779 both of which could have been derived from the Mamonia Complex. Negative
780 Eu anomalies of 0.71-1.00 are slightly higher than those in craton-derived post-
781 Archean Australia Shale (PAAS) (0.66; Taylor and McLennan, 1985) and UCC
782 (0.70; Rudnick and Gao, 2003). These ratios are comparable to those of
783 sandstones derived from mafic sources (0.71-0.95; Cullers, 2000) and/or
784 magmatic arcs (0.79-1.04; Bhatia, 1985) associated with active margin settings
785 (McLennan et al., 1990). Overall, the linear array of sandstone data (Fig. 20c)
786 is consistent with a mixture of compositionally variable young arc-derived
787 material and upper crust-sourced material (e.g., McLennan and Taylor, 1984)
788 that was probably derived from the adjacent Mamonia Complex.

789 5.5. Provenance

790 The trace element ratios of the volcanic glass, coupled with the presence of
791 some terrigenous sediment, support a continental arc affinity (Fig. 19b-c).
792 Despite this, the trace-element ratios of the sandstones generally fingerprint an
793 oceanic island arc setting. Specifically, the ratios of La/Sc (0.58±0.18), Th/Sc
794 (0.17±0.06) and La/Th (4.08±0.77) are generally comparable to those of
795 sandstones derived from an oceanic island arc setting (0.55±0.22, 0.15±0.08,
796 4.26±1.2). However, several ratios (e.g., Eu/Eu*) suggest a continental
797 contribution. The scattering towards the continental island arc field is consistent
798 with locally reduced mafic contribution or increased felsic input (Bhatia and
799 Crook, 1986; Cullers, 1995, 2000; Cullers and Podkovyrov, 2000). On the
800 ternary Th-Sc-Zr diagram (Bhatia and Crook, 1986) (Fig. 21a) all of the
801 sandstones plot in or near the oceanic island arc field.

802 The average Kannaviou Formation sandstone has negative Nb-Ta
803 anomalies compared to the UCC-normalised multi-element patterns of average
804 greywacke from several different tectonic environments (Floyd et al., 1991) (Fig.
805 21b). The negative anomalies are comparable to those of oceanic island arc-
806 sourced greywackes, suggestive of sediment sources involving subduction-
807 related magmatic rocks (Floyd et al., 1991). The variable enrichments in V-Cr-
808 Ni-Sc and the slightly positive Ti anomalies are also consistent with arc
809 provenance (either continental or oceanic). In addition, the pronounced
810 depletion in Zr and Hf precludes significant enrichment in heavy minerals (e.g.,
811 zircon). The patterns are generally consistent with a source composed
812 predominantly of subduction-related rocks of oceanic island arc affinity, plus a
813 minor continental input (McLennan et al., 1990, 1993; Floyd et al., 1991).

814

815 5.6. Tectonic-magmatic setting

816 5.6.1. Continental arc magmatism on thinned, depleted continental crust?

817 The most likely explanation of the apparent discrepancy between the
818 continental margin arc setting inferred from the glass trace element chemistry
819 and the mainly oceanic arc origin suggested by the trace and REE data is that
820 the arc magmas represented by the Kannaviou Formation were not extracted
821 from fertile asthenosphere above normal-thickness continental crust. Arc-type
822 signatures could instead result if magma was extracted from crust that was
823 relatively thin and/or depleted by previous melt extraction (Fitton et al., 1997;
824 Condie, 2003). In the case of the Kannaviou Formation, both of these situations
825 are likely to have occurred because the region was affected by Triassic rift-
826 related magmatism to form the Southern Neotethys. Early spreading of this

827 ocean basin is represented by the late Triassic MORB (Dhiarizos Group) of the
828 Mamonia Complex (Robertson and Woodcock, 1979; Malpas et al., 1992, 1993;
829 Chan et al., 2008). Active continental margins in several other regions are
830 known to have relatively primitive oceanic arc-type signatures, as indicated by
831 the chemistry of derived volcaniclastic sediments and related tuffaceous
832 deposits, for example the Brook Street Terrane in southern New Zealand
833 (Robertson et al., in press).

834 5.6.2. Arc-volcaniclastic sediment comparisons

835 Despite their inferred continental margin arc provenance, as mainly inferred
836 from the glass composition, the Kannaviou Formation sandstones accumulated
837 on oceanic crust. Examples of volcanic arc-sourced successions overlying
838 oceanic crust are well represented in the southwest and north Pacific regions
839 (e.g., Horn et al., 1969; Marsaglia, 1992; Clift et al., 1998; Kutterolf et al., 2018;
840 Robertson et al., 2018). Ancient examples of oceanic arc-derived volcaniclastic
841 sediments that accumulated on oceanic crust include the late Cretaceous
842 Nindam Formation in northwest India (Robertson and Degnan, 1994; Clift et al.,
843 2000, 2002), the Jurassic Talkeetna Volcanic Formation in Alaska (Plafker et
844 al., 1989; Clift et al., 2005; Greene et al., 2006), the Permian Takitimu Group in
845 southern New Zealand (Houghton and Landis, 1989; Spandler et al., 2005;
846 Robertson and Palamakumbura, in press; Robertson et al., in press), the
847 Jurassic Gran Cañon Formation (Critelli et al., 2002; Busby, 2004) and the
848 Cretaceous Alisitos Group (Busby et al., 2006; Marsaglia et al., 2016) in Mexico.
849 In addition, there are many instances of arc-derived successions overlying
850 continental crust (Dickinson, 1995), to name one well-documented example,

851 the late Cenozoic Central American Volcanic Arc (Carr, 1984; Kutterolf et al.,
852 2008a, b; Schindlbeck et al., 2016).

853 A key requirement for the genesis of the Kannaviou Formation sandstones
854 is for supra-subduction zone oceanic lithosphere, represented by the Troodos
855 ophiolite, to collide with an adjacent continental margin arc, following
856 subduction of intervening Neotethyan oceanic crust. The tectonic-magmatic
857 setting of the Kannaviou Formation can be broadly compared to the intersection
858 of the Mariana-Bonin forearc (counterpart of the Troodos ophiolite) with the
859 Japanese continental island arc, as exposed in the Miura and Boso Peninsulas
860 (Ogawa et al., 1985, 2008). However, no exact counterpart is known elsewhere
861 for the complex microplate setting of Cyprus during the latest Cretaceous.

862 5.6.3. Implications for late Cretaceous arc magmatism in the eastern
863 Mediterranean

864 The previously suggested source (Robertson, 1977a; Gilbert and Robertson,
865 2013) of the Kannaviou Formation is the Fourkovouno (Selvilitepe) Formation
866 of the Kyrenia Range. This is characterised by a c. 400 m thick late Cretaceous
867 subduction-related volcanogenic succession that encompasses felsic
868 tuffaceous rocks, felsic debris-flow deposits and rhyolitic lava flows (Moore,
869 1960; Poisson, 1977; Baroz, 1979, 1980; Robertson and Woodcock, 1986;
870 Huang et al., 2007; Robertson et al., 2012; Chen, 2018). However, there are
871 differences between the Kannaviou Formation source volcanism and that of the
872 Kyrenia Range continental margin arc magmatism: (1) the Kannaviou
873 Formation sandstones were derived from an incipient continental margin arc,
874 whereas the Kyrenia Range volcanic rocks represent a more evolved Andean-
875 type active continental margin; and (2) the Kannaviou Formation volcanism is

significantly older (80.1±1.1 Ma) than that of the Kyrenia Range ($^{206}Pb/^{238}U$ age of 72.9±1.0 Ma) (Chen, 2018). A possible explanation for these differences is that older, immature arc volcanism originally existed in the Kyrenia Range area but has been concealed by subsequent subduction and/or continental collision, consistent with the evidence of southward thrusting during the Middle Eocene and Late Miocene-earliest Pliocene (Baroz, 1979; Robertson et al., 2012, 2014; McCay and Robertson, 2013; Robertson and Kinnaird, 2016).

The northerly active continental margin of the Southern Neotethys, represented in north Cyprus by the Kyrenia Range (Robertson et al., 2012), extended eastwards through the Misis-Andırın lineament of southern Turkey into southeast Turkey (e.g., Robertson, 2002) (Fig. 1a). Late Cretaceous continental margin arc magmatism in southeast Turkey is also interpreted to relate to northward subduction of the Southern Neotethys beneath a northerly-located Tauride continental unit (e.g., Robertson, 2002; Parlak, 2006; Rızaoğlu et al., 2009; Robertson et al., 2006, 2007, 2012). There are two potential sources of felsic ash in southeast Turkey: (1) tholeiitic oceanic arc magmatism dated at 83-75 Ma (Aktaş and Robertson, 1984, 1990; Robertson et al., 2007; Karaoğlan et al., 2013); and (2) I-type, calc-alkaline Andean-type intrusive rocks, dated at 88-82 Ma (Santonian-Campanian) (Parlak, 2006; Robertson et al., 2006; Rızaoğlu et al., 2009; Karaoğlan et al., 2016). Unfortunately, any extrusive equivalents of the continental arc magmatism were eroded or are not exposed. Of the two occurrences of arc magmatism, based on the geochemical evidence, only the continental margin arc volcanism could be a source for the Kannaviou Formation volcanic ash, assuming long-distance transport by winds and/or currents. Prevailing easterly winds and currents have been modelled for

the late Cretaceous (e.g., Hay, 2011), such that a source well to the east of Cyprus should be considered.

5.6.4. Pyroclastic fallout dispersal efficiency

Pyroclastic fallout components such as glass shards, feldspar crystals, mafic crystals, lithic grains and pumice can be dispersed substantial distances by wind (Carey and Sigurdsson, 1982, 2000; Fisher and Schmincke, 1984; Pyle, 1989). In general, the dispersal distance is mainly controlled by a combination of grain size, prevailing wind strength and eruptive volume (i.e., column height) (Pyle, 1989; Carey, 1996). Relatively recent (<0.5 Ma) ash of grain size 32-500 µm that was derived from the continental margin Japan arc can be correlated with tuffaceous sediments of the oceanic Izu-Bonin forearc, up to 1000 km away (Kutterolf et al., 2018). Maximum grain size versus distance from source relationships are, for example, known for ash layers that were produced by the Toba eruption in Sumatra (75 ka; Ninkovich et al., 1978), the Campanian ignimbrite eruption in Italy (33 ka; Cornell et al., 1983) and the Minoan eruption of Santorini (1620 B.C.; Watkins et al., 1978). The maximum sizes of the feldspar/glass crystals and the mafic crystals (e.g., pyroxene) of the Kannaviou Formation sandstones are up to 1200 µm and c. 500 µm, respectively. Assuming the crystals were sourced from a common eruptive centre, these sizes are compatible with eruptions on the approximate scale of the Minoan eruption of Santorini (28 km^3; Watkins et al., 1978), with a likely distance of c. 100 km from the source arc (Fig. 22). This distance is significantly less than that of the known continental margin arc volcanism in southeast Turkey (c. 300 km). Also, to achieve the up to 750 m thickness of the Kannaviou Formation, repeated Santorini-scale eruptions would be needed over a relatively short time

926 period (c. 0.3 Ma), followed by channelised sediment transport of up to c. 300
927 km (e.g., Mason et al., 2004; Deligne et al., 2011). The volcaniclastic
928 sandstones are found only in western Cyprus and not overlying the Troodos
929 ophiolite as a whole, which points to a relatively local source, followed by
930 bathymetrically controlled (channelised) deposition. The most likely scenario is
931 that the Kannaviou Formation source eruptions were located close to the
932 Kyrenia Range but have since been concealed tectonically, as a result of the
933 crustal contraction that took place in response to subduction or collision.

934 5.6.5. Tectonic-magmatic model

935 Our proposed model (Fig. 23) builds on a previously proposed double
936 subduction scenario (e.g., Robertson, 2002; Parlak, 2006; Karaoğlan et al.,
937 2016), in which the Troodos ophiolite formed above an intra-oceanic subduction
938 zone (c. 90 Ma) (Mukasa and Ludden, 1987), and then moved northwards
939 related to subduction beneath Tauride microcontinent crust. Resulting early-
940 stage (incipient) continental margin arc volcanism supplied pyroclastic fallout
941 deposits to a deep-marine forearc basin to the south, coupled with gravity flow
942 reworking. In addition, terrigenous sediment, mostly siliciclastic and
943 recrystallised carbonate, was supplied from the adjacent continental margin,
944 represented by the Triassic-Cretaceous terrigenous-derived sedimentary rocks
945 of the Mamonia Complex (Robertson and Woodcock, 1979; Torley and
946 Robertson, 2018).

947

6. Conclusions

In this study we have used a combination field-based sedimentology and structural geology, optical petrography, whole-rock, glass and mineral chemistry, and also U-Pb zircon dating to infer that the late Cretaceous (80.1±1.0 Ma) arc volcanism of the Kannaviou Formation in western Cyprus was derived from an incipient continental margin arc. A similar integrated multi-technique approach has the potential to shed new light on a range of modern and ancient arc-related sediments elsewhere. The presence of terrigenous material within some of the volcaniclastic sandstones initially suggested a continental margin arc setting. The SIMS trace element analysis of relatively unaltered volcanic glass confirmed a continental influence. Despite this, several conventional trace element tectonic discriminant diagrams point to an oceanic arc source. The likely solution of this apparent discrepancy is that the continental margin arc was constructed on magmatically depleted lithosphere that was thinned during regional late Permian-early Jurassic rifting of the Southern Neotethys. Effective interpretation of comparable arc-derived volcaniclastic sandstones elsewhere therefore depends on a multi-technique approach, especially glass trace element analysis (where possible) and should not rely on interpretation of whole-rock chemical data alone.

Acknowledgements

We particularly thank Richard Hinton, Steffen Kutterolf and Dick Kroon for scientific discussion. Edinburgh University undergraduates helped transport the large volumes of rocks required for the U-Pb zircon dating back to Edinburgh. Linda Kirstein kindly advised on zircon separation and made laboratory

preparation facilities available for the U-Pb dating. Mike Hall is thanked for thin section preparation and polishing blocks for zircon analysis. Nick Odling kindly assisted with the XRF analysis. The first author gratefully acknowledges the receipt of a joint studentship of the Principal's Career Development PhD Scholarship and Edinburgh Global Research Scholarship. The authors are grateful for financial support from the Natural Environment Research Council-Ion Microprobe Facility (to A. H. F. Robertson) to carry out SIMS U-Pb dating of detrital zircon. Fieldwork and geochemical analysis were aided by financial support from the International Association of Sedimentologists [Postgraduate Grant Scheme], the Mineralogical Society of Great Britain and Ireland [Postgraduate Student Bursary Awards], and the Edinburgh Geological Society [Clough Fund]. Additional financial support for fieldwork was provided by the John Dixon Memorial Fund.

987 Reference

988 Aktaş, G., Robertson, A.H.F., 1984. The Maden Complex, SE Turkey: evolution
989 of a Neotethyan active margin. In: Dixon, J.E., Robertson, A.H.F. (Eds.),
990 The Geological Evolution of the Eastern Mediterranean. Geological
991 Society of London, Special Publications 17, pp. 375-402.

992 Aktaş, G., Robertson, A.H.F., 1990. Tectonic evolution of the Tethys suture
993 zone in SE Turkey: evidence from the petrology and geochemistry of
994 Late Cretaceous and Middle Eocene extrusives. In: Malpas, J., Moores,
995 E.M., Panayiotou, A., Xenophontos, C. (Eds.), Ophiolites-Oceanic
996 Crustal Analogues. Proceedings of the International Symposium
997 'Troodos 1987'. Geological Survey Department, Nicosia, Cyprus, pp.
998 311-329.

999 Bailey, W., Holdsworth, R., Swarbrick, R., 2000. Kinematic history of a
1000 reactivated oceanic suture: the Mamonia Complex Suture Zone, SW
1001 Cyprus. Journal of the Geological Society 157, 1107-1126.

1002 Balmer, E.M., Robertson, A.H.F., Raffi, I., Kroon, D., 2019. Pliocene–
1003 Pleistocene sedimentary development of the syntectonic Polis graben,
1004 NW Cyprus: evidence from facies analysis, nannofossil biochronology
1005 and strontium isotope dating. Geological Magazine 156, 889-917.

1006 Baroz, F., 1979. Etude géologique dans le Pentadaktylos et la Mesaoria
1007 (Chypre Septentrionale). Doctor of Science Thesis (published).
1008 Université de Nancy, France, 434 pp.

1009 Baroz, F., 1980. Volcanism and continent-island arc collision in the
1010 Pentadaktylos range, Cyprus. In: Panayiotou, A. (Ed.), Ophiolites:
1011 Proceedings of the International Ophiolite Symposium. Cyprus Ministry

1012 of Agriculture and Natural Resources, Geology Survey Department,
1013 Nicosia, Cyprus, pp. 73-85.
1014 Bauluz, B., Mayayo, M.J., Fernandez-Nieto, C., Lopez, J.M.G., 2000.
1015 Geochemistry of Precambrian and Paleozoic siliciclastic rocks from the
1016 Iberian Range (NE Spain): implications for source-area weathering,
1017 sorting, provenance, and tectonic setting. Chemical Geology 168, 135-
1018 150.
1019 Bhatia, M.R., 1985. Rare earth element geochemistry of Australian Paleozoic
1020 graywackes and mudrocks: provenance and tectonic control.
1021 Sedimentary Geology 45, 97-113.
1022 Bhatia, M.R., Crook, K.A., 1986. Trace element characteristics of graywackes
1023 and tectonic setting discrimination of sedimentary basins. Contributions
1024 to Mineralogy and Petrology 92, 181-193.
1025 Boichu, M., Villemant, B., Boudon, G., 2011. Degassing at La Soufrière de
1026 Guadeloupe volcano (Lesser Antilles) since the last eruptive crisis in
1027 1975–77: Result of a shallow magma intrusion? Journal of Volcanology
1028 and Geothermal Research 203, 102-112.
1029 Bragina, L.G., Bragin, N.Y., 1995. Radiolarians and stratigraphy of Campanian-
1030 Maestrichtian deposits of southwestern Cyprus. Stratigraphic and
1031 Geological Correlation 3, 147-155.
1032 Bryant, C., Arculus, R., Eggins, S., 2003. The geochemical evolution of the Izu-
1033 Bonin arc system: A perspective from tephras recovered by deep-sea
1034 drilling. Geochemistry, Geophysics, Geosystems 4, 1094,
1035 doi:10.1029/2002GC000427.

1036 Burnham, C.W., Jahns, R.H., 1962. A method for determining the solubility of
1037 water in silicate melts. American Journal of Science 260, 721-745.
1038 Busby, C., 2004. Continental growth at convergent margins facing large ocean
1039 basins: a case study from Mesozoic convergent-margin basins of Baja
1040 California, Mexico. Tectonophysics 392, 241-277.
1041 Busby, C., Adams, B.F., Mattinson, J., Deoreo, S., 2006. View of an intact
1042 oceanic arc, from surficial to mesozonal levels: Cretaceous Alisitos arc,
1043 Baja California. Journal of Volcanology and Geothermal Research 149,
1044 1-46.
1045 Busby, C.J., Tamura, Y., Blum, P., Guèrin, G., Andrews, G.D.M., Barker, A.K.,
1046 Berger, J.L.R., Bongiolo, E.M., Bordiga, M., DeBari, S.M., Gill, J.B.,
1047 Hamelin, C., Jia, J., John, E.H., Jonas, A.S., Jutzeler, M., Kars, M.A.C.,
1048 Kita, Z.A., Konrad, K., Mahony, S.H., Martini, M., Miyazaki, T., Musgrave,
1049 R.J., Nascimento, D.B., Nichols, A.R.L., Ribeiro, J.M., Sato, T.,
1050 Schindlbeck, J.C., Schmitt, A.K., Straub, S.M., Vautravers, M.J., Yang,
1051 Y., 2017. The missing half of the subduction factory: shipboard results
1052 from the Izu rear arc, IODP Expedition 350. International Geology
1053 Review 59, 1677-1708.
1054 Carey, S.N., 1996. Modeling of tephra fallout from explosive eruptions. In:
1055 Scarpa, R., Tilling, R. (Eds.), Monitoring and mitigation of volcano
1056 hazards. Springer, Berlin, pp. 429-461.
1057 Carey, S.N., Schneider, J.-L., 2011. Volcaniclastic processes and deposits in
1058 the deep-sea. In: Huneke, H., Mulder, T. (Eds.), Developments in
1059 Sedimentology 63. Elsevier, Amsterdam, pp. 457-515.

1060 Carey, S.N., Sigurdsson, H., 1982. Influence of particle aggregation on
1061 deposition of distal tephra from the May 18, 1980, eruption of Mount St.
1062 Helens volcano. Journal of Geophysical Research: Solid Earth 87, 7061-
1063 7072.
1064 Carey, S.N., Sigurdsson, H., 2000. Grain size of Miocene volcanic ash layers
1065 from Sites 998, 999, and 1000: Implications for source areas and
1066 dispersal. In: Leckie, R.M., Sigurdsson, H., Acton, G.D., Draper, G.
1067 (Eds.), Proceedings of the Ocean Drilling Program, Scientific Results
1068 165. Ocean Drilling Program, College Station, TX, pp. 101-113.
1069 Carr, M.J., 1984. Symmetrical and segmented variation of physical and
1070 geochemical characteristics of the Central American volcanic front.
1071 Journal of Volcanology and Geothermal Research 20, 231-252.
1072 Carr, M.J., Patino, L.C., Feigenson, M.D., 2007. Petrology and geochemistry of
1073 lavas. In: Jochen Bundschuh, G.E.A. (Ed.), Central America-geology,
1074 resources and hazards. A. A. Balkema, Rotterdam, Netherlands, pp.
1075 565-577.
1076 Chan, G.H.-N., Malpas, J., Xenophontos, C., Lo, C.-H., 2008. Magmatism
1077 associated with Gondwanaland rifting and Neo-Tethyan oceanic basin
1078 development: evidence from the Mamonia Complex, SW Cyprus.
1079 Journal of the Geological Society 165, 699-709.
1080 Chen, G., 2018. Provenance-related studies of Triassic-Miocene Tethyan
1081 sedimentary and igneous rocks from Cyprus. Unpublished PhD thesis.
1082 University of Edinburgh, UK, 484 pp.

1083 Clift, P.D., Blusztajn, J., 1999. The trace-element characteristics of Aegean and
1084 Aeolian volcanic arc marine tephra. Journal of Volcanology and
1085 Geothermal Research 92, 321-347.

1086 Clift, P.D., Degnan, P.J., Hannigan, R., Blusztajn, J., 2000. Sedimentary and
1087 geochemical evolution of the Dras forearc basin, Indus suture, Ladakh
1088 Himalaya, India. Geological Society of America Bulletin 112, 450-466.

1089 Clift, P.D., Dixon, J.E., 1994. Variations in arc volcanism and sedimentation
1090 related to rifting of the Lau Basin (southwest Pacific). In: Hawkins, J.W.,
1091 Parson, L.M., Allan, J.F., Resig, J., Weaver, P. (Eds.), Proceedings of
1092 the Ocean Drilling Program, Scientific Results 135. Ocean Drilling
1093 Program, College Station, TX, pp. 23-50.

1094 Clift, P.D., Draut, A.E., Kelemen, P.B., Blusztajn, J., Greene, A., 2005.
1095 Stratigraphic and geochemical evolution of an oceanic arc upper crustal
1096 section: The Jurassic Talkeetna Volcanic Formation, south-central
1097 Alaska. Geological Society of America Bulletin 117, 902-925.

1098 Clift, P.D., Fitton, J.G., 1998. Trace and rare earth element chemistry of
1099 volcanic ashes from sites 918 and 919: implications for Icelandic
1100 volcanism. In: Saunders, A.D., Larsen, H.C., Wise, S.H. (Eds.),
1101 Proceedings of the Ocean Drilling Program, Scientific Results 152.
1102 Ocean Drilling Program, College Station, TX, pp. 67-84.

1103 Clift, P.D., Hannigan, R., Blusztajn, J., Draut, A.E., 2002. Geochemical
1104 evolution of the Dras–Kohistan Arc during collision with Eurasia:
1105 evidence from the Ladakh Himalaya, India. Island Arc 11, 255-273.

1106 Clift, P.D., MacLeod, C.J., Tappin, D.R., Wright, D.J., Bloomer, S.H., 1998.
1107 Tectonic controls on sedimentation and diagenesis in the Tonga Trench

and forearc, southwest Pacific. Geological Society of America Bulletin 110, 483-496.

Clube, T.M.M., Creer, K., Robertson, A., 1985. Palaeorotation of the Troodos microplate, Cyprus. Nature 317, 522-525.

Clube, T.M.M., Robertson, A.H.F., 1986. The palaeorotation of the Troodos microplate, Cyprus, in the Late Mesozoic-Early Cenozoic plate tectonic framework of the Eastern Mediterranean. Survey in Geophysics 8, 375-437.

Condie, K.C., 1993. Chemical composition and evolution of the upper continental crust: contrasting results from surface samples and shales. Chemical Geology 104, 1-37.

Condie, K.C., 2003. Incompatible element ratios in oceanic basalts and komatiites: tracking deep mantle sources and continental growth rates with time. Geochemistry, Geophysics, Geosystems 4, 1005, doi:10.1029/2002GC000333.

Condie, K.C., Wronkiewicz, D., 1990. The Cr/Th ratio in Precambrian pelites from the Kaapvaal Craton as an index of craton evolution. Earth and Planetary Science Letters 97, 256-267.

Cornell, W., Carey, S., Sigurdsson, H., 1983. Computer simulation of transport and deposition of the Campanian Y-5 ash. Journal of Volcanology and Geothermal Research 17, 89-109.

Critelli, S., Marsaglia, K.M., Busby, C.J., 2002. Tectonic history of a Jurassic backarc-basin sequence (the Gran Cañon Formation, Cedros Island,

1131 Mexico), based on compositional modes of tuffaceous deposits.
1132 Geological Society of America Bulletin 114, 515-527.

1133 Cullers, R.L., 1995. The controls on the major-and trace-element evolution of
1134 shales, siltstones and sandstones of Ordovician to Tertiary age in the
1135 Wet Mountains region, Colorado, USA. Chemical Geology 123, 107-131.
1136 Cullers, R.L., 2000. The geochemistry of shales, siltstones and sandstones of
1137 Pennsylvanian–Permian age, Colorado, USA: implications for
1138 provenance and metamorphic studies. Lithos 51, 181-203.
1139 Cullers, R.L., Podkovyrov, V.N., 2000. Geochemistry of the Mesoproterozoic
1140 Lakhanda shales in southeastern Yakutia, Russia: implications for
1141 mineralogical and provenance control, and recycling. Precambrian
1142 Research 104, 77-93.
1143 Deer, W.A., Howie, R.A., Zussman, J., 2013. An introduction to the rock-forming
1144 minerals. Mineralogical Society, London, 494 pp.
1145 Deligne, N., Coles, S., Sparks, R., 2010. Recurrence rates of large explosive
1146 volcanic eruptions. Journal of Geophysical Research: Solid Earth 115,
1147 B06203, doi:10.1029/2009JB006554.
1148 Dickinson, W.R., 1995. Forearc Basins. In: Busby, C., Ingersoll, R. (Eds.),
1149 Tectonics of Sedimentary Basins. Blackwell Science, Oxford, pp. 221-
1150 262.
1151 Dickinson, W.R., Beard, L.S., Brakenridge, G.R., Erjavec, J.L., Ferguson, R.C.,
1152 Inman, K.F., Knepp, R.A., Lindberg, F.A., Ryberg, P.T., 1983.
1153 Provenance of North American Phanerozoic sandstones in relation to
1154 tectonic setting. Geological Society of America Bulletin 94, 222-235.

Dickinson, W.R., Suczek, C.A., 1979. Plate tectonics and sandstone compositions. American Association of Petroleum Geologists Bulletin 63, 2164-2182.

Feng, R., Kerrich, R., 1990. Geochemistry of fine-grained clastic sediments in the Archean Abitibi greenstone belt, Canada: implications for provenance and tectonic setting. Geochimica et Cosmochimica Acta 54, 1061-1081.

Fisher, R.V., Schmincke, H.-U., 1984. Pyroclastic rocks. Springer-Verlag, Berlin Heidelberg, 472 pp.

Fitton, J.G., Godard, M., 2004. Origin and evolution of magmas on the Ontong Java Plateau. In: Fitton, J.G., Mahoney, J.J., Wallace, P.J., Saunders, A.D. (Eds.), Origin and Evolution of the Ontong Java Plateau. Geological Society of London, Special Publications 229, pp. 151-178.

Fitton, J.G., Saunders, A., Larsen, L., Hardarson, B., Norry, M., 1998. Volcanic rocks from the southeast Greenland margin at 63°N: composition, petrogenesis and mantle sources. In: Saunders, A.D., Larsen, H.C., Wise, S.W., Jr. (Eds.), Proceedings of the Ocean Drilling Program, Scientific Results 152. Ocean Drilling Program, College Station, TX, pp. 331-350.

Fitton, J.G., Saunders, A.D., Norry, M.J., Hardarson, B.S., Taylor, R.N., 1997. Thermal and chemical structure of the Iceland plume. Earth and Planetary Science Letters 153, 197-208.

Floyd, P., Leveridge, B., 1987. Tectonic environment of the Devonian Gramscatho basin, south Cornwall: framework mode and geochemical

1179 evidence from turbiditic sandstones. Journal of the Geological Society
1180 144, 531-542.
1181 Floyd, P., Shail, R., Leveridge, B., Franke, W., 1991. Geochemistry and
1182 provenance of Rhenohercynian synorogenic sandstones: implications
1183 for tectonic environment discrimination. In: Morton, A.C., Todd, S.P.,
1184 Haughton, P.D.W. (Eds.), Developments in Sedimentary Provenance
1185 Studies. Geological Society of London, Special Publication 57, pp. 173-
1186 188.
1187 Gass, I.G., 1968. Is the Troodos Massif of Cyprus a Fragment of Mesozoic
1188 Ocean Floor? Nature 220, 39-42.
1189 Geringer, G., Botha, B., Pretorius, J., Ludick, D., 1986. Calc-alkaline volcanism
1190 along the eastern margin of the Namaqua Mobile Belt, South Africa-a
1191 possible middle Proterozoic volcanic arc. Precambrian Research 33,
1192 139-170.
1193 Gilbert, M.F., Robertson, A.H.F., 2013. Field relations, geochemistry and origin
1194 of the Upper Cretaceous volcaniclastic Kannaviou Formation in western
1195 Cyprus: evidence of a southerly Neotethyan volcanic arc. In: Robertson,
1196 A.H.F., Parlak, O., Ünlügenç, U.C. (Eds.), Geological Development of
1197 Anatolia and the Easternmost Mediterranean Region. Geological
1198 Society of London, Special Publications 372, pp. 273-298.
1199 Graham, S.A., Ingersoll, R.V., Dickinson, W.R., 1976. Common provenance for
1200 lithic grains in Carboniferous sandstones from Ouachita Mountains and
1201 Black Warrior Basin. Journal of Sedimentary Research 46, 620-632.

1202 Greene, A.R., Debari, S.M., Kelemen, P.B., Blusztajn, J., Clift, P.D., 2006. A
1203 detailed geochemical study of island arc crust: the Talkeetna arc section,
1204 south–central Alaska. Journal of Petrology 47, 1051-1093.
1205 Hannah, R.S., Vogel, T.A., Patino, L.C., Alvarado, G.E., Pérez, W., Smith, D.R.,
1206 2002. Origin of silicic volcanic rocks in Central Costa Rica: a study of a
1207 chemically variable ash-flow sheet in the Tiribi Tuff. Bulletin of
1208 Volcanology 64, 117-133.
1209 Hartley, M.E., Thordarson, T., 2013. The 1874-1876 volcano-tectonic episode
1210 at Askja, North Iceland: Lateral flow revisited. Geochemistry,
1211 Geophysics, Geosystems 14, 2286-2309.
1212 Hay, W.W., 2011. Can humans force a return to a 'Cretaceous' climate?
1213 Sedimentary Geology 235, 5-26.
1214 Hayward, C., 2011. High spatial resolution electron probe microanalysis of
1215 tephras and melt inclusions without beam-induced chemical modification.
1216 The Holocene 22, 119-125.
1217 Horn, D.R., Delach, M.N., Horn, B.M., 1969. Distribution of volcanic ash layers
1218 and turbidites in the North Pacific. Geological Society of America Bulletin
1219 80, 1715-1724.
1220 Houghton, B., Landis, C., 1989. Sedimentation and volcanism in a Permian arc-
1221 related basin, southern New Zealand. Bulletin of Volcanology 51, 433-
1222 450.
1223 Howell, D.G., Normark, W.R., 1982. Sedimentology of submarine fans. In:
1224 Scholle, P.A., D., S. (Eds.), Sandstone depositional environments.
1225 American Association of Petroleum Geologists, Memoir 31, pp. 365-404.

1226 Hu, Z., Gao, S., 2008. Upper crustal abundances of trace elements: a revision
1227 and update. Chemical Geology 253, 205-221.

1228 Huang, K., Malpas, J., Xenophontos, C., 2007. Geological studies of igneous
1229 rocks and their relationships along the Kyrenia Range. In: Moumani, K.,
1230 Shawabkeh, K., Al-Malabeh, A., Abdelghafoor, M. (Eds.), 6th
1231 International Congress of Eastern Mediterranean Geology, Amman,
1232 Jordan, pp. 53.

1233 Ingersoll, R.V., Bullard, T.F., Ford, R.L., Grimm, J.P., Pickle, J.D., Sares, S.W.,
1234 1984. The effect of grain size on detrital modes: a test of the Gazzi-
1235 Dickinson point-counting method. Journal of Sedimentary Research 54,
1236 103-116.

1237 Inwood, J., Anderson, M.W., Morris, A., Robertson, A.H.F., 2009. Successive
1238 structural events in the Hatay ophiolite of southeast Turkey:
1239 Distinguishing oceanic, emplacement and post-emplacement phases of
1240 faulting. Tectonophysics 473, 208-222.

1241 Irvine, T., Baragar, W., 1971. A guide to the chemical classification of the
1242 common volcanic rocks. Canadian Journal of Earth Sciences 8, 523-548.

1243 Karaoğlan, F., Parlak, O., Hejl, E., Neubauer, F., Kloetzli, U., 2016. The
1244 temporal evolution of the active margin along the Southeast Anatolian
1245 Orogenic Belt (SE Turkey): Evidence from U–Pb, Ar–Ar and fission track
1246 chronology. Gondwana Research 33, 190-208.

1247 Karaoğlan, F., Parlak, O., Robertson, A., Thöni, M., Klötzli, U., Koller, F., Okay,
1248 A.İ., 2013. Evidence of Eocene high-temperature/high-pressure
1249 metamorphism of ophiolitic rocks and granitoid intrusion related to
1250 Neotethyan subduction processes (Doğanşehir area, SE Anatolia). In:

1251 Robertson, A.H.F., Parlak, O., Ünlügenç, U.C. (Eds.), Geological
1252 Development of Anatolia and the Easternmost Mediterranean Region.
1253 Geological Society of London, Special Publications 372, pp. 249-272.
1254 Kelly, N., Hinton, R., Harley, S., Appleby, S., 2008. New SIMS U–Pb zircon
1255 ages from the Langavat Belt, South Harris, NW Scotland: implications
1256 for the Lewisian terrane model. Journal of the Geological Society 165,
1257 967-981.
1258 Kuno, H., 1966. Lateral variation of basalt magma type across continental
1259 margins and island arcs. Bulletin of Volcanology 29, 195-222.
1260 Kutterolf, S., Freundt, A., Perez, W., Mörz, T., Schacht, U., Wehrmann, H.,
1261 Schmincke, H.U., 2008a. Pacific offshore record of plinian arc volcanism
1262 in Central America: 2. Tephra volumes and erupted masses.
1263 Geochemistry, Geophysics, Geosystems 9, Q02S02,
1264 doi:10.1029/2007GC001791.
1265 Kutterolf, S., Freundt, A., Peréz, W., Mörz, T., Schacht, U., Wehrmann, H.,
1266 Schmincke, H.U., 2008b. Pacific offshore record of plinian arc volcanism
1267 in Central America: 1. Along-arc correlations. Geochemistry,
1268 Geophysics, Geosystems 9, Q02S01, doi:10.1029/2007GC001631.
1269 Kutterolf, S., Schindlbeck, J., Robertson, A., Avery, A., Baxter, A., Petronotis,
1270 K., Wang, K.L., 2018. Tephrostratigraphy and Provenance From IODP
1271 Expedition 352, Izu-Bonin Arc: Tracing Tephra Sources and Volumes
1272 From the Oligocene to Recent. Geochemistry, Geophysics, Geosystems
1273 19, 150-174.
1274 Kutterolf, S., Schindlbeck, J.C., Scudder, R.P., Murray, R.W., Pickering, K.T.,
1275 Freundt, A., Labanieh, S., Heydolph, K., Saito, S., Naruse, H.,

Underwood, M.B., Wu, H., 2014. Large volume submarine ignimbrites in the Shikoku Basin: An example for explosive volcanism in the Western Pacific during the Late Miocene. Geochemistry, Geophysics, Geosystems 15, 1837-1851.

Lapierre, H., 1968. Découverte d'une série volcanosédimentaire probablement d'âge Crétacé supérieur au SW de l'île de Chypre. Comptes Rendus de l'Académie des Sciences D266, 1876-1878.

Lapierre, H., 1975. Les Formations Sédimentaires et Éruptives Des Nappes de Mamonia et Leurs Relations Avec Le Massif Du Troodos (Chypre Occidentale). Mémoires de la Société géologique de France 123, Paris, 131 pp.

Lapierre, H., Bosch, D., Narros, A., Mascle, G., Tardy, M., Demant, A., 2007. The Mamonia Complex (SW Cyprus) revisited: remnant of Late Triassic intra-oceanic volcanism along the Tethyan southwestern passive margin. Geological Magazine 144, 1-19.

Le Bas, M.J., Le Maitre, R., Streckeisen, A., Zanettin, B., 1986. A chemical classification of volcanic rocks based on the total alkali-silica diagram. Journal of Petrology 27, 745-750.

Leake, B.E., Woolley, A.R., Arps, C.E.S., Birch, W.D., Gilbert, M.C., Grice, J.D., Hawthorne, F.C., Kato, A., Kisch, H.J., Krivovichev, V.G., Linthout, K., Laird, J., Mandarino, J.A., Maresch, W.V., Nickel, E.H., Rock, N.M.S., Schumacher, J.C., Smith, D.C., Stephenson, N.C.N., Ungaretti, L., Whittaker, E.J.W., Youzhi, G., 1997. Nomenclature of amphiboles: report of the subcommittee on amphiboles of the International

1300 Mineralogical Association, Commission on New Minerals and Mineral
1301 Names. Mineralogical Magazine 61, 295-321.
1302 Lord, A.R., Panayides, I., Urquhart, E., Xenophontos, C., 2000. A
1303 biochronostratigraphical framework for the Late Cretaceous-Recent
1304 circum-Troodos sedimentary sequence, Cyprus. In: Panayides, I.,
1305 Xenophontos, C., Malpas, J. (Eds.), Proceedings of the Third
1306 International Conference on the Geology of the Eastern Mediterranean.
1307 Cyprus Geological Survey Department, Nicosia, Cyprus, pp. 289-298.
1308 Lowe, D.J., Shane, P.A., Alloway, B.V., Newnham, R.M., 2008. Fingerprints
1309 and age models for widespread New Zealand tephra marker beds
1310 erupted since 30,000 years ago: a framework for NZ-INTIMATE.
1311 Quaternary Science Reviews 27, 95-126.

1312 Ludwig, K.R., 2012. Users manual for Isoplot 3.75. Berkeley Geochronology
1313 Centre Special Publication No. 5, 75 pp.
1314 MacLeod, C.J., 1990. Role of the Southern Troodos Transform Fault in the
1315 rotation of the Cyprus microplate: evidence from the Eastern Limassol
1316 Forest Complex. In: Malpas, J., Moores, E.M., Panayiotou, A.,
1317 Xenophontos, C. (Eds.), Ophiolites oceanic crustal analogues:
1318 proceedings of the symposium 'Troodos 1987'. Cyprus Geological
1319 Survey Department, Nicosia, Cyprus, pp. 75-86.
1320 MacLeod, C.J., Murton, B.J., 1993. Structure and tectonic evolution of the
1321 Southern Troodos Transform Fault Zone, Cyprus. In: Prichard, H.M.,
1322 Alabaster, T., Harris, N.B., Neary, C.R. (Eds.), Magmatic Processes and
1323 Plate Tectonics. Geological Society of London, Special Publications 76,
1324 pp. 141-176.

1325 Malpas, J., Calon, T., Squires, G., 1993. The development of a late Cretaceous
1326 microplate suture zone in SW Cyprus. In: Prichard, H.M., Alabaster, T.,
1327 Harris, N.B., Neary, C.R. (Eds.), Magmatic Processes and Plate
1328 Tectonics. Geological Society of London, Special Publications 76, pp.
1329 177-195.
1330 Malpas, J., Xenophontos, C., Williams, D., 1992. The Ayia Varvara Formation
1331 of SW Cyprus: A product of complex collisional tectonics.
1332 Tectonophysics 212, 193-211.
1333 Marsaglia, K.M., 1992. Petrography and provenance of volcaniclastic sands
1334 recovered from the Izu-Bonin Arc, Leg 126. In: Taylor, B., Fujioka, K., et
1335 al. (Eds.), Proceedings of the Ocean Drilling Program, Scientific Results
1336 126. Ocean Drilling Program, College Station, TX, pp. 139-154.
1337 Marsaglia, K.M., Barone, M., Critelli, S., Busby, C., Fackler-Adams, B., 2016.
1338 Petrography of volcaniclastic rocks in intra-arc volcano-bounded to fault-
1339 bounded basins of the Rosario segment of the Lower Cretaceous Alisitos
1340 oceanic arc, Baja California, Mexico. Sedimentary Geology 336, 138-
1341 146.
1342 Marsaglia, K.M., Ingersoll, R.V., 1992. Compositional trends in arc-related,
1343 deep-marine sand and sandstone: a reassessment of magmatic-arc
1344 provenance. Geological Society of America Bulletin 104, 1637-1649.
1345 Mason, B.G., Pyle, D.M., Oppenheimer, C., 2004. The size and frequency of
1346 the largest explosive eruptions on Earth. Bulletin of Volcanology 66, 735-
1347 748.

McBride, E.F., 1963. A classification of common sandstones. Journal of Sedimentary Research 33, 664-669.

McCay, G.A., Robertson, A.H.F., 2013. Upper Miocene–Pleistocene deformation of the Girne (Kyrenia) Range and Dar Dere (Ovgos) lineaments, northern Cyprus: role in collision and tectonic escape in the easternmost Mediterranean region. In: Robertson, A.H.F., Parlak, O., Ünlügenç, U.C. (Eds.), Geological Development of Anatolia and the Easternmost Mediterranean Region. Geological Society, London, Special Publications 372, pp. 421-445.

McLennan, S.M., Hemming, S., McDaniel, D., Hanson, G., 1993. Geochemical approaches to sedimentation, provenance, and tectonics. In: Johnsson, M.J., Basu, A. (Eds.), Processes Controlling the Composition of Clastic Sediments. Geological Society of America, Special Paper 284, pp. 21-40.

McLennan, S.M., Taylor, S., Eriksson, K., 1983. Geochemistry of Archean shales from the Pilbara Supergroup, western Australia. Geochimica et Cosmochimica Acta 47, 1211-1222.

McLennan, S.M., Taylor, S., McCulloch, M., Maynard, J., 1990. Geochemical and Nd-Sr isotopic composition of deep-sea turbidites: crustal evolution and plate tectonic associations. Geochimica et Cosmochimica Acta 54, 2015-2050.

McLennan, S.M., Taylor, S.R., 1984. Archaean sedimentary rocks and their relation to the composition of the Archaean continental crust. In: Kröner, A., Hanson, G.N., Goodwin, A.M. (Eds.), Archaean geochemistry: the

origin and evolution of the Archaean continental crust. Springer-Verlag, Berlin, pp. 47-72.

Mercier, J., Vergely, P., Delibassis, N., 1973. Comparison between deformation deduced from the analysis of recent faults and from focal mechanisms of earthquakes (an example: the Paphos region, Cyprus). Tectonophysics 19, 315-332.

Moore, J.G., Nakamura, K., Alcaraz, A., 1966. The 1965 Eruption of Taal Volcano. Science 151, 955-960.

Moore, T.A., 1960. The geology and mineral resources of the Astromeritis-Kormakiti area. Geological Survey Department, Memoir 6, Nicosia, Cyprus, 96 pp.

Moores, E.M., Vine, F.J., 1971. The Troodos Massif, Cyprus and other ophiolites as oceanic crust: evaluation and implications. Philosophical Transactions of the Royal Society of London. Series A, Mathematical and Physical Sciences 268, 443-466.

Morag, N., Haviv, I., Katzir, Y., 2016. From ocean depths to mountain tops: Uplift of the Troodos ophiolite (Cyprus) constrained by low-temperature thermochronology and geomorphic analysis. Tectonics 35, 622-637.

Morimoto, N., 1988. Nomenclature of pyroxenes. Mineralogy and Petrology 39, 55-76.

Morris, A., 1996. A review of palaeomagnetic research in the Troodos ophiolite, Cyprus. In: Morris, A., Tarling, D.H. (Eds.), Palaeomagnetism and Tectonics of the Mediterranean Region. Geological Society of London, Special Publications 105, pp. 311-324.

1396 Morris, A., Anderson, M.W., Robertson, A.H.F., 1998. Multiple tectonic rotations
1397 and transform tectonism in an intraoceanic suture zone, SW Cyprus.
1398 Tectonophysics 299, 229-253.
1399 Morris, A., Creer, K.M., Robertson, A.H.F., 1990. Palaeomagnetic evidence for
1400 clockwise rotations related to dextral shear along the southern Troodos
1401 transform fault, Cyprus. Earth and Planetary Science Letters 99, 250-
1402 262.
1403 Morris, A., Robertson, A.H.F., Anderson, M.W., Hodgson, E., 2015. Did the
1404 Kyrenia Range of northern Cyprus rotate with the Troodos–Hatay
1405 microplate during the tectonic evolution of the eastern Mediterranean?
1406 International Journal of Earth Sciences 105, 399-415.
1407 Mukasa, S.B., Ludden, J.N., 1987. Uranium-lead isotopic ages of
1408 plagiogranites from the Troodos ophiolite, Cyprus, and their tectonic
1409 significance. Geology 15, 825-828.
1410 Murton, B., 1986. Anomalous oceanic lithosphere formed in a leaky transform
1411 fault: evidence from the Western Limassol Forest Complex, Cyprus.
1412 Journal of the Geological Society 143, 845-854.
1413 Murton, B.J., Cass, I.G., 1986. Western Limassol Forest complex, Cyprus: part
1414 of an Upper Cretaceous leaky transform fault. Geology 14, 255-258.
1415 Nesbitt, H.W., Markovics, G., Price, R.C., 1980. Chemical processes affecting
1416 alkalis and alkaline earths during continental weathering. Geochimica et
1417 Cosmochimica Acta 44, 1659-1666.
1418 Nielsen, C.H., Sigurdsson, H., 1981. Quantitative methods for electron
1419 microprobe analysis of sodium in natural and synthetic glasses.
1420 American Mineralogist 66, 547-552.

1421 Ninkovich, D., Sparks, R., Ledbetter, M., 1978. The exceptional magnitude and
1422 intensity of the Toba eruption, Sumatra: an example of the use of deep-
1423 sea tephra layers as a geological tool. Bulletin of Volcanology 41, 286-
1424 298.

1425 Nisbet, E.G., Pearce, J.A., 1977. Clinopyroxene composition in mafic lavas
1426 from different tectonic settings. Contributions to Mineralogy and
1427 Petrology 63, 149-160.

1428 Nishimura, A., Marsaglia, K.M., Rodolfo, K.S., Colella, A., Hiscott, R.N., Tazakl,
1429 K., Gill, J.B., Janecek, T., Firth, J., Isiminger-Kelso, M., Herman, Y.,
1430 Taylor, R.N., Taylor, B., Fujioka, K., Leg 126 Scientific Party, 1991.
1431 Pliocene-quaternary submarine pumice deposits in the Sumisu Rift area,
1432 Izu-Bonin Arc. In: Fisher, R.V., Smith, G.A. (Eds.), Sedimentation in
1433 Volcanic Settings. Society of Economic Paleontologists and
1434 Mineralogists Special Publication 45, pp. 201-208.

1435 Ogawa, Y., Horiuchi, K., Taniguchi, H., Naka, J., 1985. Collision of the Izu arc
1436 with Honshu and the effects of oblique subduction in the Miura-Boso
1437 Peninsulas. Tectonophysics 119, 349-379.

1438 Ogawa, Y., Takami, Y., Takazawa, S., 2008. Oblique subduction in an island
1439 arc collision setting: unique sedimentation, accretion, and deformation
1440 processes in the Boso TTT-type triple junction area, NW Pacific. In:
1441 Draut, A.E., Clift, P.D., Scholl, W.D. (Eds.), Formation and Applications
1442 of the Sedimentary Record in Arc Collision Zones. Geological Society of
1443 America, Special Paper 436, pp. 155-170.

1444 Parlak, O., 2006. Geodynamic significance of granitoid magmatism in the
1445 southeast Anatolian orogen: geochemical and geochronogical evidence

from Göksun–Afşin (Kahramanmaraş, Turkey) region. International Journal of Earth Sciences 95, 609-627.

Patino, L.C., Carr, M.J., Feigenson, M.D., 2000. Local and regional variations in Central American arc lavas controlled by variations in subducted sediment input. Contributions to Mineralogy and Petrology 138, 265-283.

Payne, A.S., Robertson, A.H.F., 1995. Neogene supra-subduction zone extension in the Polis graben system, west Cyprus. Journal of the Geological Society 152, 613-628.

Payne, A.S., Robertson, A.H.F., 2000. Structural evolution and regional significance of the Polis graben system, western Cyprus. In: Panayides, I., Xenophontos, C., Malpas, J. (Eds.), Proceedings of the Third International Conference on the Geology of the Eastern Mediterranean. Cyprus Geological Survey Department, Nicosia, Cyprus, pp. 45-60.

Pearce, J.A., 1983. Role of the sub-continental lithosphere in magma genesis at active continental margins. In: Hawkersworth, C.J., Norry, M.J. (Eds.), Continental Basalts and Mantle Xenoliths. Shiva, Cheshire, UK, pp. 230-249.

Pearce, J.A., Robinson, P.T., 2010. The Troodos ophiolitic complex probably formed in a subduction initiation, slab edge setting. Gondwana Research 18, 60-81.

Pickering, K., Hiscott, R., 2016. Deep Marine Systems: Processes, Deposits, Environments, Tectonics and Sedimentation. Wiley, Chichester, UK, 672 pp.

Piper, D.J., von Huene, R., Duncan, J.R., 1973. Late Quaternary sedimentation in the active eastern Aleutian Trench. Geology 1, 19-22.

1471 Plafker, G., Nokleberg, W., Lull, J., 1989. Bedrock geology and tectonic
1472 evolution of the Wrangellia, Peninsular, and Chugach terranes along the
1473 Trans-Alaska Crustal Transect in the Chugach Mountains and southern
1474 Copper River Basin, Alaska. Journal of Geophysical Research: Solid
1475 Earth 94, 4255-4295.

1476 Plank, T., 2005. Constraints from Thorium/Lanthanum on Sediment Recycling
1477 at Subduction Zones and the Evolution of the Continents. Journal of
1478 Petrology 46, 921-944.

1479 Poisson, A., 1977. Récherches Géologiques dans les Taurides Occidentales,
1480 Turquie. Doctor of Science Thesis (published). Université Paris-Sud,
1481 France, 795 pp.

1482 Poole, A.J., Robertson, A.H.F., 1998. Pleistocene fanglomerate deposition
1483 related to uplift of the Troodos Ophiolite, Cyprus. In: Robertson, A.H.F.,
1484 Emeis, K., Richter, C., Camerlenghi, A. (Eds.), Proceedings of the
1485 Ocean Drilling Program, Scientific Results 160. Ocean Drilling Program,
1486 College Station, TX, pp. 544-568.

1487 Pyle, D.M., 1989. The thickness, volume and grainsize of tephra fall deposits.
1488 Bulletin of Volcanology 51, 1-15.

1489 Rızaoğlu, T., Parlak, O., Höck, V., Koller, F., Hames, W.E., Billor, Z., 2009.
1490 Andean-type active margin formation in the eastern Taurides:
1491 Geochemical and geochronogical evidence from the Baskil granitoid
1492 (Elazığ, SE Turkey). Tectonophysics 473, 188-207.

1493 Robertson, A.H.F., 1975. Cyprus umbers: basalt-sediment relationships on a
1494 Mesozoic ocean ridge. Journal of the Geological Society 131, 511-531.

1495 Robertson, A.H.F., 1976. Pelagic chalks and calciturbidites from the lower
1496 Tertiary of the Troodos Massif, Cyprus. Journal of Sedimentary
1497 Research 46, 1007-1016.
1498 Robertson, A.H.F., 1977a. The Kannaviou Formation, Cyprus: volcaniclastic
1499 sedimentation of a probable Late Cretaceous volcanic arc. Journal of the
1500 Geological Society 134, 269-292.
1501 Robertson, A.H.F., 1977b. The Moni Melange, Cyprus: an olistostrome formed
1502 at a destructive plate margin. Journal of the Geological Society 133, 447-
1503 466.

1504 Robertson, A.H.F., 1977c. Tertiary uplift history of the Troodos massif, Cyprus.
1505 Geological Society of America Bulletin 88, 1763-1772.

1506 Robertson, A.H.F., 1990. Tectonic evolution of Cyprus. In: Malpas, J., Moores,
1507 E.M., Panayiotou, A., Xenophontos, C. (Eds.), Ophiolites-Oceanic
1508 Crustal Analogues: Proceedings of the International Symposium
1509 'Troodos 1987'. Cyprus Geological Survey Department, Nicosia, Cyprus,
1510 pp. 235-250.
1511 Robertson, A.H.F., 2002. Overview of the genesis and emplacement of
1512 Mesozoic ophiolites in the Eastern Mediterranean Tethyan region. Lithos
1513 65, 1-67.
1514 Robertson, A.H.F., Degnan, P., 1994. The Dras arc complex: lithofacies and
1515 reconstruction of a Late Cretaceous oceanic volcanic arc in the Indus
1516 suture zone, Ladakh Himalaya. Sedimentary Geology 92, 117-145.
1517 Robertson, A.H.F., Hudson, J.D., 1974. Pelagic sediments in the Cretaceous
1518 and Tertiary history of the Troodos Massif, Cyprus. In: Hsü, K.J.,

1519 Jenkyns, H.C. (Eds.), Pelagic Sediments: on Land and Under the Sea.
1520 Blackwell Scientific Publications, Oxford, pp. 403-436.
1521 Robertson, A.H.F., Kinnaird, T.C., 2016. Structural development of the central
1522 Kyrenia Range (north Cyprus) in its regional setting in the eastern
1523 Mediterranean region. International Journal of Earth Sciences 105, 417-
1524 437.
1525 Robertson, A.H.F., Kutterolf, S., Avery, A., Baxter, A.T., Petronotis, K., Acton,
1526 G.D., Carvallo, C., Schindlbeck, J.C., 2018. Depositional setting,
1527 provenance, and tectonic-volcanic setting of Eocene–Recent deep-sea
1528 sediments of the oceanic Izu–Bonin forearc, northwest Pacific (IODP
1529 Expedition 352). International Geology Review 60, 1816-1854.
1530 Robertson, A.H.F., McCay, G.A., Tasli, K., Yıldız, A., 2014. Eocene
1531 development of the northerly active continental margin of the Southern
1532 Neotethys in the Kyrenia Range, north Cyprus. Geological Magazine
1533 151, 692-731.
1534 Robertson, A.H.F., Palamakumbura, R.N., 2019. Geological development and
1535 regional significance of an oceanic magmatic arc and its sedimentary
1536 cover: Permian Brook Street Terrane, South Island, New Zealand. In:
1537 Robertson, A.H.F. (Ed.), Paleozoic-Mesozoic Geology of South Island,
1538 New Zealand: Subduction-related Processes Adjacent to SE Gondwana.
1539 Geological Society of London, Memoirs 49 (in press).
1540 Robertson, A.H.F., Palamakumbura, R.N., Campbell, H., 2019. Permian-
1541 Triassic felsic tuffs in South Island, New Zealand: significance for
1542 oceanic and active continental margin subduction. In: Robertson, A.H.F.
1543 (Ed.), Paleozoic-Mesozoic Geology of South Island, New Zealand:

1544 Subduction-related Processes Adjacent to SE Gondwana. Geological
1545 Society of London, Memoirs 49 (in press).
1546 Robertson, A.H.F., Parlak, O., Rizaoğlu, T., Ünlügenç, Ü., İnan, N., Tasli, K.,
1547 Ustaömer, T., 2007. Tectonic evolution of the South Tethyan ocean:
1548 evidence from the Eastern Taurus Mountains (Elaziğ region, SE Turkey).
1549 In: Ries, A.C., Butler, R.W.H., Graham, R.H. (Eds.), Deformation of the
1550 Continental Crust: The Legacy of Mike Coward. Geological Society of
1551 London, Special Publications 272, pp. 231-270.
1552 Robertson, A.H.F., Tasli, K., İnan, N., 2012. Evidence from the Kyrenia Range,
1553 Cyprus, of the northerly active margin of the Southern Neotethys during
1554 Late Cretaceous–Early Cenozoic time. Geological Magazine 149, 264-
1555 290.
1556 Robertson, A.H.F., Ustaömer, T., Parlak, O., Ünlügenç, U.C., Taşlı, K., İnan, N.,
1557 2006. The Berit transect of the Tauride thrust belt, S Turkey: Late
1558 Cretaceous–Early Cenozoic accretionary/collisional processes related
1559 to closure of the Southern Neotethys. Journal of Asian Earth Sciences
1560 27, 108-145.
1561 Robertson, A.H.F., Woodcock, N.H., 1979. Mamonia Complex, southwest
1562 Cyprus: Evolution and emplacement of a Mesozoic continental margin.
1563 Geological Society of America Bulletin 90, 651-665.
1564 Robertson, A.H.F., Woodcock, N.H., 1986. The role of the Kyrenia Range
1565 Lineament, Cyprus, in the geological evolution of the eastern
1566 Mediterranean area. Philosophical Transactions of the Royal Society of
1567 London. Series A, Mathematical and Physical Sciences 317, 141-177.

1568 Robertson, A.H.F., Xenophontos, C., 1993. Development of concepts
1569 concerning the Troodos ophiolite and adjacent units in Cyprus. n:
1570 Prichard, H.M., Alabaster, T., Harris, N.B.W., Neary, C.R. (Eds.),
1571 Magmatic Processes and Plate Tectonics. Geological Society of London,
1572 Special Publications 76, pp. 85-119.
1573 Robinson, P.T., Malpas, J., 1990. The Troodos ophiolite of Cyprus: new
1574 perspectives on its origin and emplacement. In: Malpas, J., Moores, E.M.,
1575 Panayiotou, A., Xenophontos, C. (Eds.), Ophiolites, Oceanic Crustal
1576 Analogues. Cyprus Geological Survey Department, Nicosia, Cyprus, pp.
1577 13-26.
1578 Roser, B.P., Korsch, R.J., 1986. Determination of tectonic setting of sandstone-
1579 mudstone suites using SiO_2 content and K_2O/Na_2O ratio. The Journal of
1580 Geology 94, 635-650.
1581 Rubatto, D., 2002. Zircon trace element geochemistry: partitioning with garnet
1582 and the link between U–Pb ages and metamorphism. Chemical Geology
1583 184, 123-138.
1584 Rudnick, R., Gao, S., 2003. Composition of the continental crust. In: Holland,
1585 H.D., Turekian, K.K. (Eds.), Treatise on Geochemistry 3, Elsevier-
1586 Pergamon, Oxford, pp. 1-64.
1587 Schindlbeck, J.C., Kutterolf, S., Freundt, A., Alvarado, G., Wang, K.L., Straub,
1588 S., Hemming, S., Frische, M., Woodhead, J., 2016. Late Cenozoic
1589 tephrostratigraphy offshore the southern Central American Volcanic Arc:
1590 1. Tephra ages and provenance. Geochemistry, Geophysics,
1591 Geosystems 17, 4641-4668.

1592 Schindlbeck, J.C., Kutterolf, S., Freundt, A., Scudder, R., Pickering, K.T.,
1593 Murray, R., 2013. Emplacement processes of submarine volcaniclastic
1594 deposits (IODP Site C0011, Nankai Trough). Marine Geology 343, 115-
1595 124.
1596 Schweller, W.J., Kulm, L.D., Prince, R.A., 1981. Tectonics, structure, and
1597 sedimentary framework of the Peru-Chile Trench. In: Kulm, L.V.D.,
1598 Dymond, J., Dasch, E.J., Hussong, D.M., Roderick, R. (Eds.), Nazca
1599 Plate: Crustal Formation and Andean Convergence. Geological Society
1600 of America Memoirs 154, pp. 323-349.
1601 Söderlund, U., Hofmann, A., Klausen, M.B., Olsson, J.R., Ernst, R.E., Persson,
1602 P.-O., 2010. Towards a complete magmatic barcode for the Zimbabwe
1603 craton: Baddeleyite U–Pb dating of regional dolerite dyke swarms and
1604 sill complexes. Precambrian Research 183, 388-398.
1605 Spandler, C., Worden, K., Arculus, R., Eggins, S., 2005. Igneous rocks of the
1606 Brook Street Terrane, New Zealand: implications for Permian tectonics
1607 of eastern Gondwana and magma genesis in modern intra-oceanic
1608 volcanic arcs. New Zealand Journal of Geology and Geophysics 48, 167-
1609 183.
1610 Stern, R.J., Fouch, M.J., Klemperer, S.L., 2003. An overview of the Izu-Bonin-
1611 Mariana subduction factory. In: Eiler, J. (Ed.), Inside the Subduction
1612 Factory. American Geophysical Union 138, Washington, D. C., pp. 175-
1613 222.
1614 Straub, S.M., 2003. The evolution of the Izu Bonin - Mariana volcanic arcs (NW
1615 Pacific) in terms of major element chemistry. Geochemistry, Geophysics,
1616 Geosystems 4, 1018, doi:10.1029/2002GC000357.

1617 Straub, S.M., Layne, G.D., 2003. Decoupling of fluids and fluid-mobile elements
1618 during shallow subduction: Evidence from halogen-rich andesite melt
1619 inclusions from the Izu arc volcanic front. Geochemistry, Geophysics,
1620 Geosystems 4, 9003, doi:10.1029/2002GC000349.
1621 Sun, S.-s., McDonough, W.F., 1989. Chemical and isotopic systematics of
1622 oceanic basalts: implications for mantle composition and processes. In:
1623 Saunders, A.D., Norry, M.J. (Eds.), Magmatism in the Ocean Basins.
1624 Geological Society of London, Special Publications 42, pp. 313-345.
1625 Swarbrick, R.E., 1980. The Mamonia complex of S.W. Cyprus: a Mesozoic
1626 continental margin and its relationship to the Troodos Complex. In:
1627 Panayiotou, A. (Ed.), Ophiolites: Proceedings of the International
1628 Ophiolite Symposium. Cyprus Ministry of Agriculture and Natural
1629 Resources, Geology Survey Department, Nicosia, Cyprus, pp. 86-92.
1630 Swarbrick, R.E., 1993. Sinistral strike-slip and transpressional tectonics in an
1631 ancient oceanic setting: the Mamonia Complex, southwest Cyprus.
1632 Journal of the Geological Society 150, 381-392.
1633 Swarbrick, R.E., Naylor, M.A., 1980. The Kathikas melange, SW Cyprus: late
1634 Cretaceous submarine debris flows. Sedimentology 27, 63-78.
1635 Swarbrick, R.E., Robertson, A.H.F., 1980. Revised stratigraphy of the Mesozoic
1636 rocks of southern Cyprus. Geological Magazine 117, 547-563.
1637 Taylor, S.R., McLennan, S.M., 1985. The Continental Crust: its Composition
1638 and Evolution. Blackwell Scientific Publications, United States, 312 pp.
1639 Torley, J.M., Robertson, A.H.F., 2018. New evidence and interpretation of
1640 facies, provenance and geochemistry of late Triassic-early Cretaceous
1641 Tethyan deep-water passive margin-related sedimentary rocks (Ayios

Photios Group), SW Cyprus in the context of eastern Mediterranean geodynamics. Sedimentary Geology 377, 82-110.

Ulmer-Scholle, D.S., Scholle, P.A., Schieber, J., Raine, R.J., 2015. A color guide to the petrography of sandstones, siltstones, shales and associated rocks. American Association of Petroleum Geologists, Memoir 109, Tulsa, 509 pp.

Urquhart, E., Banner, F.T., 1994. Biostratigraphy of the supra-ophiolite sediments of the Troodos Massif, Cyprus: the Cretaceous Perapedhi, Kannaviou, Moni and Kathikas formations. Geological Magazine 131, 499-518.

Ustaömer, P.A., Ustaömer, T., Robertson, A., 2012. Ion probe U-Pb dating of the Central Sakarya basement: a peri-Gondwana terrane intruded by late Lower Carboniferous subduction/collision-related granitic rocks. Turkish Journal of Earth Sciences 21, 905-932.

Van der Plas, L., Tobi, A., 1965. A chart for judging the reliability of point counting results. American Journal of Science 263, 87-90.

Watkins, N., Sparks, R., Sigurdsson, H., Huang, T., Federman, A., Carey, S., Ninkovich, D., 1978. Volume and extent of the Minoan tephra from Santorini Volcano: new evidence from deep-sea sediment cores. Nature 271, 122-126.

Woodhead, J., Eggins, S., Gamble, J., 1993. High field strength and transition element systematics in island arc and back-arc basin basalts: evidence for multi-phase melt extraction and a depleted mantle wedge. Earth and Planetary Science Letters 114, 491-504.

Wronkiewicz, D.J., Condie, K.C., 1987. Geochemistry of Archean shales from the Witwatersrand Supergroup, South Africa: source-area weathering and provenance. Geochimica et Cosmochimica Acta 51, 2401-2416.

Yamamoto, T., 2009. Sedimentary processes caused by felsic caldera-forming volcanism in the Late Miocene to Early Pliocene intra-arc Aizu basin, NE Japan arc. Sedimentary Geology 220, 337-348.

Listing of Figures

Fig. 1. (a) Simplified map showing Cyprus in the eastern Mediterranean. The locations of the late Cretaceous volcanogenic sediments (FF; blue box) in the Kyrenia Range, northern Cyprus and the late Cretaceous arc-related rocks in southeast Turkey (green box) are indicated; (b) Outline geological map of western Cyprus, showing the main outcrops of the late Cretaceous Kannaviou Formation, and their relationship to the Troodos ophiolite and Mamonia Complex (modified after Robertson, 1977a; Robertson and Woodcock, 1979; Swarbrick, 1980). Abbreviations: STTFZ, South Troodos Transform Fault Zone; FF, Fourkovouno (Selvilitepe) Formation.

Fig. 2. Main geological units in western Cyprus; see Fig. 4 for detailed sedimentary logs of local successions and keys (data from Robertson, 1977a, and this study).

Fig. 3. Geological map of the main outcrop of the Kannaviou Formation near Kannaviou village (modified from Lapierre, 1975). Stratigraphic sections (a-d) are indicated. Dash lines for generalised sections; solid lines for measured sections.

Fig. 4. Summary logs showing local facies and thickness variations. See Fig. 3 for locations of sections a-d and the Supplementary material for e-j. Dash lines for generalised sections; solid lines for measured sections.

Fig. 5. Field photographs of the Kannaviou Formation. (a) Volcanogenic clay and siltstone with interspersed lenticular volcaniclastic sandstone, 1 km ENE of Kannaviou village. Samples (nos. 16-04, 16-13) are from this outcrop; (b) Thick-bedded, lenticular sandstone, interbedded with claystone and mudstone; overlying the uppermost Troodos extrusives (lava breccias) near the Paleomylon River (see section in Fig. 4b). Samples 16-16, 18.4 and 18.5 are from this section; (c) Bioturbation on bedding surface (<3 cm long) (see Fig. 5a for location); (d) Matrix-supported basaltic breccia (hyaloclastite) with palagonite clasts; within lenticular volcaniclastic sandstone (see Fig. 5b for location); (e) Sandstone showing convolute lamination and slumping, 1 km WNW of Istinjo (see section in Fig. 4h); (f) Lenticular (channelised) sandstone, up to 20 m thick, occupying the upper part of the succession, 1 km NNW of Lasa.

Fig. 6. Photomicrographs of the Kannaviou Formation sandstones. (a) Microlitic volcanic fragment (Lvf). Surrounding detrital grains include volcanic glass (Vg), pyroxene (Px) and feldspar (Fg) (cross-polarised light); (b) Foliated, detrital mica-schist fragments (Lm) composed of quartz and muscovite (cross-polarised light); (c) Angular chert fragment (Ls) (plane-polarised light); (d) Well-preserved radiolarians (R) and planktic foraminifera (F) from the upper part of the succession (plane-polarised light). Sandstone sample number is indicated in the top-left corner.

Fig. 7. Optical micrographs (a-i) and scanning electron micrographs (j-l) of Kannaviou Formation sandstones illustrating glass shards: (a-f) and (j-l) near Kannaviou village; (g) near the Paleomylon River; (h-i) south of Lapithiou. Sandstone sample number is indicated in the top-left corner. (a) subangular, highly vesicular, pumiceous glass; (b) angular blocky and cuspate bubble-wall shards; (c) cuspate shard; (d) pinkish (mafic) blocky shard with tiny tubular vesicle; (e) pinkish (mafic) and colourless (felsic) cuspate bubble-wall glass and spindle-like glass; (f) subrounded, 'frothy' glass shard; (g) thin tubular vesicle; (h) subrounded, brownish glass (mafic); (i) subangular to subrounded blocky glass (felsic) with microlitic texture; (j) conchoidal glassy fracture surface of vesicular pumice; (k) blocky, pumiceous and cuspate glass; (l) highly vesicular bubble wall glass. Abbreviation: B, blocky; C, cuspate; F, frothy; P, pumiceous; S, spindle; T, tabular.

Fig. 8. Point-count data of the Kannaviou Formation sandstones. (a) QFL (quartz-feldspar-lithic fragments) diagram for lithological classification (after McBride, 1963); (b) Ternary QFL (quartz-feldspar-lithic fragments) plot for discrimination of tectonic settings (after Dickinson et al., 1983); (c) QFL (quartz-feldspar-lithic fragments) plot with fields from Marsaglia and Ingersoll (1992) for comparison; also shown are the average data for the total dataset and the separate sample localities; (d) LmLvLs (metamorphic-volcanic-sedimentary lithic fragments) plot with fields from Marsaglia and Ingersoll (1992) for comparison; also shown are the average data for the total dataset and the separate sample localities.

Fig. 9. Na_2O+K_2O vs. SiO_2 diagram for volcanic glass (after Le Bas et al., 1986). The alkaline-subalkaline boundary line is from Irvine and Baragar (1971). Values are in wt. % and recalculated on a volatile-free basis.

Fig. 10. Normal mid-ocean ridge basalt (N-MORB)-normalised trace-element distributions of the volcanic glass from the Kannaviou Formation sandstones. N-MORB data after Sun and McDonough (1989).

Fig. 11. Geochemical plots for mineral grains of the Kannaviou Formation sandstones. (a) Anorthite-Albite-Orthoclase ternary diagram (after Deer et al., 2013) for feldspar; (b) Pyroxene ternary diagram (after Morimoto, 1988); (c) Classification of amphibole (after Leake et al., 1997).

Fig. 12. Selected cathodoluminescence images of zircon grains analysed from the Kannaviou Formation sandstones. Locations of the ion probe analysis spots and the corresponding ages ($^{206}Pb/^{238}U \pm 1\sigma$) are indicated. Scale bar=20 μm.

Fig. 13. Zircon analysis from the Kannaviou Formation sandstones. (a) An enlarged plot showing 5 analyses of magmatic zircon grains from sample 14-04 near Armou village; (b) An enlarged plot showing 11 analyses of magmatic zircon grains from samples near the Kannaviou village; (c) Wetherill Concordia diagram for the combined 8 concordant analyses, yielding a $^{206}Pb/^{238}U$ age of 80.44±1.0 Ma. One analysis (zircon 7; black arrow) with an apparently old age was excluded for Fig. 13d; (d) $^{206}Pb/^{238}U$ weighted mean diagram for zircon.

Fig. 14. Total alkali vs. silica diagram for the Kannaviou Formation sandstones (after Le Bas et al., 1986). The alkaline-subalkaline boundary line is from Irvine and Baragar (1971).

1760 Fig. 15. Upper continental crust (UCC)-normalised multi-element diagrams for
1761 sandstones from the Kannaviou Formation. Grey shaded areas indicate the
1762 total range of data. Normalising values from Rudnick and Gao (2003) and Hu
1763 and Gao (2008).

1764 Fig. 16. Chondrite-normalised REE diagrams for the Kannaviou Formation
1765 sandstones and deep-sea sands from various settings. Grey shaded areas
1766 indicate the total range of data from the Kannaviou Formation sandstones.
1767 Normalising values of chondrite are from Taylor and McLennan (1985). UCC
1768 and deep-sea sands of various settings data are from Rudnick and Gao (2003),
1769 Hu and Gao (2008) and McLennan et al. (1990), respectively.

1770 Fig. 17. Inferred palaeotopography of southwest Cyprus (see black box of inset
1771 for location) during the early Maastrichtian (in present geographical co-
1772 ordinates). The Kannaviou Formation transgresses an irregular fault-controlled
1773 ocean-floor topography, represented by the Troodos ophiolite. The fault scarps
1774 represent part of the westward extension of the South Troodos Transform Fault
1775 Zone (modified from Robertson, 1977a).

1776 Fig. 18. Geochemical plots of the Kannaviou Formation sandstones. (a)
1777 Correlation diagram of LOI vs. CaO for the whole-rock data; (b) Diagram
1778 showing the relationship between total silica contents of volcanic glass from all
1779 sites with their apparent volatile contents (100%-analytical total) (after Clift and
1780 Dixon, 1994).

1781 Fig. 19. Geochemical plots for glass and pyroxene of the Kannaviou Formation
1782 sandstones. (a) Ternary AFM (Na_2O+K_2O-FeO-MgO) plot showing the magma
1783 series and volcanic affinity of the glass; division between the calc-alkaline and

1784 the tholeiitic fields after Irvine and Baragar (1971); (b) U/Th vs. Th/Nb (after
1785 Bryant et al., 2003) for volcanic glass; (c) Th/La vs. Sm/La (after Plank, 2005)
1786 for volcanic glass; (d) Ternary TiO_2-MnO-Na_2O diagram for pyroxene (after
1787 Nisbet and Pearce, 1977). Abbreviations: VAB, volcanic arc basalt; OFB,
1788 ocean-floor basalt; WPA, within-plate alkali basalt; WPT, within-plate tholeiitic
1789 basalt.

1790 Fig. 20. Comparative plots for discriminating the provenance of the Kannaviou
1791 Formation sandstones. (a) Th/Sc vs. Zr/Sc diagram (after McLennan et al.,
1792 1993). Asterisks mark the average compositions of felsic volcanic rock,
1793 andesite and basalt (after Condie, 1993). Grey squares represent the average
1794 compositions of UCC (Rudnick and Gao, 2003; Hu and Gao, 2008); (b) La/Th
1795 vs. Hf diagram (after Floyd and Leveridge, 1987); (c) Ternary plot of La-Th-Sc.
1796 Values of potential source rocks (grey squares) are from McLennan and Taylor
1797 (1984).

1798 Fig. 21. Comparative chemical plots for the Kannaviou Formation. (a) Th-Sc-
1799 Zr/10 ternary plot (after Bhatia and Crook, 1986); (b) Normalised multi-element
1800 patterns for average Kannaviou Formation sandstone composition, and also for
1801 greywacke data (averaged) from different tectonic environments (after Floyd et
1802 al., 1991). Upper continental crust-normalisation values from Rudnick and Gao
1803 (2003) and from Hu and Gao (2008).

1804 Fig. 22. Variation in maximum grain size for the Toba, Campanian, and
1805 Santorini marine tephra fall layers (from Fisher and Schmincke, 1984).
1806 Horizontal lines with arrows show the maximum feldspar crystal sizes in the
1807 Kannaviou Formation. Vertical dashed line corresponds to the probable

1808 distance (c. 100 km) from the source arc to the Kannaviou Formation
1809 volcaniclastic sediments.

1810 Fig. 23. Plate tectonic model for the Campanian (c. 80 Ma) arc-type magmatism
1811 in Cyprus. (a) Map view showing the Kannaviou Formation accumulates in a
1812 deep-marine forearc basin setting to the south of Tauride continental crust. This
1813 is bordered by oceanic crust and also by continental crust, represented by the
1814 Mamonia Complex (to the west), which supplies small amounts of terrigenous
1815 material, especially to the upper part of the Kannaviou Formation. The Troodos
1816 ophiolite forms by incipient spreading above a separate subduction zone farther
1817 south. (b) Cross-sections showing the Kannaviou Formation being created by
1818 arc volcanism located in a distal (southerly) part of the Tauride microcontinent.
1819 Cross-section line is indicated in Fig. 23a.

1820

Listing of Tables

1833 Listing of Supplementary material

1834 Supplementary Appendix A. References, standardisation protocols and errors
1835 for SIMS analysis of glass trace elements in the Kannaviou Formation.

1836 Supplementary Appendix B. Fault distribution and kinematic analysis along the
1837 southwest margin of Troodos ophiolite.

1838 Supplementary Figure 1. Geological map of the Peristerona to Lasa region
1839 showing an additional outcrop of the Kannaviou Formation in western Cyprus
1840 (modified from Lapierre, 1975). Stratigraphic sections (e-j) are indicated.

1841 Supplementary Figure 2. Stereoplots showing the orientation of fault planes and
1842 kinematic results. (a-b) near Asproyia; (c) Kannaviou Dam area; (d) Ezousa
1843 River area; (e) near Kannaviou village; (f) near Kritou Marottou; (g) west of
1844 Istinjo; (h) Zakharia area.

1845 Supplementary Figure 3. Major element binary plots of glass shards in the
1846 Kannaviou Formation sandstones.

1847 Supplementary Figure 4. Major element binary plots of the Kannaviou
1848 Formation sandstones.

1849 Supplementary Table 1. Point-count data for the Kannaviou Formation,
1850 calculated from no less than 400 points. For framework parameters (with
1851 explanatory notes) see Table 2.

1852 Supplementary Table 2. Major element oxides and trace elements, analysed by
1853 XRF; also trace elements and rare earth elements analysed by ICP-MS for the
1854 Kannaviou Formation sandstones.

Supplementary Table 3. Electron microprobe analyses of volcanic glass, feldspar, pyroxene and amphibole grains in the Kannaviou Formation sandstones. Major elements in wt. %.

Supplementary Table 4. Analyses of trace elements in volcanic glass of the Kannaviou Formation sandstones; analysed by secondary ion mass spectrometry (SIMS). Trace elements in ppm.

Supplementary Table 5. SIMS zircon U-Pb analyses of the zircon grains separated from the Kannaviou Formation sandstones.

Supplementary Table 6. Table of correlation coefficients for the Kannaviou Formation sandstones.

Fig. 1

Click here to download high resolution image

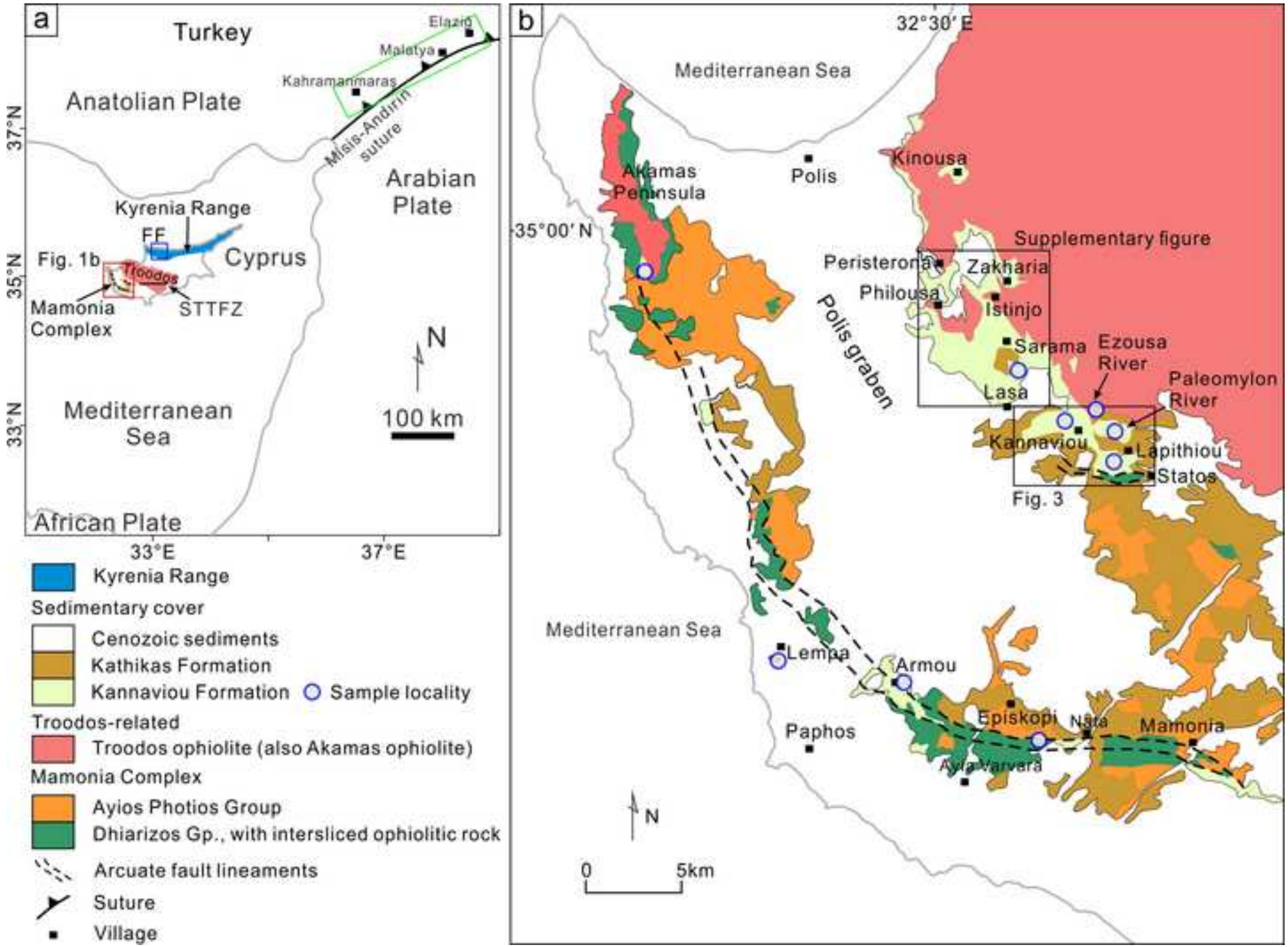

Fig. 2

Click here to download high resolution image

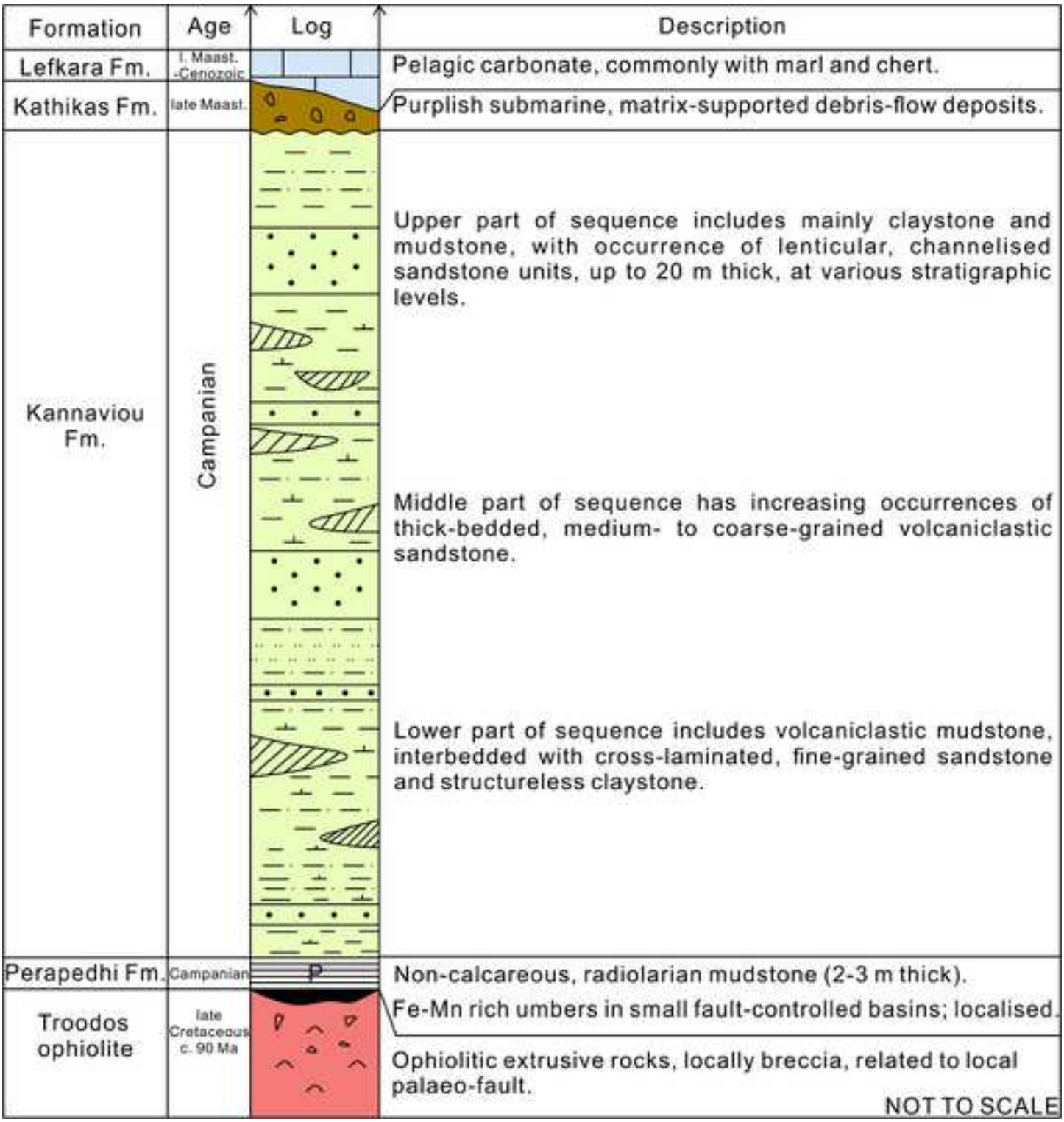

Fig. 3

Click here to download high resolution image

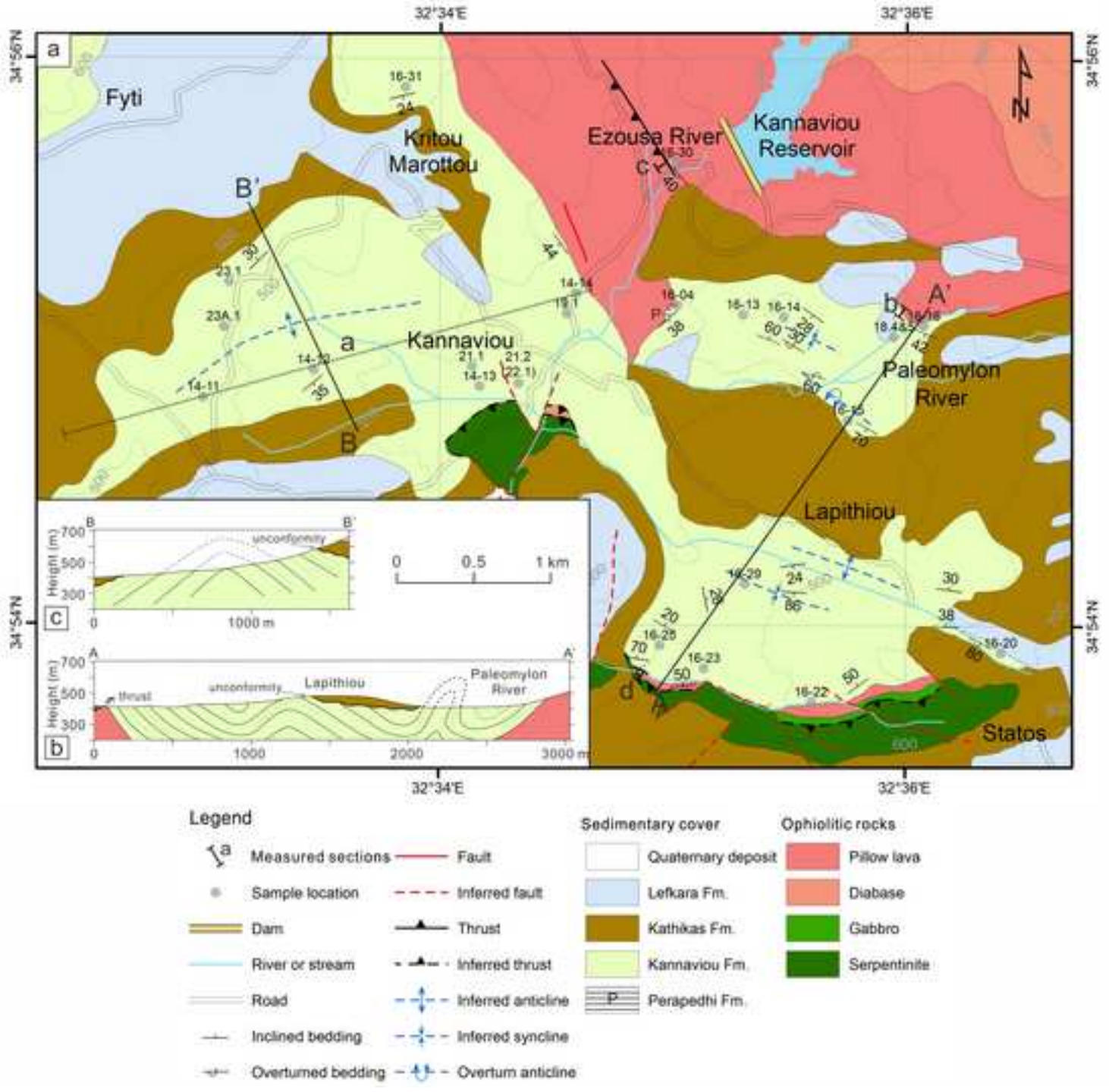

Fig. 4

Click here to download high resolution image

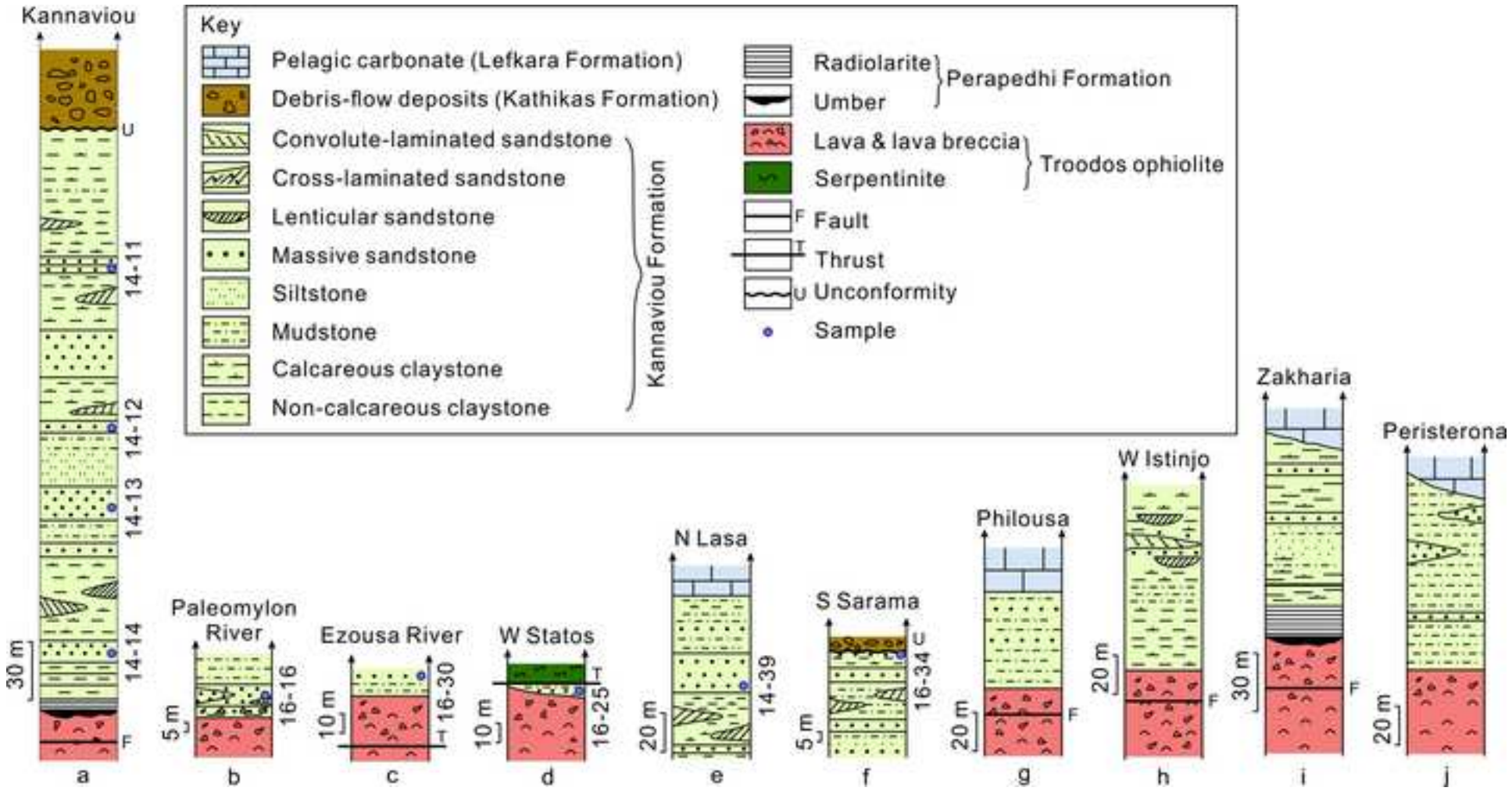

Fig. 5

Click here to download high resolution image

Fig. 6

Click here to download high resolution image

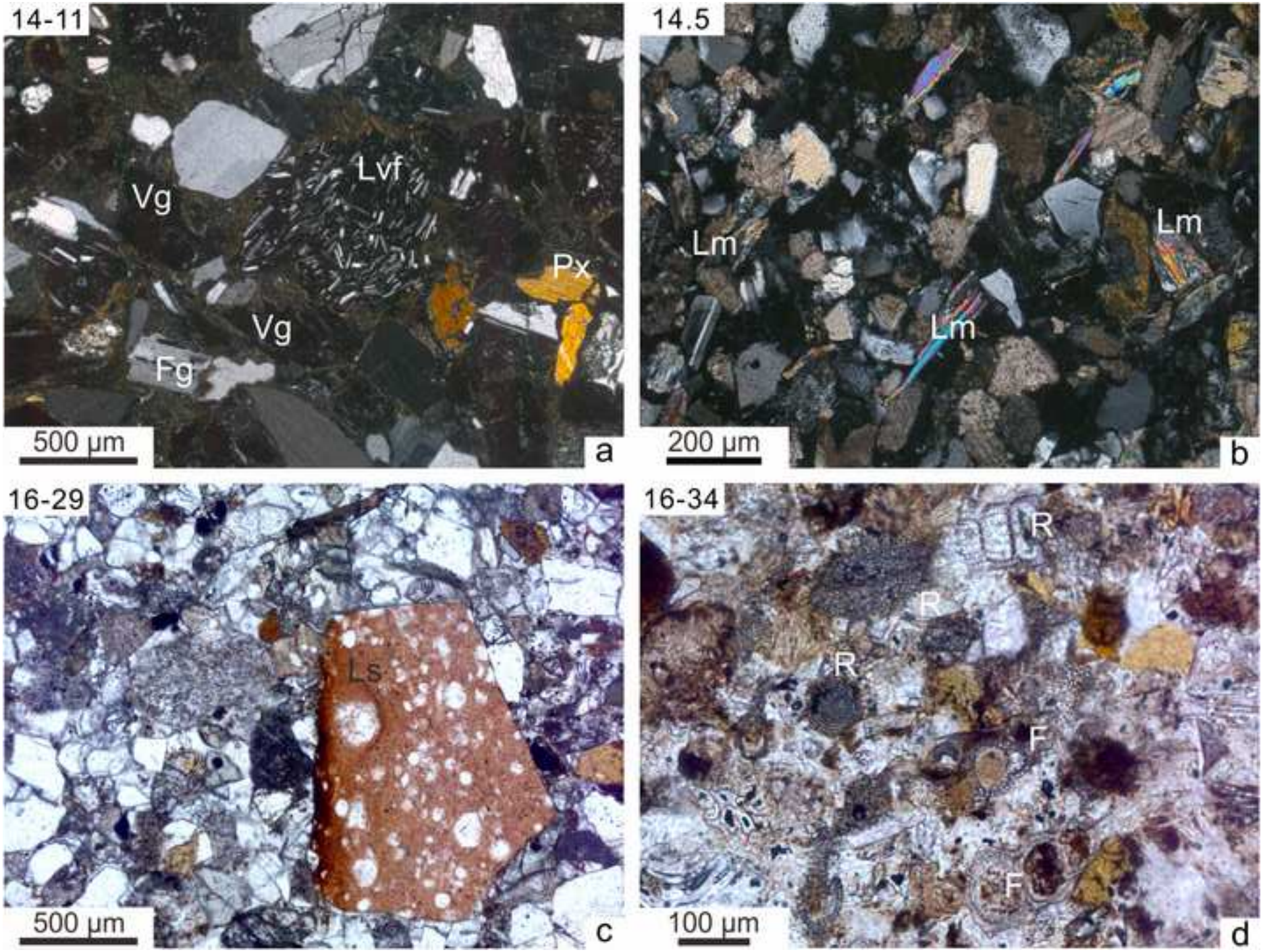

Fig. 7

Click here to download high resolution image

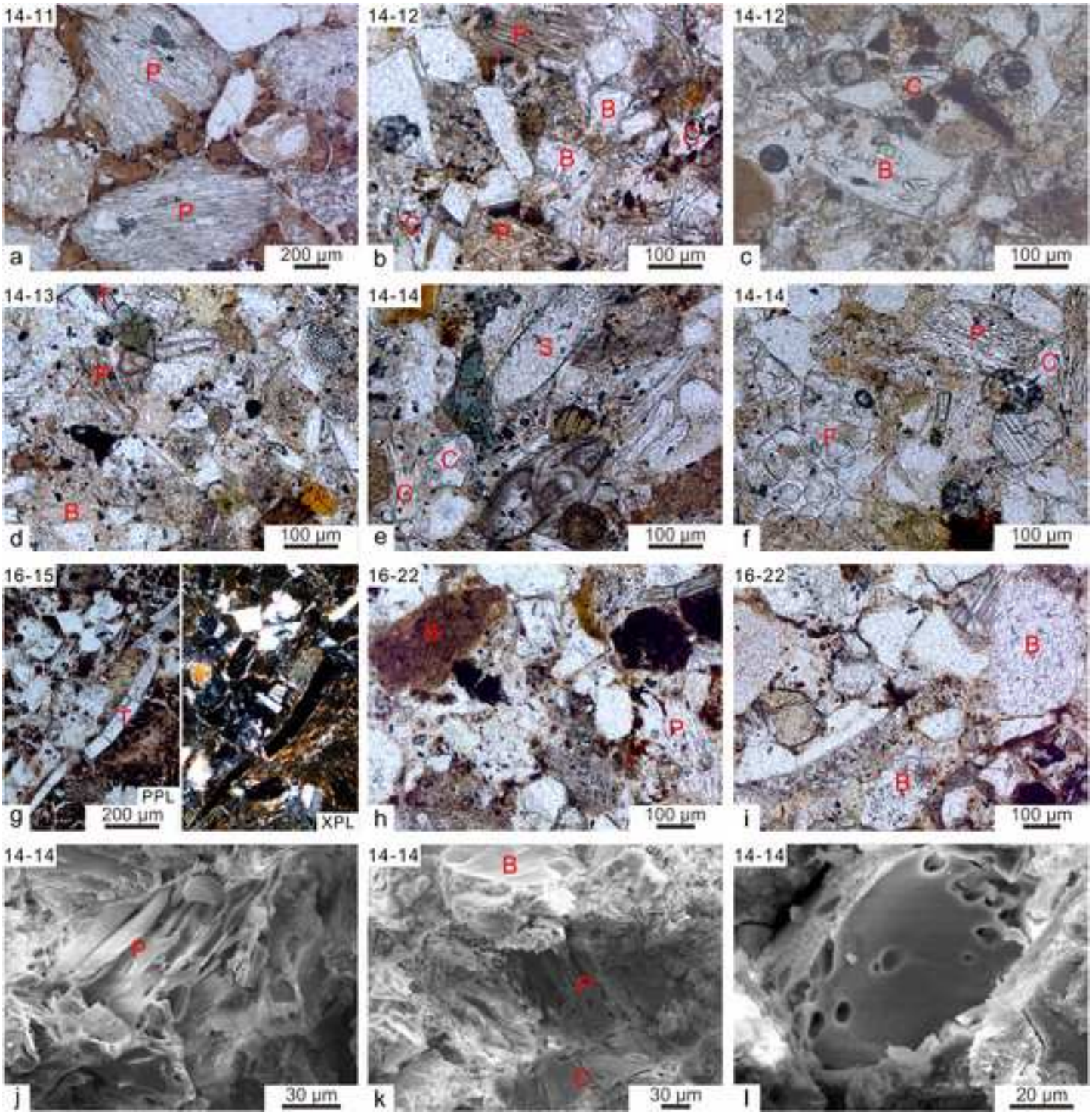

Fig. 8

Click here to download high resolution image

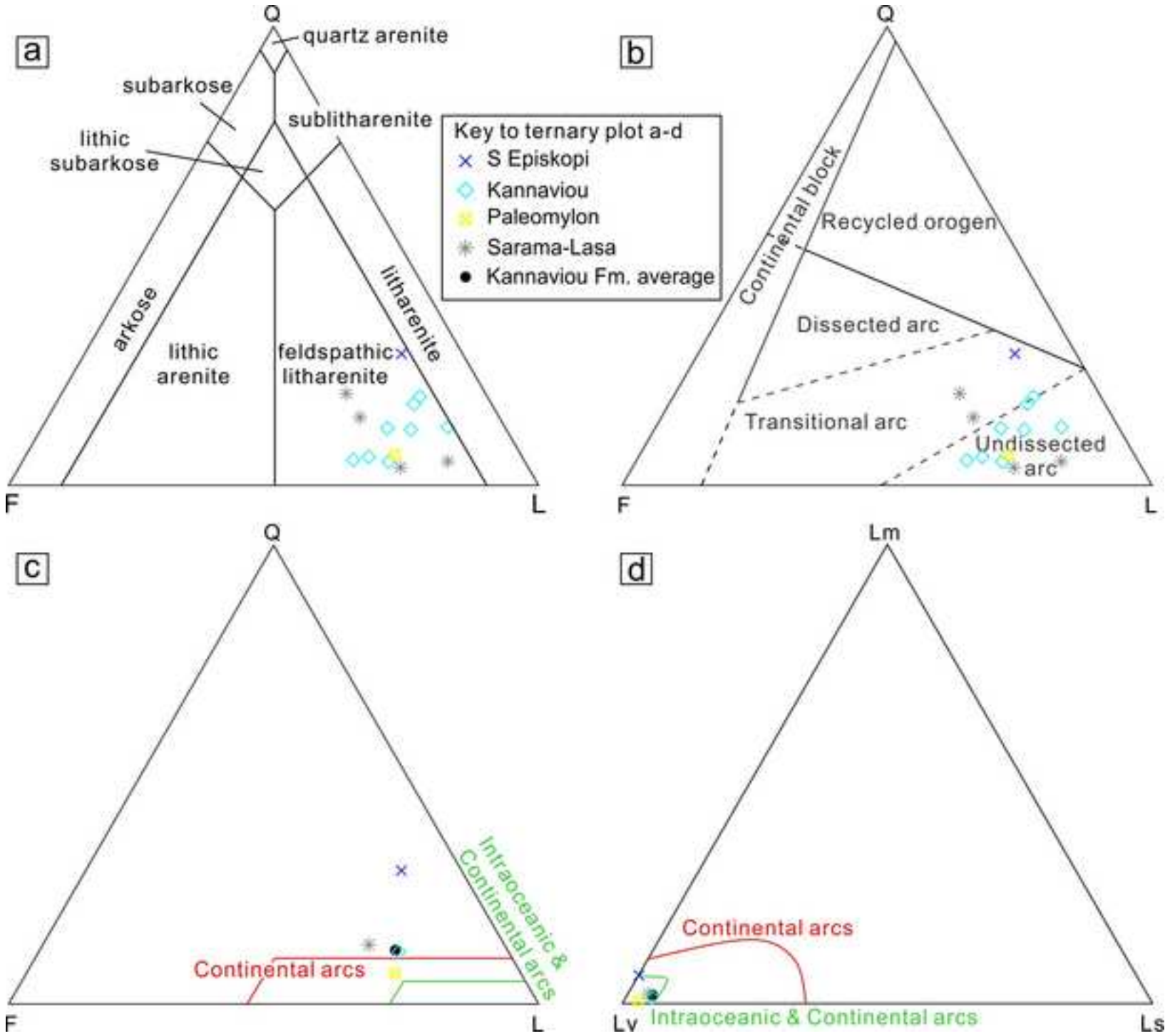

Fig. 9

Click here to download high resolution image

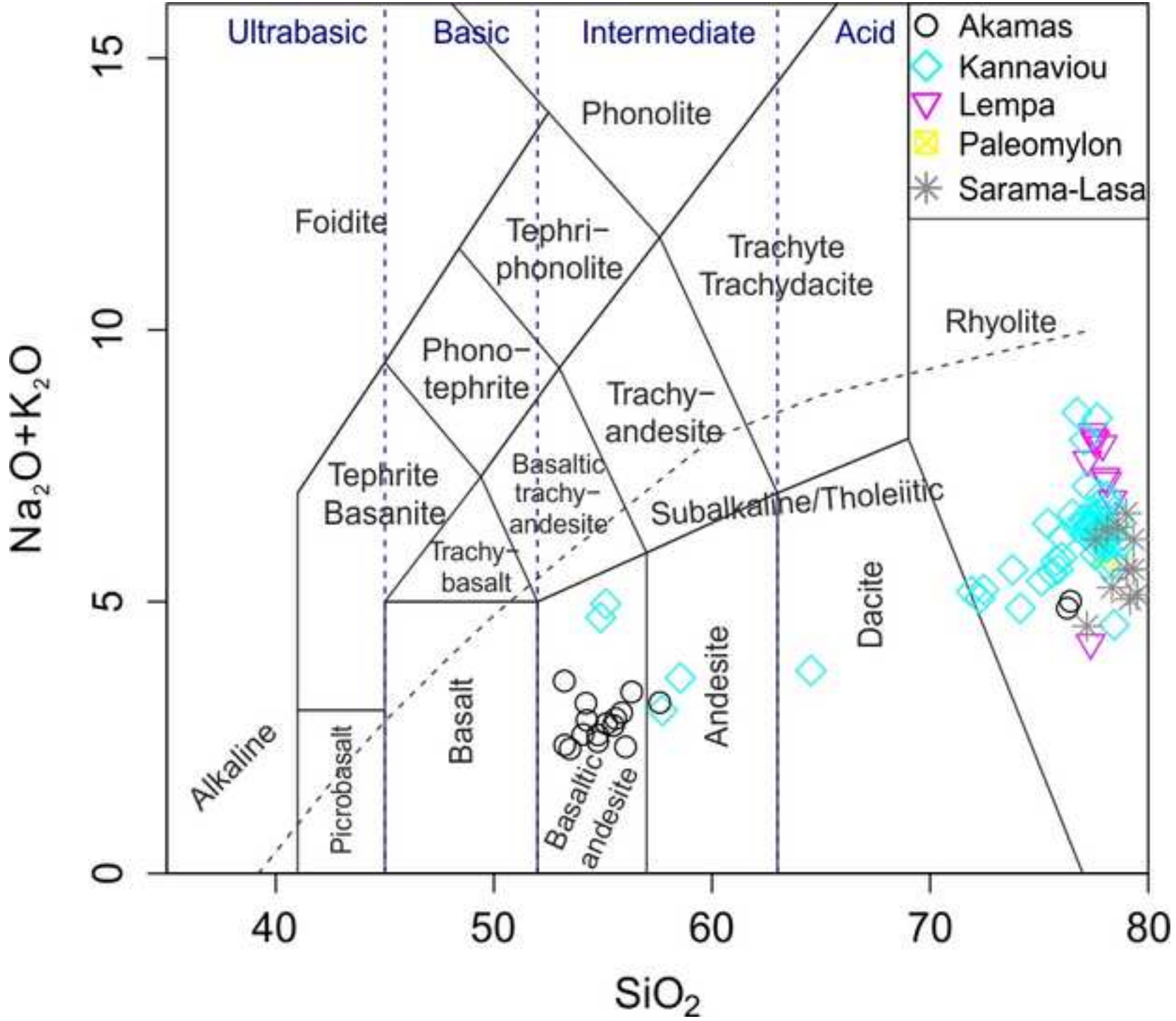

Fig. 10

Click here to download high resolution image

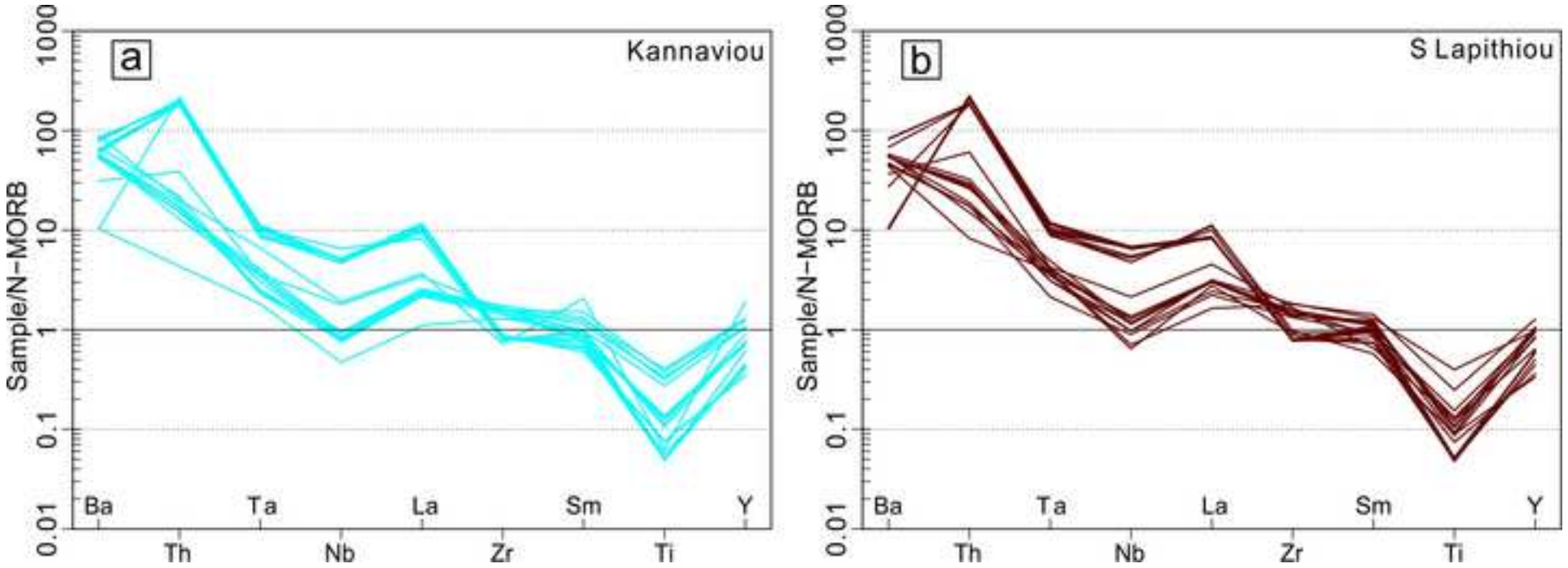

Fig. 11

Click here to download high resolution image

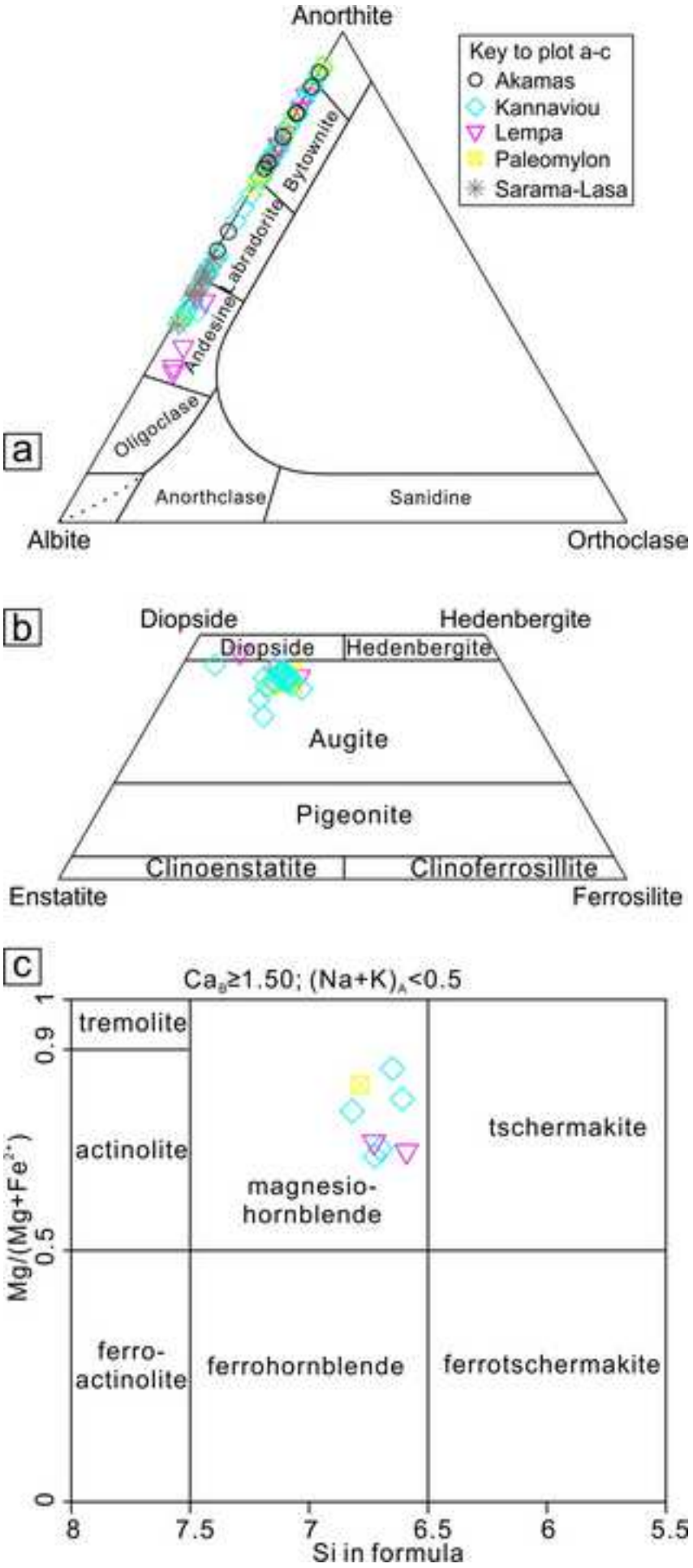

Fig. 12

Click here to download high resolution image

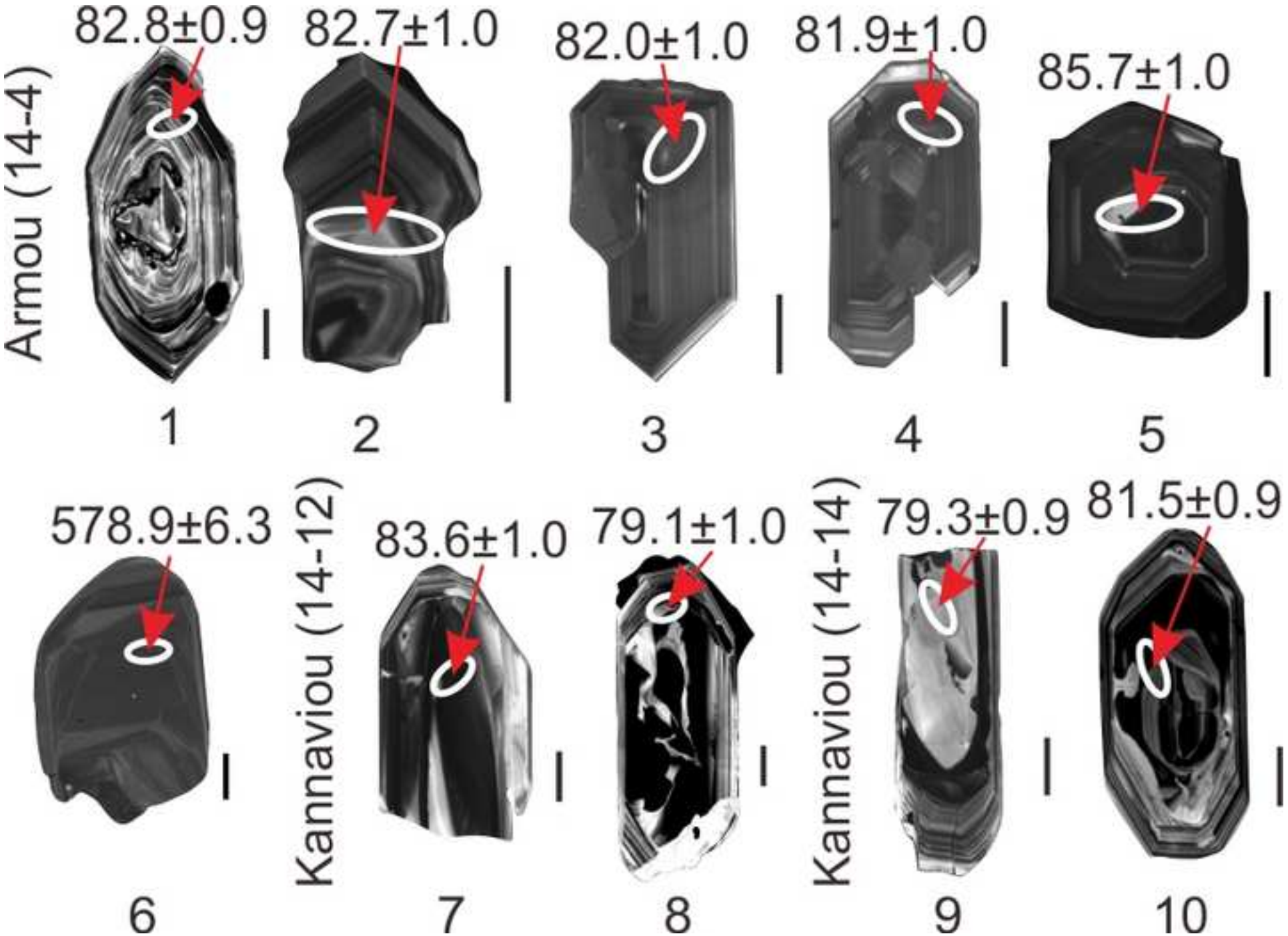

Fig. 13

Click here to download high resolution image

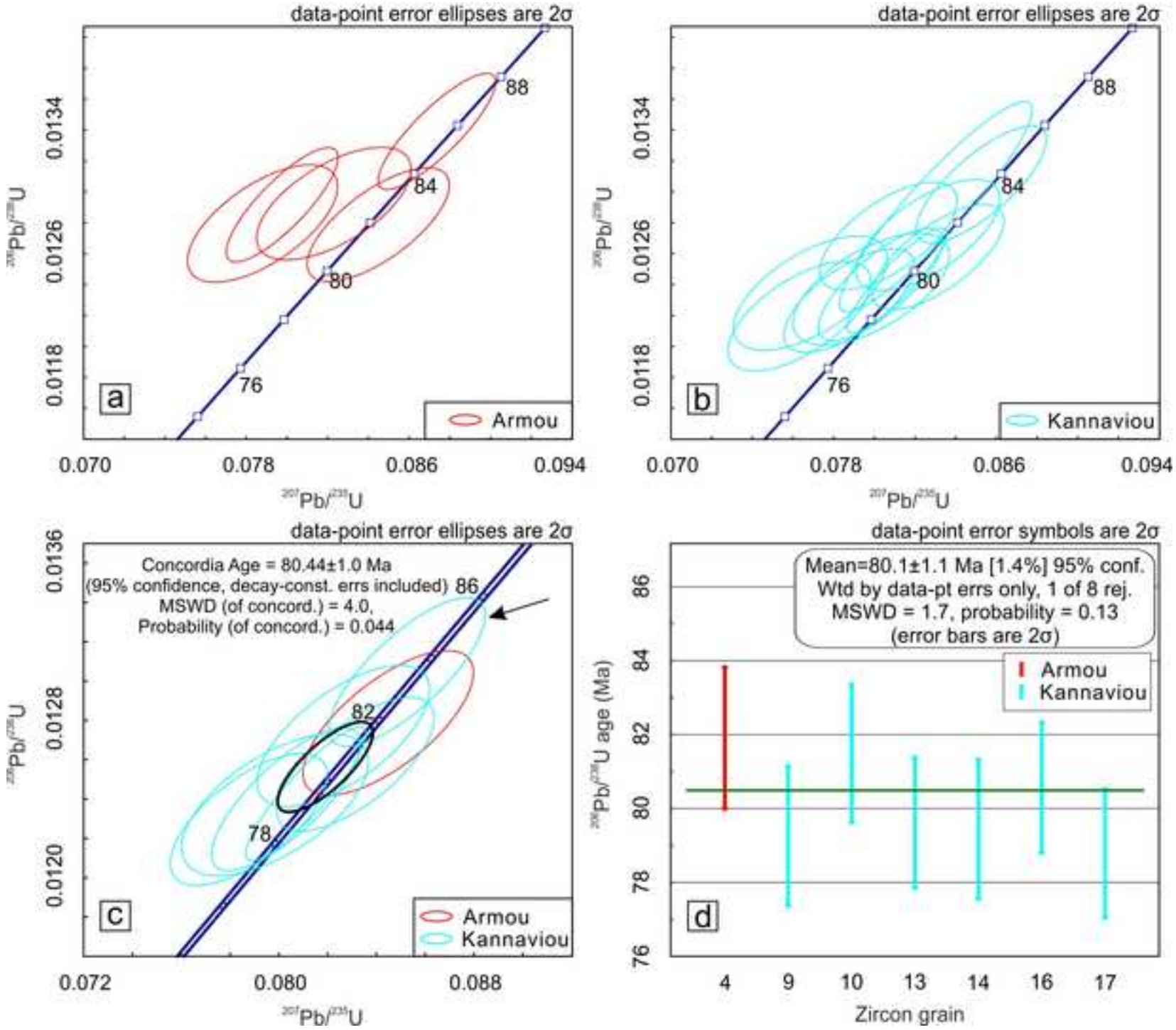

Fig. 14

Click here to download high resolution image

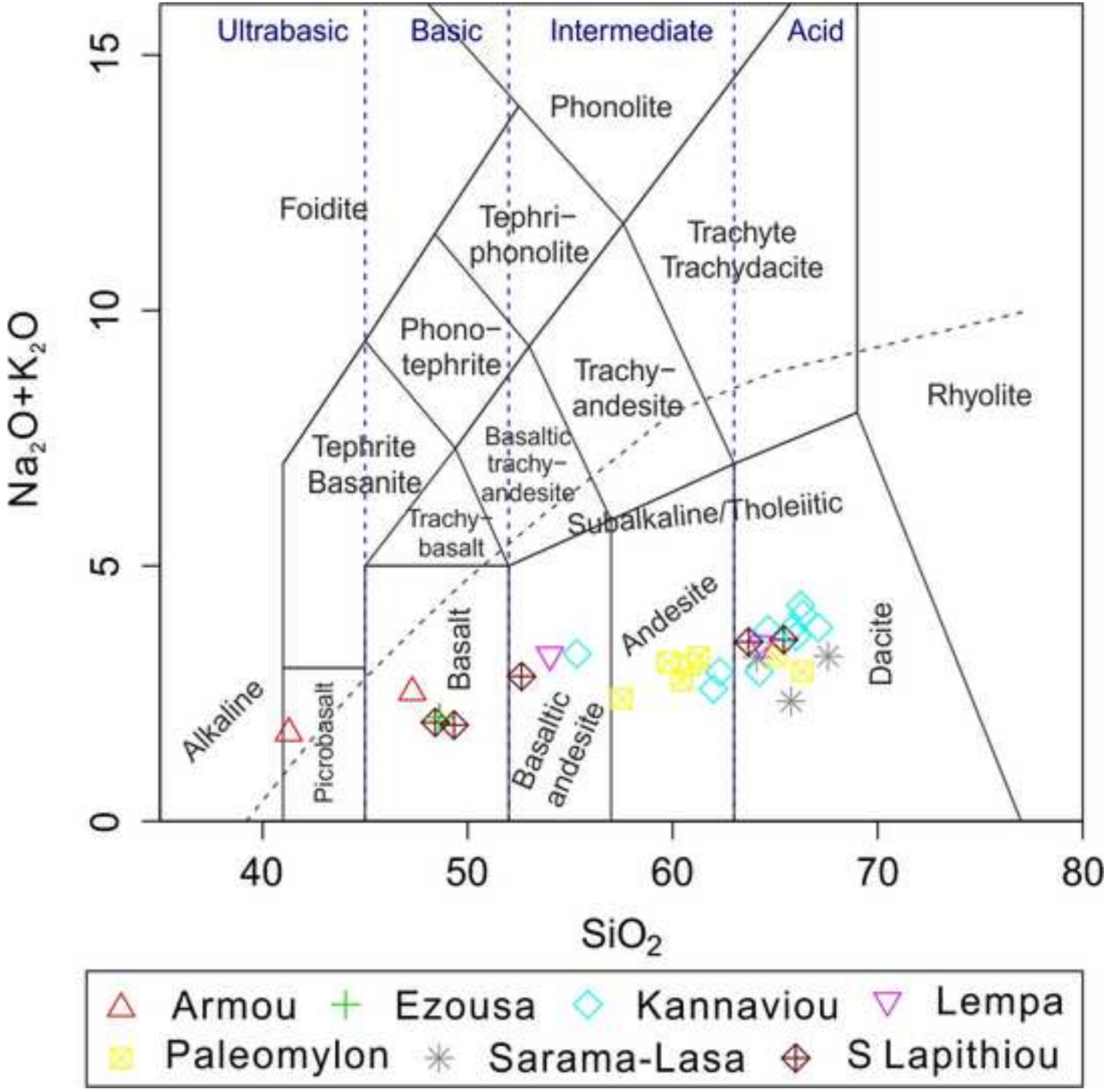

Fig. 15

Click here to download high resolution image

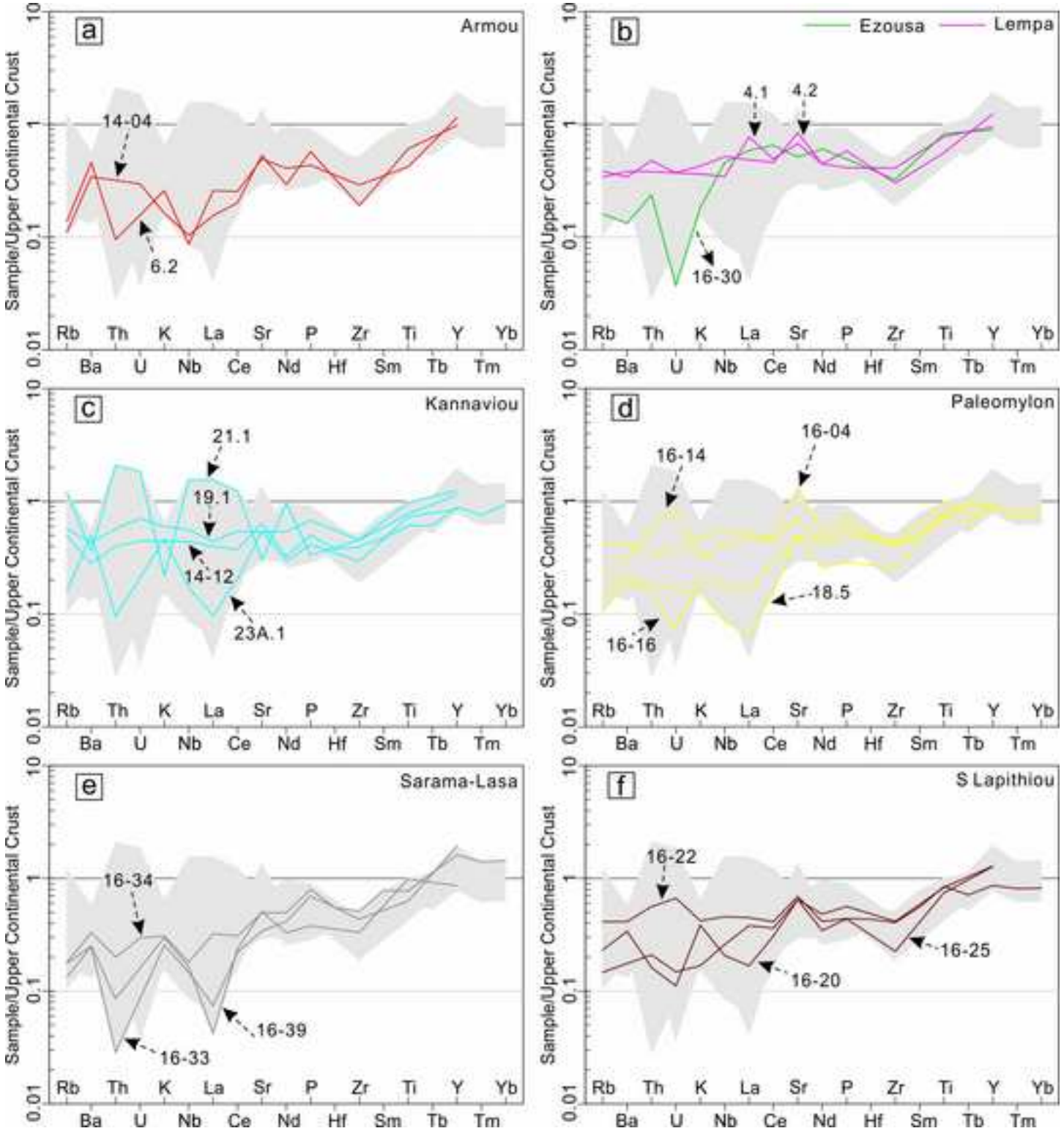

Fig. 16

Click here to download high resolution image

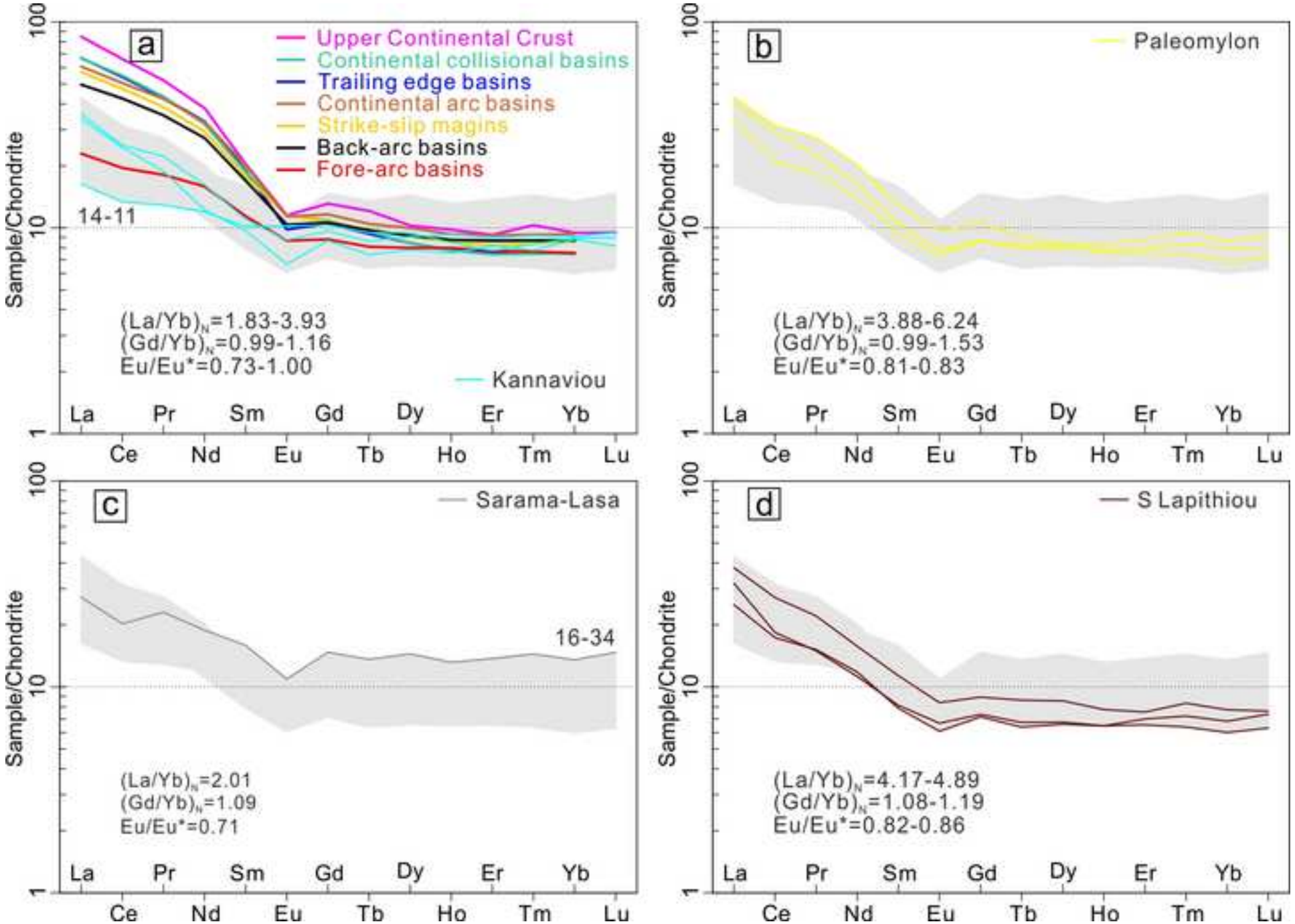

Fig. 17

Click here to download high resolution image

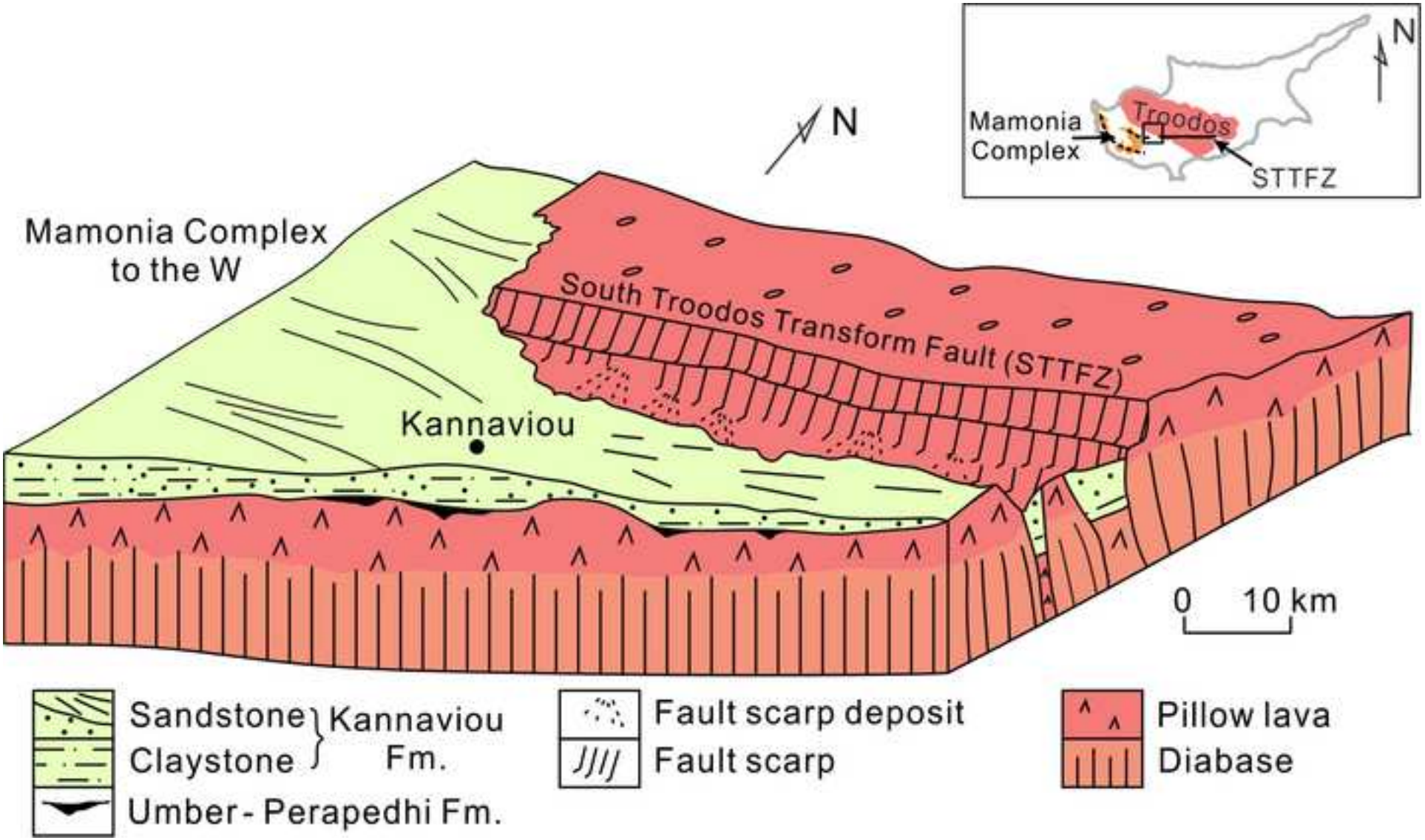

Fig. 18

Click here to download high resolution image

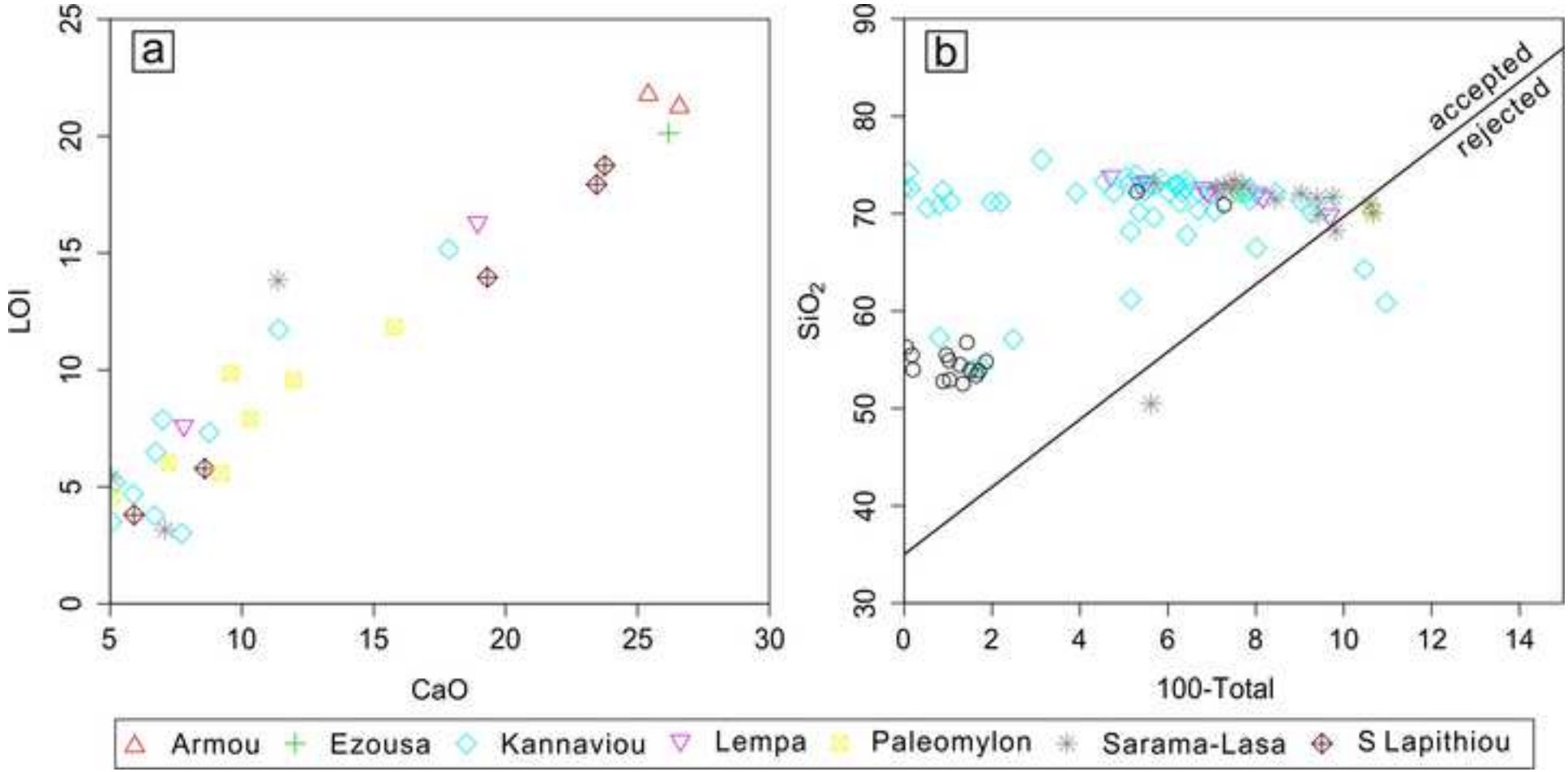

Fig. 19

Click here to download high resolution image

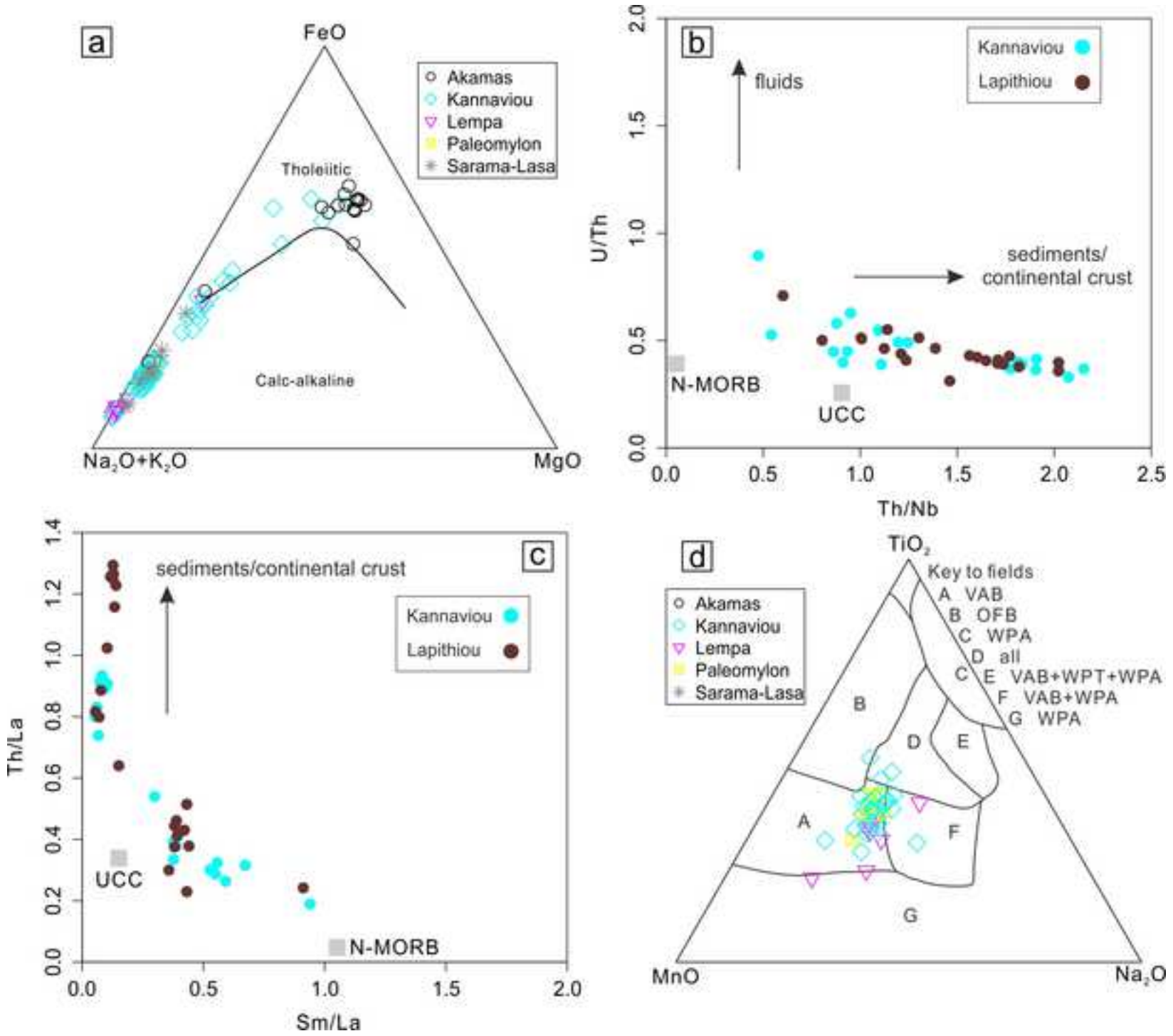

Fig. 20

Click here to download high resolution image

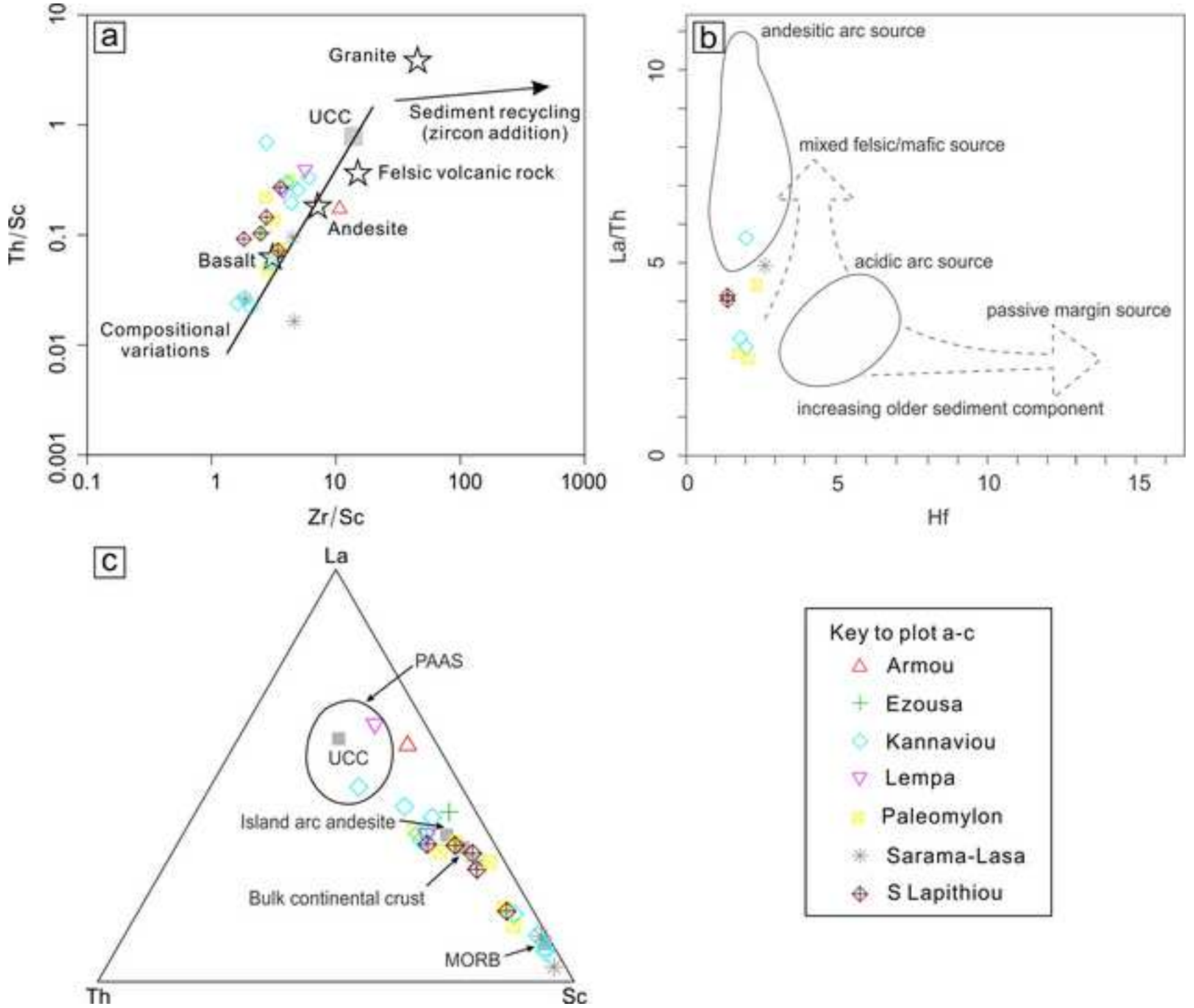

Fig. 21

Click here to download high resolution image

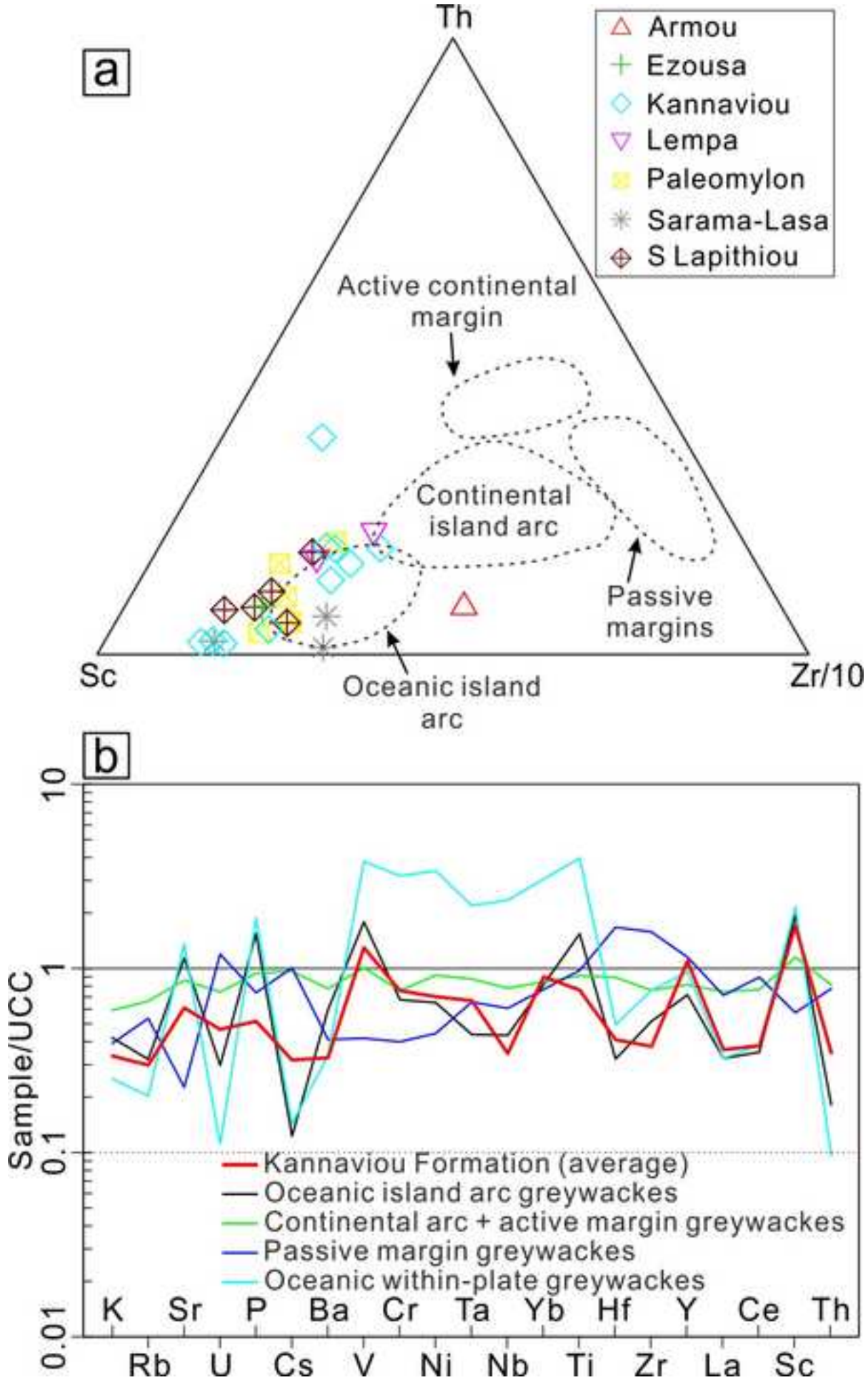

Fig. 22

Click here to download high resolution image

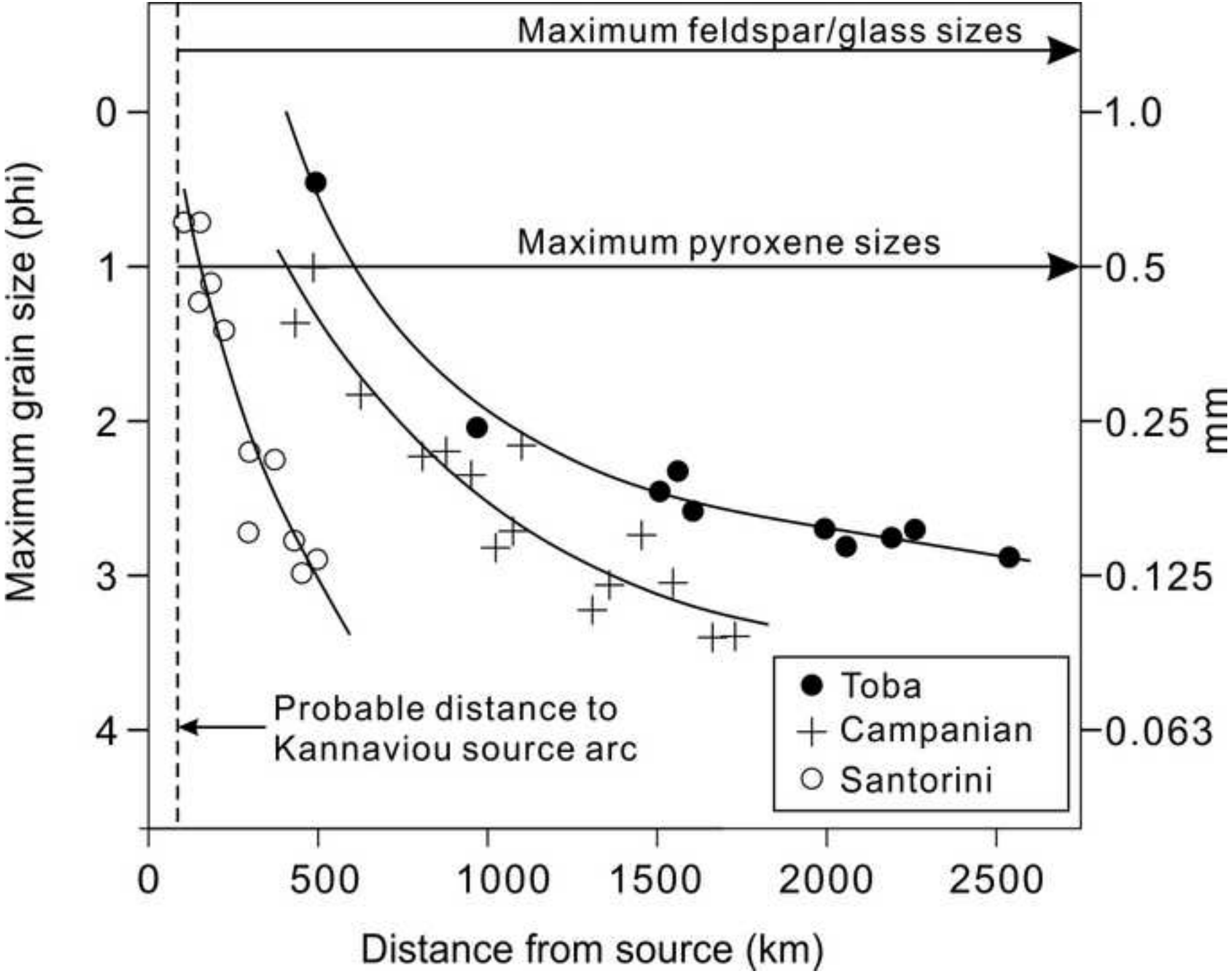

Fig. 23

Click here to download high resolution image

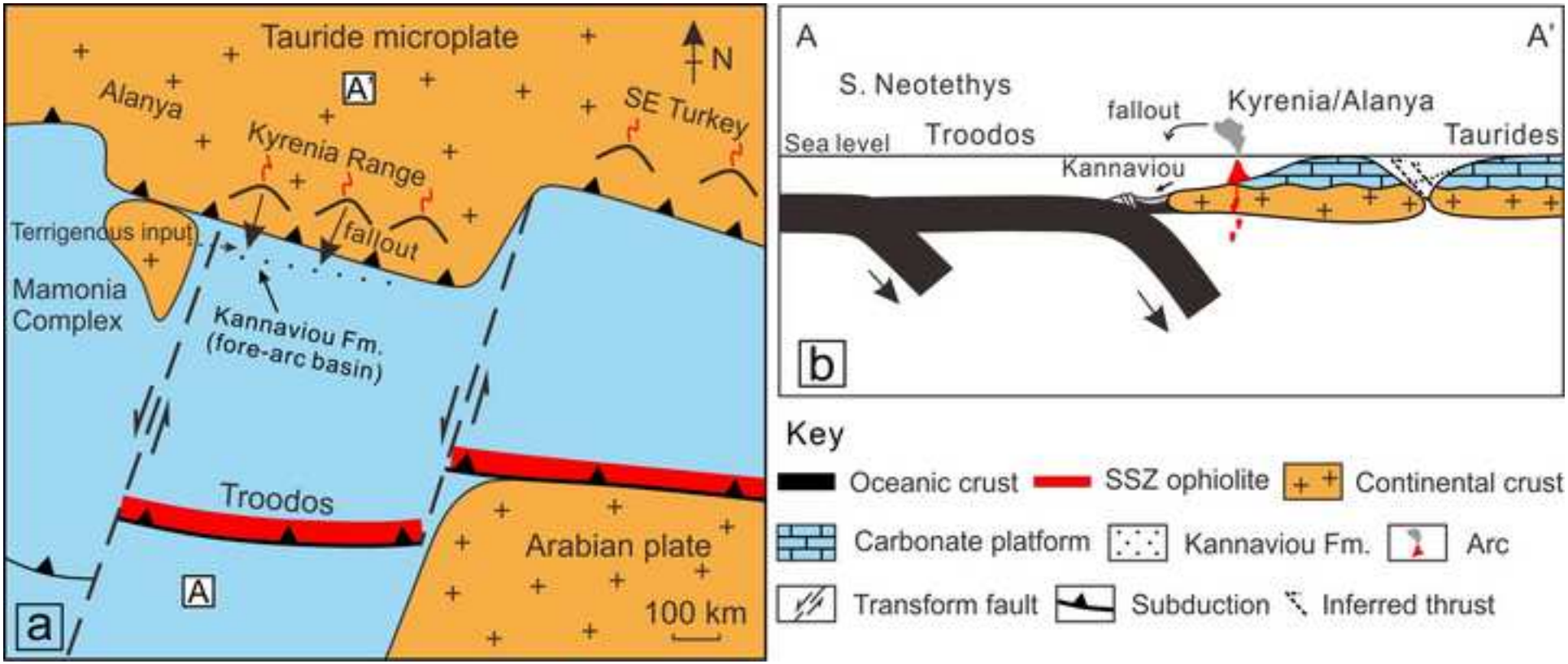

Table 1

Click here to download Table: Table 1.xlsx

Sample	Geographic location	Geographic coordinates	QFL	XRF[a]	ICP-MS	EMPA[a]	IMS-4f	U-Pb	Note[b]
14-04	Armou	34°47'40"N, 32°28'19"E		X				X	
14-11	Kannaviou	34°54'48"N, 32°32'59"E	X	X	X		X		
14-12	Kannaviou	34°54'53"N, 32°33'29"E	X	X	X			X	
14-13	Kannaviou	34°54'53"N, 32°34'16"E	X	X					
14-14	Kannaviou	34°55'20"N, 32°34'34"E	X	X	X		X	X	
16-04	Paleomylon	34°55'08"N, 32°35'01"E		X	X				
16-13	Paleomylon	34°55'06"N, 32°35'18"E		X	X				
16-14	Paleomylon	34°55'02"N, 32°35'29"E		X	X				
16-15	Paleomylon	34°54'44"N, 32°35'44"E		X					
16-16	Paleomylon	34°55'03"N, 32°36'03"E		X					
16-20	south of Lapithiou	34°53'55"N, 32°36'25"E		X			X		
16-22	south of Lapithiou	34°53'44"N, 32°35'36"E		X	X		X		
16-23	south of Lapithiou	34°53'50"N, 32°35'07"E		X	X				
16-25	south of Lapithiou	34°53'54"N, 32°34'51"E		X					
16-29	south of Lapithiou	34°54'09"N, 32°35'19"E		X	X				
16-30	Ezousa River	34°55'36"N, 32°35'00"E		X					
16-31	Kannaviou-Kri. Marottou	34°55'50"N, 32°33'53"E		X					
16-33	Sarama	34°57'25"N, 32°32'28"E		X					
16-34	Sarama	34°56'52"N, 32°32'02"E		X	X				
16-39	Lasa	34°55'47"N, 32°31'51"E		X					Newly collected
4.1	Lempa	34°48'52"N, 32°24'08"E		X[a]					
4.2	Lempa	34°48'52"N, 32°24'08"E		X[a]		X[a]			
6.2	Armou	34°47'43"N, 32°28'22"E		X[a]					
14.5	south of Episkopi	34°46'08"N, 32°32'28"E	X						
18.4	Paleomylon	34°55'02"N, 32°36'00"E		X[a]					
18.5	Paleomylon	34°55'02"N, 32°36'00"E	X	X[a]		X[a]			
19.1	Kannaviou	34°55'07"N, 32°34'33"E	X	X[a]		X[a]			
21.1	Kannaviou	34°54'53"N, 32°34'10"E		X[a]		X[a]			
21.2	Kannaviou	34°54'48"N, 32°34'20"E	X	X[a]		X[a]			
22.1	Kannaviou	34°54'48"N, 32°34'20"E	X						
23.1	Kannaviou	34°55'14"N, 32°33'09"E	X	X[a]					
23A.1	Kannaviou	34°55'03"N, 32°33'05"E		X[a]		X[a]			Gilbert and Robertson (2013)
1074	Akamas	34°59'31"N, 32°19'56"E				X			
2124	Lasa	NA	X						
2141	Sarama	NA	X						
2156	Sarama	NA	X						
2158	Sarama	NA	X						
2164	Sarama	NA				X			Robertson (1977a)

QFL: petrographic thin section study for point counting;
XRF: major and trace element analysed by X-ray fluorescence spectrometry;
ICP-MS: trace and rare earth element analysed by inductively coupled plasma mass spectrometry;
EMPA: mineral chemistry analysed by electron microprobe;
IMS-4f: glass trace element analysed by ion microprobe;
U-Pb: zircon U-Pb geochronology analysed by secondary-ion mass spectrometry;

[a] Data from Gilbert and Robertson (2013);

[b] Thin section, polished section source.

Table 2

Click here to download Table: Table 2.xlsx

Main parameter		*Calculated parameter*	
Qm	Monocrystalline quartz	Q	Total quartz grains (=Qm+Qp)
Qp	Polycrystalline quartz	F	Total feldspar grains (=Fg)
Fg[a]	Feldspar grains	Lv	Volcanic lithics (=Vg+Lvm+Lvf)
Fl	Feldspar in lithics	Lsm	Sedimentary and metamorphic lithics (=Ls+Lm)
Vg[b]	Volcanic glass	L	Total unstable lithic fragments (=Lv+Lsm+Lo+Fl)
Lvm[c]	Intermediate to mafic volcanic lithics	Lt	Total lithic fragments (=L+Qp)
Lvf[d]	Felsic volcanic lithics		
Ls	Sedimentary lithics		
Lm	Metamorphic lithics		
Lo	Other lithics		
Px	Detrital pyroxenes		
Am	Detrital amphiboles		
Bt	Detrital biotite grains		
Ms	Detrital muscovite flakes		
Cal	Carbonate grains		
Bio	Bioclastic detritus		
M	Matrix		
C	Cement		

[a] no differentiation of feldspar;

[b] volcanic glass (relatively pure, with very minor phenocrysts);

[c] dark coloured volcanic lithics, with common pyroxene and opaque crystals;

[d] pale coloured volcanic lithics with common quartz and feldspar laths.

Table 3

Click here to download Table: Table 3.xlsx

	Kannaviou Formation							Sediment from felsic sources[a]		Sediment from mafic sources[a]	
	Armou	Ezousa	Kanaviou	Lempa	Paleomylon	Sarama-Lasa	S Lapithiou	Coarse fractions	Fine fractions	Coarse fractions	Fine fractions
La/Co	-	-	0.24-0.84	-	0.69-1.13	0.59	0.67	1.8-13.8	1.4-22.4	0.14-0.38	-
Th/Co	-	-	0.05-0.31	-	0.16-0.44	0.12	0.21	0.67-19.4	0.3-7.5	0.04-1.4	-
Th/Cr	0.03	0.01	0.03-0.71	0.08	0.03-0.12	0.02-0.05	0.05	0.13-2.7	0.067-4.0	0.018-0.046	0.002-0.045
La/Sc	0.27-1.58	-	0.08-1.52	0.70-2.30	0.04-0.77	0.04-0.45	0.47	2.5-16.3	0.7-27.7	0.43-0.86	0.4-1.1
Th/Sc	0.17	-	0.69	0.26-0.39	0-0.32	0.02-0.10	0.14	0.84-20.5	0.64-18.1	0.05-0.22	0.05-0.4
Eu/Eu*	-	-	0.73-1.00	-	0.81-0.83	0.71	0.81-0.86	0.40-0.94	0.32-0.83	0.71-0.95	0.7-1.02

[a] data from Cullers (1995, 2000)

Supplementary Appendix A

Click here to download Supplementary material for on-line publication only: Supplementary Appendix A.docx

Supplementary Appendix B

Click here to download Supplementary material for on-line publication only: Supplementary Appendix B.docx

Supplementary Figure 1

Click here to download Supplementary material for on-line publication only: Supplementary Figure 1.jpg

Supplementary Figure 2

Click here to download Supplementary material for on-line publication only: Supplementary Figure 2.jpg

Supplementary Figure 3

Click here to download Supplementary material for on-line publication only: Supplementary Figure 3.jpg

Supplementary Figure 4

Click here to download Supplementary material for on-line publication only: Supplementary Figure 4.jpg

Supplementary Table 1

Click here to download Supplementary material for on-line publication only: Supplementary Table 1.xlsx

Supplementary Table 2

Click here to download Supplementary material for on-line publication only: Supplementary Table 2.xlsx

Supplementary Table 3

Click here to download Supplementary material for on-line publication only: Supplementary Table 3.xlsx

Supplementary Table 4

Click here to download Supplementary material for on-line publication only: Supplementary Table 4.xlsx

Supplementary Table 5

Click here to download Supplementary material for on-line publication only: Supplementary Table 5.xlsx

Supplementary Table 6

Click here to download Supplementary material for on-line publication only: Supplementary Table 6.xlsx